Abstract

Yujie, Lu. Solution and Surface Properties of Helical Rod-like Polyguanidines (Under the direction of Bruce M. Novak)

Helical polymers are of increasing interest because of the wide variety of applications for them, which include uses in optical devices, chiral columns for HPLC separations, asymmetric supports for catalysis, components in organic/inorganic hybrid materials and biomimetic application.

Polymerization of achiral monomers (with optically inactive catalysts) always yields a racemic mixture of right and left helical senses since the enantiomers are of equal energy. Our research goal is to synthesize polymers with a biased helical sense and investigate their properties, such as chirality and liquid crystallinity. To this end, two kinds of approaches for the preparation of helical polyguanidines have been demonstrated: significant amplification of chirality was observed in polyguanidines containing chiral side chains and the optically active polyguanidines can also be produced from achiral monomers by helix-sense selective catalysts. The chirality of polymer arises from helical conformation of polymer chains with an excess of single screw sense.

Furthermore, we investigated a new method of preparing self-assembled monolayers (SAMs) of thiol terminated polyguanidines. These end-capped polymers were prepared through the living polymerization of carbodiimides. The features of living polymerization allow us to functionalize the polymer during the initiation step. Polarization modulation infrared reflection absorption spectroscopy (PM-IRRAS), monitoring the infrared signature peak of polyguanidines at 1649 cm^{-1}, ellipsometry, and contact-angle goniometry were used to detect the formation and properties of these polymeric SAMs on gold surfaces. The gold-

polyguanidines nanocomposites have been also prepared by the surface initiated polymerization on gold nanoparticles. Because these polymers possess helical structures reminiscent of polypeptides, these work should allow us to probe chiral interactions and energies on surfaces that are biologically relevant.

SOLUTION AND SURFACE PROPERTIES OF HELICAL ROD-LIKE POLYGUANIDINES

by

Yujie Lu

A dissertation submitted to the Graduate Faculty of
North Carolina State University
in partial fulfillment of the
requirements for the Degree of
Doctor of Philosophy

Department of Chemistry

Raleigh

2005

APPROVED BY:

_____	_____
Bruce M. Novak (Chairman)	T. Brent Gunnoe
_____	_____
Tatyana I. Smirnova	Jeffery L. White

Dedication

This work is dedicated to my parents, Shuying Sun and Qingduo Lu, and my wife, Rui Xiao.

Thank you for all of your love, support and encouragement.

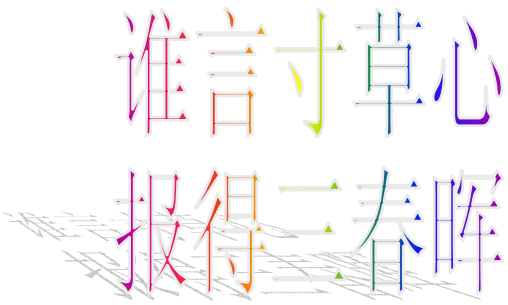

Biography

The author was born on Sept. 18, 1973 in Lanzhou, China. During the 6 years of education at Lanzhou High School, Yujie was inspired intensively to pursue a career in science. Upon graduation of high school, he attended the Peking University in Beijing, China and received a bachelor degree in chemistry in 1997. In 1997, he began his graduate education in Beijing Research Institute of Chemical Industry and worked with Dr. Jinliang Qiao. His research project was on the modification of the properties of polypropylene, especially on the melting strength of PP, and a patent has been applied for this work. He got much industry experience there and earned his MS degree in 2000. Since the fall of 2000, he joined Dr. Novak's research group in North Carolina State University to begin working on the investigation of the helical polymer and polymer surface chemistry.

Acknowledgements

I would first like to thank Dr. Bruce Novak. He is the best research advisor I ever had. He provides not only excellent facilities, resources, and a remarkable working environment to make progress in research, but those good suggestions allowing me to explore my own ideas. Under his supervision, I learn to think systematically, thoroughly and independently.

The Novak's group has been a cozy family to me. I enjoy the international atmosphere of the group. Dr. Gonglu Tian and Dr. Hong-zhi Tang, two talented postdocs, helped me lots on my experiments and paper writing. I also benefited from the valuable discussion with them. Thanks other group fellows, Haibo, Yoko, Keitaro and Hyun-su, your contributions to my work are greatly appreciated. The past members of our team have been a blessing, and I thank them all for their advice, encouragement and friendship.

I am grateful to Professors Stefan Franzen (Department of Chemistry), Jan Genzer (Department of Chemical Engineering) Harald Ade (Department of Physics) and Clay Clark (Department of Biochemistry) in North Carolina State University for providing generous help on the equipment access.

Finally, I would like express my deepest gratitude to all of my friends, especially to Xinhui Lou. Your precious advice, help and friendship are significant to me along the way.

Table of Contents

List of Figures……x

List of Schemes……xv

List of Tables……xvi

Chapter I

An Overview of the Helical Polymers

1.1. Chirality overview……1

1.1.1. Enantiomers……...1

1.1.2. Diastereomers……4

1.1.3. Configurational and conformational asymmetry……...5

1.2. Helical structure……5

1.2.1. Helical polymers……6

1.2.2. Natural helical polymers……7

1.2.3. Synthetic helical polymers……8

Polysilylenes……8

Polymethacrylate……...10

Polyisocyanides……12

Polyisocyanates……13

Polyguanidines……..14

1.3. Synthesis of helical polymers……17

1.3.1. Helix-sense-selective polymerization……17

1.3.2. Amplification of chirality……....18

1.3.3. Cooperativity……...19

1.4. Polyguandines……22

1.4.1. Carbodiimide monomer……...22

1.4.2. Living polymerization of carbodiimides……23

1.4.3. Liquid crystalline properties of polyguanidines……..24

1.4.4. The cooperativity of polyguanidines……...27

1.4.5. Characterization of polyguanidines……29

1.5. Reference and notes……31

Chapter II

Influencing Macromolecular Chirality in Subtle Ways

2.1. Introduction……36

2.1.1. Helical reversals and inversion barrier……36

2.1.2. Regioselectivity in carbodiimide polymerizations……..38

2.1.3. Motivation: highly ordered helical polyguanidines……39

2.2. Amplification of chirality……...43

2.2.1. Preparation of materials……...43

Monomers……..43

Polymers……45

2.2.2. Amplification of chirality……46

2.3. Regioselectivity……..50

2.4. Annealing behaviors……...56

2.4.1. Optical Rotation……...56

2.4.2. Circular Dichroism……..59

2.4.3. ^{19}F NMR……..61

2.5. Activation energy for the polymer reorganization..……...65

2.6. Molecular weight dependence of optical rotation of polyguanidines……68

2.7. Cooperativity through chiral seeding……70

2.8. Helix-sense-selective polymerization of carbodiimides from achiral monomers……..76

2.9. Conclusion……..81

2.10. Experimental section……83

2.10.1. General procedures and characterization……...83

2.10.2. Experimental procedures and characterizations……84

2.11. References and notes……96

Chapter III.

The Adsorption of Thiol Terminated Rod-like Polyguanidines on Gold Surfaces

3.1. Introduction to ultrathin organic films……...98

3.1.1. Langmuir-Blodgett films……98

Origin……98

The formation of LB films……99

Transfer ratio……...101

Applications……101

3.1.2. Self-assembled monolayers……...102

Features and applications……103

History……104

Structure……..105

3.1.3. Monolayers of alkanethiols on gold……..106

Mechanism and kinetics of the formation……...107

Application in biotechnology……..108

3.1.4. Motivation: formation of SAMs with functionalized polyguanidines……..109

3.2. The adsorption of thiol-terminated polyguanidines on gold……111

3.2.1. Preparation of thiol-terminated polyguanidines……111

3.2.2. Analysis of the SAMs by polarization-modulation infrared reflection adsorption spectroscopy (PM-IRRAS)……112

3.2.3. Properties of monolayer films formed from polyguanidines as a function of the chain length……114

3.2.4. Kinetics of formation of monolayers……118

3.2.5. Solvent effect on monolayer formation……120

3.2.6. AFM images of the SAMs of polyguanidines on gold……..123

3.3. Gold-polyguanidine nanocomposites……...126

3.4. Experimental section……132

3.4.1. General procedures and characterizations……132

3.4.2. Experimental procedures and characterizations……132

3.5. References and notes……138

List of Figures

Figure 1.1. Configuration of enantiomers and diastereomers…….……2

Figure 1.2. The structure of helical hexahelicene…….……..6

Figure 1.3. The α-helical structure of polypeptide…….…….7

Figure 1.4. The structure of 1-phenyldibenzosuberyl methacrylate…….…….11

Figure 1.5. Polyisocyanide's 4/1 helical conformation.....…...13

Figure 1.6. Circular dichroism and UV spectra of deuterated polyisocyanates…….....15

Figure 1.7. The structural relationship between polyisocyanates, polyisocyanides and the hybrid polymer derived from the polymerization of carbodiimdes……..16

Figure 1.8. Optically inactive helical polymer chain….……...17

Figure 1.9. Cooperativity within a helical polymer chain…….……20

Figure 1.10. The pyramid of cooperativity……21

Figure 1.11. The enantiomeric conformers of carbodiimides……...22

Figure 1.12. Effective catalysts for the polymerization of carbodiimides……25

Figure 1.13. The mechanism of polymerization of carbodiimide monomer using a Ti(IV) catalyst……...26

Figure 1.14. Structures of some of the liquid crystalline polyguanidines……..…28

Figure 2.1. An energy diagram for helical inversion……..……...37

Figure 2.2. Two possible insertion pathways in the polymerization of unsymmetrical carbodiimides……38

Figure 2.3. Regiospecificities which may arise upon polymerization of asymmetric carbodiimides……39

Figure 2.4. Diastereomeric nature between right and left handed helices for polymers composed of chiral monomers……..42

Figure 2.5. Catalysts used in this work……..45

Figure 2.6. Annealing behavior of Poly-**2**……47

Figure 2.7. Circular dichroism and UV spectra for Poly-**3** in hexane at room temperature……49

Figure 2.8. CD spectra of poly-**4** and poly-**5**……51

Figure 2.9. Possible decomposition products for polyguanidines……53

Figure 2.10. ^{13}C NMR and IR data for polyguanidines……55

Figure 2.11. Proposed mechanism for regioselective polymerization of non-symmetric aryl carbodiimides……57

Figure 2.12. Specific optical rotation of poly-**3** as the function of time at different annealing temperatures……..58

Figure 2.13. Variable temperature CD spectra of poly-**3** in hexane ($c = 4.1 \times 10^{-5}$ M, path length = 1.0 cm)……60

Figure 2.14. The CD spectra of poly-**3** in the octane solution during the annealing process ($c = 7.38 \times 10^{-5}$ M, path length = 1.0 cm)……..61

Figure 2.15. Fluorinated carbodiimide monomers……62

Figure 2.16. ^{19}F NMR spectra of Poly-**10** in the solution of $CDCl_3$ annealed at 50 °C……64

Figure 2.17. Specific optical rotation of poly-**10** as the function of time annealing at 50°C……...65

Figure 2.18. Kinetic vs. thermodynamic control over helical conformation…….66

Figure 2.19. The rate of helix inversion of poly-**3**……67

Figure 2.20. Arrhenius plot for annealing poly-**3**….....67

Figure 2.21. Two possible mechanisms for lose helical reversals……69

Figure 2.22. The evolution of the optical rotation of poly-3 of different molecular weights at 70 ºC……..70

Figure 2.23. Optical Rotation for s series of polyisocyanates containing different amount of (*R*)-2,6- dimethylheptyl isocyanate (sergeant) and *n*-hexyl isocyanate (solider)……..72

Figure 2.24. Optical rotation for a series of poly(**3**-*co*-**6**) containing different amounts of sergeant and soldier monomers. ……...73

Figure 2.25. The specific optical rotation of annealing poly(**3**-*co*-**6**) as the function of time……74

Figure 2.26. The more realistic two-dimensional depictions of the polyisocyanate chain and polyguanidines……...75

Figure 2.27. CD spectra of enantiotopic poly-**6**……79

Figure 2.28. The specific rotation of poly-**6** as a function of time and annealing temperature……80

Figure 3.1. Conventional schematic of the LB technique using a hydrophilic substrate…100

Figure 3.2. A schematic diagram on SPR gas detection system…….102

Figure 3.3. A schematic view of the structure and the forces in a self-assembled monolayer……105

Figure 3.4. SAMs formed by rod-like helical polymers……..110

Figure 3.5. The PM-IRRAS spectra measured for the monolayers formed from poly-**4**…113

Figure 3.6. Evolution of PM-IRRAS spectra of imine stretching mode with increasing poly-**4** chain length……..115

Figure 3.7. Ellipsometric thickness as the function of the repeat unit in the polyguanidines chains……..116

Figure 3.8. Contact angles as the function of the number of repeat units in the polguanidines chains…….....118

Figure 3.9. The immersion time dependence of SAMs formation.....119

Figure 3.10. The effect of solvent on the formation of thiol-terminated polyguanidines...121

Figure 3.11. PM-IRRAS measurements of the SAMs formed in different solvents (from top to bottom: chloroform, toluene, THF, hexane and benzene……122

Figure 3.12. AFM tapping mode analysis of a SAMs of 50:1 poly(*N,N'*-di-*n*-hexylguanidine) absorbed from benzene to gold substrate……...….124

Figure 3.13. AFM tapping mode analysis of a SAMs of 100:1 poly*(N,N'*-di-*n*-hexylguanidine) absorbed from benzene to gold substrate…….125

Figure 3.14. UV-Vis absorption spectra of gold seeds and gold-polyguanidine nanocomposites……...……129

Figure 3.15. Size distributions of the particles by light scattering: gold seeds and gold-polyguanidines nanocomposites.…….……..…..130

Figure 3.16. TEM images of gold seeds and gold-polyguanidines nanocomposites ..……...131

List of Schemes

Scheme 1.1. Enantiomer-selective reaction by enzyme……..3

Scheme 1.2. The Wurtz-type reduction of poly(di-alkylsilylene)s…….9

Scheme 1.3. Helix-sense-selection anionic polymerization of TrMA……..10

Scheme 1.4. Polymerization of isocyanides……..12

Scheme 2.1.The previous works on the polyguanidine prepared from homo-chiral monomer and its annealing behavior.....…...40

Scheme 2.2. Synthetic route of the chiral monomer of **2** and **3**……44

Scheme 2.3. Polymerization of carbodiimide **2**…….46

Scheme 2.4. Polymerization of carbodiimides **4** and **5**…….51

Scheme 2.5. Preparation of optically active catalysts **III** and **IV**.....77

Scheme 2.6.Polymerization of achiral carbodiimide monomer-**6** with the chiral titanium catalysts…….78

Scheme 3.1. Polymerization of carbodiimide with a Ti catalyst……..111

Scheme 3.2. Synthetic route of initiator **II** and poly-**4**……112

Scheme 3.3. Preparation of gold-polyguanidines nanocomposites…….127

List of Tables

Table 2.1. The specific optical rotations of monomers and polymers……...47

Table 2.2. The specific optical rotations of poly-**3** (virgin) with different molecular weight……70

Chapter I: An Overview of Helical Polymers

1.1. Chirality overview

The three-dimensional world we live in has important consequences at all length scales. The relationship between an actual object and its mirror image is fundamental to understand molecular interactions. As we know, each object has a mirror image, but it is not necessary that the image is identical to the original object. When an object exactly matches its mirror image, it is called superimposable. Superimposable objects can be "placed" on each other so that each feature of one precisely coincides in space with an equivalent feature in the other. If complete registry is not achieved, these are called nonsuperimposable objects. A common example of nonsuperimposable objects are our hands.

Like the macro world, stereochemistry impacts chemical interactions in three dimensions. The mirror image concept we mentioned can be extended from macroscopic objects to molecules. A molecule that has no center of symmetry and a non-superimposable mirror image is called chiral.[1-3] A molecule is chiral if it contains a single tetrahedral carbon atom attached to four different atoms or groups of atoms. Chirality at the molecular level differentiates one molecule from the next, determines the activity of a drug, and allows life to proceed. Due to its important significance in biology and the pharmaceutical industry, chirality plays a paramount role in scientific research.[4]

1.1.1. Enantiomers

Two stereoisomers related as nonsuperimposable mirror images are called enantiomers (Figure 1.1). Enantiomers of a chiral molecule have the same physical properties, such as heat of formations, densities, melting and boiling points. They also have

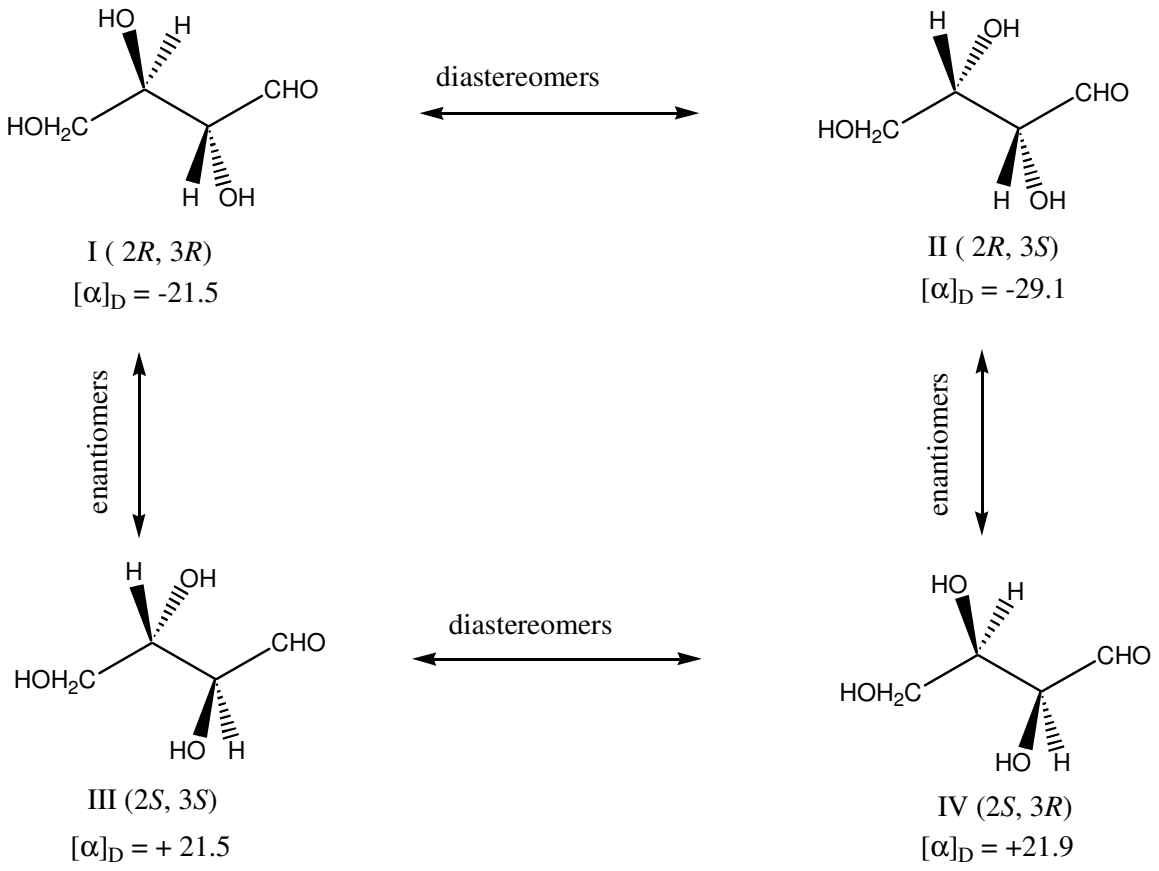

Figure 1.1. Configuration of enantiomers and diastereomers.

the same chemical properties in an achiral environment. However, their chemistry can substantially differ in a chiral environment. This difference is important in many processes in biocatalytic reactions. For example, only one of a pair of enantiomers fits into a specific

site in a biological molecule such as an enzyme catalyst because the site on the enzyme that binds the enantiomer is chiral. An example of such stereoselective process is the enzyme (*Pseudomonas cepacia lipase*) is able to acetylate efficiently the (*R*)-enantiomer of 4-hydroxyl-4-phenyl-butan-2-one with >99% ee (Scheme 1.1).[5]

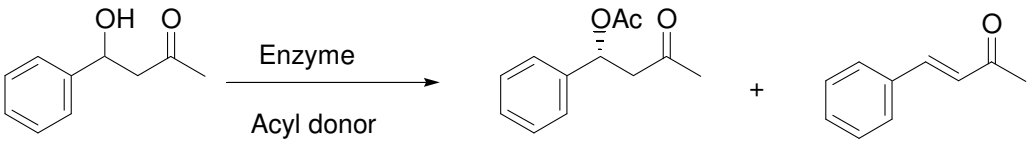

Scheme 1.1. Enantiomer-selective reaction by an enzyme.

Although enantiomers have identical chemical properties in achiral environments, they differ in one physical property: enantiomers behave differently when interacting with plane polarized light. The separated enantiomers have an ability to rotate the plane of polarized monochromatic light in equal but opposite directions.[6,7] This difference is used to distinguish a chiral molecule from its enantiomer in the laboratory.

A material with an excess of one enantiomer rotates plane-polarized light, so it is optically active. Conversely, achiral molecules or racemic mixtures with an enantiomeric excess of zero are optically inactive since they do not rotate plane-polarized light. Optical activity is the ability of a chiral substance to rotate the plane of polarized light and it is measured using an instrument called a polarimeter. The degree of rotation is called optical rotation, α, of enantiomers. The amount of rotation observed in a polarimeter depends on the structure of the substance, the number of molecules encountered by the light and measurement condition, including temperature, wavelength and solvent. To account for the

effects of path length and concentration, chemist have defined the term specific rotation, given the symbol [α], which is calculated from the observed rotation according to equation 1:

$$[\alpha] = \frac{100\,\alpha}{cl} \qquad (1)$$

Where c is the concentration of sample in grams per 100 mL of solution, and l is the length of the polarimeter cell in decimeters.[3,6]

And enantiomeric excess (*ee*), equation 2, is another expression to show how pure a chiral material is.[8] From this equation, it can be seen that a racemic mixture (50% of each enantiomer) would have both a zero optical purity and enantiomeric excess of zero.

$$\%ee = \frac{[R]-[S]}{[R]+[S]} \qquad (2)$$

1.1.2. Diastereomers

Now, let's consider stereoisomers that are not enantiomers. If two or more stereoisomers with atoms connected in the same order are not related as mirror images, they are called diastereomers (Figure 1.1).[3,5] Different from enantiomers, diastereomers may have very different physical properties. And this characteristic of diastereomers could be applied to separate the enantiomers. For example, a racemic mixture can react with another optically pure compound to produce a mixture of diastereomers, which can be separated on the basis of solubility differences. Then each enantiomer is recovered from its diastereomeric derivative by another chemical reaction. The entire process is called resolution of enantiomers. Diastereomers are also thermodynamically inequivalent. At any

given temperature one diastereomer will be lower in energy, and that diastereomeric conformation will be the thermodynamic favored form.

1.1.3. Configurational and conformational asymmetry

There are two kinds of asymmetry that results in the optical activity of molecules, configuration of the substituents around a particular atom, or conformation adopted by molecules. These two phenomena are fundamentally different. Configurational asymmetry implies a particular atom is chemically substituted in an irregular fashion (i.e. chemical bonds must be broken to destroy the chirality). The configuration of molecule is fixed; it can only be changed via chemical means. Conformational asymmetry implies a molecule or material is chiral by virtue of its geometry (i.e., rotations around bonds will eliminate the chirality). The conformation of a molecule is dynamic and may change upon exposure to heat, light, pH, or other means.[9,10]

1.2. Helical structures

The helical structure is one type of conformational asymmetry. Like asymmetric centers in small molecular chirality, the helix itself is a chiral entity due to the different spin directions, left-handed and right-handed.[11] A single handed helix can display very large optical rotations. A helix is defined as the structure generated from the combined rotation and translation of a point around a line, the helix axis, at a constant distance from the axis. In some polyaromatic derivatives, like hexahelicene, the phenomenon of steric crowding is obvious (Figure 1.2).[6,12,13] Steric constraints give rise to a helical form with an energy

barrier to interconversion between the right- and left- handed enantiomers that is high enough to permit their resolution.

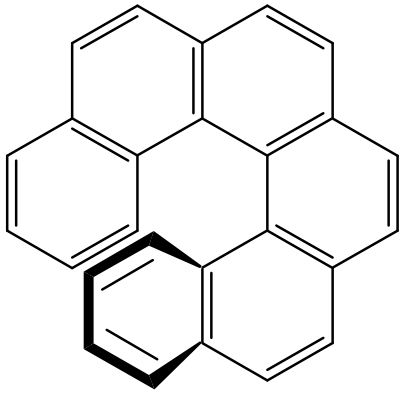

Figure 1.2. The structure of helical hexahelicene.

1.2.1. Helical polymers

Macromolecules exist in a variety of conformational forms. These range from randomly coiled chains to more spatially ordered structures. As a consequence of orderly repeat units, polymers with regular internal rotational angles (dihedral angles) along the backbone can adopt helical structures. Polymers with single-handed screw-senses in solution or in the solid state are of particularly interest. According to the nomenclature of Cahn, Ingold and Prelog,[56] the helix can be characterized by a central axis (*c*-axis), a screw sense and a pitch. For a helical polymer the pitch, *P*, is the distance traveled along the *c*-axis corresponding to one full 360 degree turn, and *h*, is the monomer repeat height projected onto the *c*-axis, where $P = n \times h$. Helix symmetry is designated by *N/m*, where *N* residues reside in *m* turns of the helical screw. Such geometry is encountered among

polymers of both natural and synthetic origin, and some of the most common examples are polypeptides, such as poly(γ-benzyl glutamate), which is well known to adopt a α-helix stabilized by the intra-molecule H-bonding.[14]

1.2.2. Natural helical polymers

In the early 1950s, *α*-helical structure for natural polypeptides (Figure 1.3) was proposed by Pauling[15] and the double-helix for DNA was found by Watson and Crick. [16]

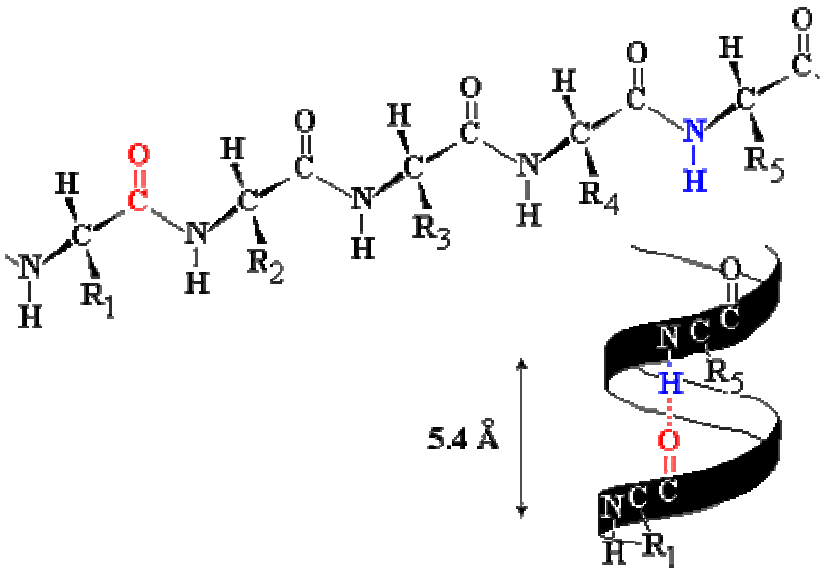

Figure 1.3. The α-helical structure of polypeptide.[118]

These two findings were considered as major milestones in the area of molecular biology. Because of their precisely ordered stereostructures, these biologically derived macromolecules, including polypeptides, proteins and nuclei acids, possess high functionalities. The helix exists as one of the most fundamental structures of these biopolymers and plays a significant role in realizing many biological activities.[17] For

example, in the case of amino acid derived biomolecules, biological systems can occasionally turn to the enantiomeric amino acids to accomplish specific structural objectives.[18] In vivo, though, the biological mechanisms at work block the use of "wrong" enantiomer acids in the formation of proteins, and this necessitates the use of isomerizing enzymes to introduce these mirror isomers.[19]

1.2.3. Synthetic helical polymers

By augmenting biological helical polymers, synthetic helical polymers are expected to broaden the application of these materials into many new areas. The potential applications include molecular recognition (separation,[20-29] catalysis,[30-36] sensory functions), optical data storage,[37, 38] as molecular scaffolds for controlled alignment of functional groups or chromophores, and ordered molecular alignment in the solid phase such as that in liquid crystalline materials.[39] These applications make the helix attractive target for synthetic polymer scientists.

The single-handed helical conformation could be induced to achrial polymers by adding optically active molecules, which are called chaperones, such as chiral amines and alcohols. The macromolecular conformation is determined by small chaperones. These interactions between polymers and chaperones may be very subtle, arising through van der Waals interactions, or they may be strong, relying on hydrogen or ionic bonding.[120,121]

Relatively few synthetic polymers adopt helical secondary structures in solution. The ones that are known are polysilylenes, poly(cis-acetylenes), poly(iso-methacrylates), polyisocyanides, polyisocyanates, and polyguanidines.

<u>Polysilylenes</u>

Most polysilylenes, including poly(dialkylsilylene)s, poly(alkylarylsilylene)s and poly(diarylsilylene)s, are synthesized by the sodium-mediated condensation of the corresponding dichlorodiorganosilanes in an inert solvent using the Wurtz-type reductive coupling reaction (Scheme 1.2).[57,58] Polysilylenes adopts a 7/3 helical structure (7 monomers units per 3 turns) in the crystalline state.[59,60] Optically active polysilylenes

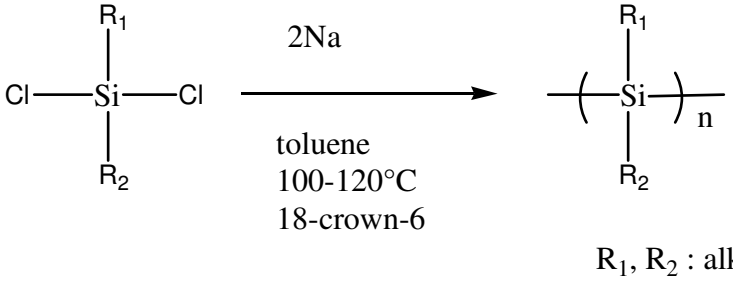

Scheme 1.2. The Wurtz-type reduction of poly(di-alkylsilylene)s.

bearing chiral side chains might be among the most suitable to elucidate the inherent nature of the helical structure because they embody a chromophoric and fluorophoric main chain exhibiting intense UV, CD and FL bands as a result of the Siσ-Siσ* transition (σ-conjugation) around 300-400 nm, the moment of which is parallel to the main chain axis (not to the side groups). Moreover, the desired molecular weights are isolated ranging from 10^3 to 10^7 by fractional precipitation. The spectral characteristics of optically active polysilylene homopolymers and copolymers, including the signal intensity, spectral width, wavelength, and linewidth, vary sensitively with the change in the main chain conformation,

stiffness of the main chain, degree of the polymerization, temperature and solvent polarity.[61-64]

Polymethacrylates

In 1979, Okamoto reported that optically active poly(triphenylmethylmethacrylate), poly(TrMA), was synthesized by asymmetric anionic polymerization (helix-sense-selective polymerization) with a complex of *n*-BuLi and (-)-sparteine (Scheme 1.3). The poly(TrMA)s possess a completely isotactic configuration and large optical rotations ($[\alpha]_D$ up to 400°). In comparison with poly(methylmethacrylate)s (PMMAs) which show very small rotation using same method, the large optical rotation of poly(TrMA)s must be attributed to the helicity of the rigid isotactic TrMA sequence as well as the polarizability of the phenyl groups. The single-handed helical conformation is stabilized by steric repulsion of the bulky side groups that prevent main-chain bond rotations.[65-67]

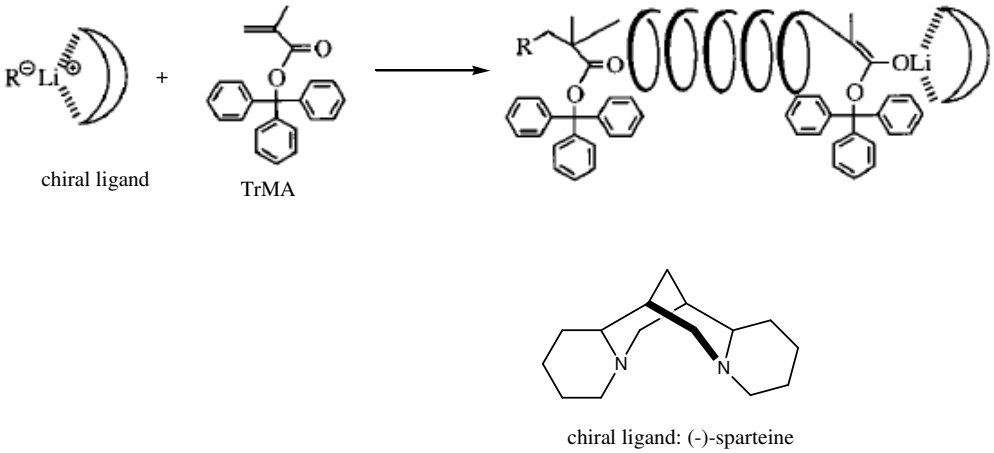

Scheme 1.3. Helix-sense-selection anionic polymerization of TrMA.

Optically active polymers with helical conformations have been obtained from the analogous methacrylates with one of the aromatic rings on the ester group replaced by aliphatic chains, cycloalkane or heteratomic rings. The structure of the ester group has significant effect on the polymerization and the optical activity. Groups that are too bulky cannot form high molecular weight polymer, and if the ester groups are too small and flexible, the stable helix will not form and a syndiotactic polymer is often obtained. 1-Phenyldibenzosuberyl methacrylate (Figure 1.4) was synthesized and polymerized using anionic techniques with optically active initiators. The monomer gave a one-handed helical, highly isotactic polymer. Noteworthy, this monomer also produced a highly isotactic polymer (mm > 98%) by radical polymerization in toluene at 40°C. In comparison, TrMA polymerized by radical polymerization was obtained with an isotacticity degree of 65%. The high stereoregulation in the radical polymerization of this monomer seems to be based on the bulky structure of the ester group.[68]

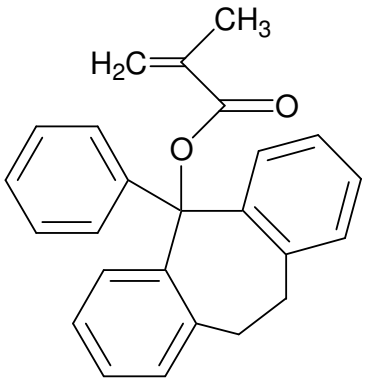

Figure 1.4. The structure of 1-phenyldibenzosuberyl methacrylate.

Optically active poly(TrMA) with a one-handed helix is extremely effective as a chiral stationary phase for optical resolution of various racemic compounds by high-performance liquid chromatography. In order to overcome the problem of the brittleness of poly(TrMA), macroporous silica gel was used as support for soluble poly(TrMA) that is conformationally stable enough to maintain its helical structure in solution at room temperature. These modified gels led to improved column efficiency.[69]

Polyisocyanides

Polyisocyanides have a structure which is highly unusual in polymers, with each carbon atom of the chain having a double bond to a nitrogen atom. This brings about a restricted rotation about the C-C single bonds of the chains and hence results in the formation of stable, rigid helices. The polymerization of isocyanides takes place, for example, in the presence of Ni (II) salts (Scheme 1.4). A helix-sense-selective

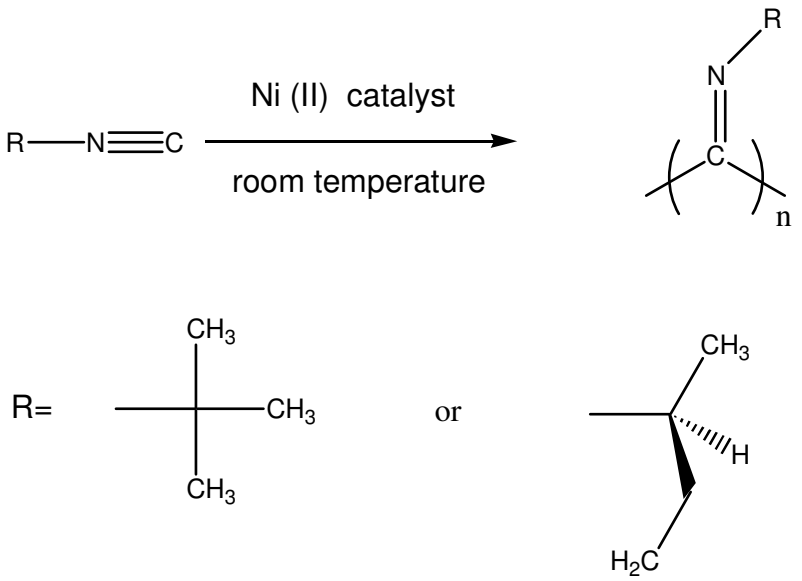

Scheme 1.4. Polymerization of isocyanides.

polymerization has been reported using optically active Ni catalysts to produce optically active polymer.[70-72]

Polyisocyanides have a 4/1 helix (Figure 1.5) and adopt the wormlike conformation in solution with relatively short persistence length, e.g., 30 Å for poly(1-phenylethyl isocyanide).[81] The persistence length is defined as the length over which the polymer chain remains straight without bending. These polymers do not racemize at room temperature due to their high helical inversion barrier, i.e., ≥ 27 kcal/mol for poly(*t*-butylisocyanide.[70] Because of the potential for a rigid helical structure, attempts have been made to use polyisocyanides as mimics of biological molecules such as ion channel and enzymes.[82-84]

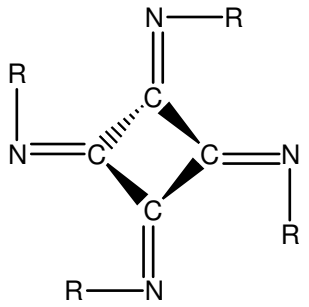

Figure 1.5. The 4/1 helical conformation of a polyisocyanide.

Polyisocyanates

Polyisocyanates have been studied intensively for a long time. The polymer is rod-like due to a combination of steric hindrance and partial conjugation. Comparatively, their persistence lengths are longer, e.g., 600 Å for poly(*n*-butylisocyanate) and the inversion

barrier is lower, e.g., 19 kcal/mol for poly(2-butylhexyl isocyanate). Figure 1.6 shows that stereoselective replacement of deuterium for one of the diastereotopic hydrogens of either the methylene group α and β to the amide function in poly (*n*-hexylisocyanate) leads to an intense circular dichroism spectrum, which is caused by a large excess of one helical sense.[73,74]

Polyguanidines

In order to combine all of the salient features of both of these helical polymers, the high barrier to helix inversion from the polyisocyanides and the long persistence lengths from the polyisocyanates, into a single polymer, which would adopt a static helical conformation in solution, we thought this could be accomplished by replacing the carbonyl group in the polyisocyanate backbone with the more sterically demanding imine group of a polyisocyanide (Figure 1.7).

The polyguanidines are in many respects the most promising candidates for biomimetic applications. Listed here are some of their important characteristics. Polyguanidines

- Are built on guanidine repeat units, a ubiquitous entity in biological systems.
- Adopt regular 6/1 helical conformation in both solution and the solid state.
- Possess dimensions comparable to helical polypeptides.
- Have a wide range of solubilities including water solubility.
- Tolerate both high and low pH extremes.
- Are not susceptible to degradation by digestive enzymes.

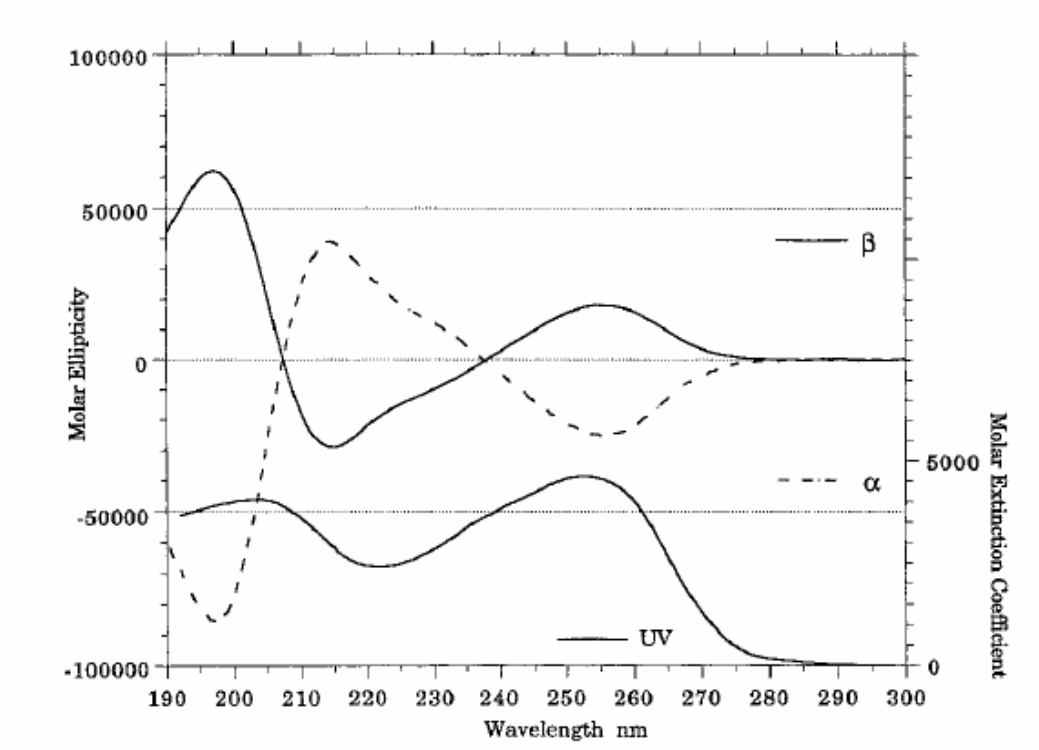

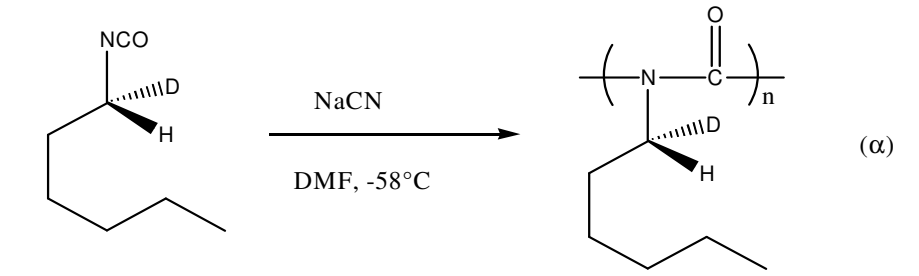

[α]= + 0.65° (neat) [α]= -444° (n-hexane)

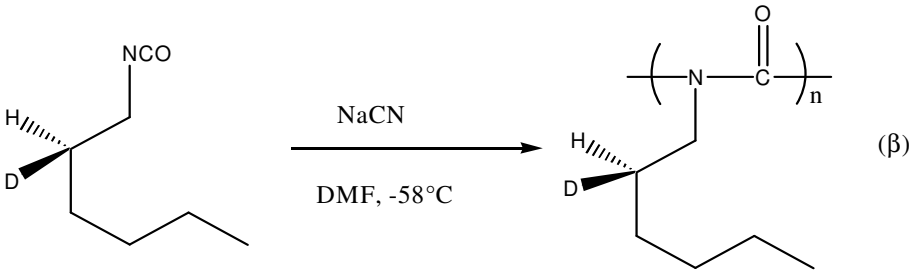

[α]= - 0.44° (neat) [α]= +302° (n-hexane)

Figure 1.6. Circular dichroism and UV spectra of deuterated polyisocyanates.[73]

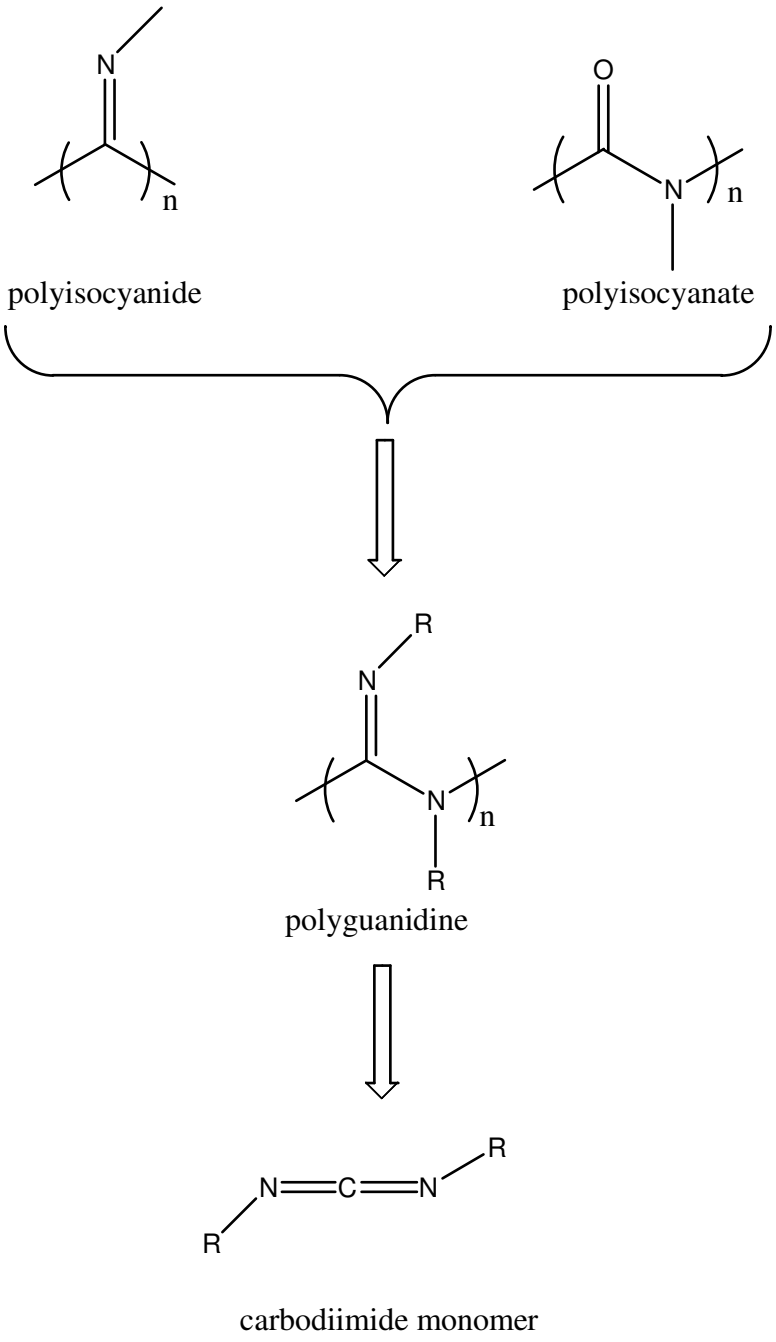

Figure 1.7. The structural relationship between polyisocyanates, polyisocyanides and the hybrid polymer derived from the polymerization of carbodiimides.

- And are more conformationally robust than polypeptides vis-à-vis pH, temperature, and denaturing reagents.

1.3. Synthesis of helical polymers

Most synthetic helical polymers in the crystalline state, such as polypeptides (achiral) and highly tactic poly(α-olefins), are not optically active, because the polymer chains exist as a series of blocks of right and left-handed regions separated by helical reversals (Figure 1.8).[40,41] The left- and right-handed helices are enantiomers and have equivalent free energy, so neither conformation is thermodynamically preferred. Therefore, many researchers are interested in generating helical polymers which consist predominantly of a single handedness.

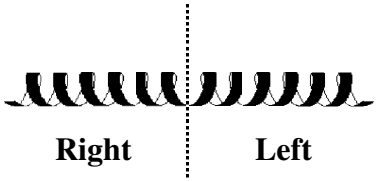

Figure 1.8. Optically inactive helical polymer chain.

1.3.1. Helix-sense-selective polymerization

Designing and synthesizing single handed helix polymers is a challenge to chemists. The observation of optical activity in polymers is usually limited to materials derived from helix-sense-selective polymerization, including the polymerization of optically active monomers,[42-45] or the asymmetric polymerization of racemic or achiral monomers with optically active catalysts.[46-51] In a few cases, optically active polymers can

be prepared through separation of enantiomeric polymers from a racemic mixture.[52-55] If the product of the polymerization has an excess of one screw sense, the polymer will be optically active.

When optically active catalysts are used, a helix-sense-selective polymerization can be classified into two categories according to the structure of monomers: fluxional and nonfluxional chains.[86] Fluxional chains have low helix inversion barriers that allow frequent occurrences of helix reversals. Conformations separating left- and right-handed helical segments are referred to as helical reversals. Examples of fluxional chain polymers include polysilylenes, polyisocyanates, and poly(*cis*-acetylenes). The removal and introduction of helix reversals can be a dynamic process, and reversible equilibrium between the two helical states (*P*- and *M*-handed) can be sometimes observed. Also, these helical conformations of polymers are under thermodynamic control at normal temperatures, and as a result, these helical polymers undergo rapid racemization (helical inversion). Nonfluxional helices, the rarer of the two categories, have higher inversion barriers typically introduced by incorporating bulky side chains that hinder main chain bond rotations. Examples include isotactic poly(trityl methylacrylate), polychloral, and polyisocyanides. The helical conformation is formed under kinetic rather than thermodynamic control. Once formed, these conformations are locked in by the high helix inversion barriers of these polymers. Because of these barriers, there are examples where materials can be isolated in kinetically controlled conformations, KCCs, which do not correspond to the thermodynamically controlled conformation (TCC) minimum.

1.3.2. Amplification of chirality

In helix-sense-selective polymerization, optically inactive initiators can be used to catalyze the polymerization of chiral monomers. Goodman and Chen[87] were the first to take advantage of the pendant chiral group to control the helix conformation. They synthesized polyisocyanates from two optically active monomers and found exceptionally high optical activities, associated with the recurring amide group chromophore, centered in the ultraviolet region. This observation reasonably implied that the left- and right-handed helices, now cast into diastereomeric states, were no longer equally populated. According to this idea, Mark Green and co-workers[73,74,77] synthesized another member of polyisocyanate family, poly[(*R*)-1-deutero-*n*-hexylisocyanate], from the chiral monomer (Figure 1.6). Although the chiral perturbation favoring one helical sense in the polymer is driven only by the difference between hydrogen and deuterium, the strong temperature-dependent optical activity and circular dichroism suggest a large preference for one helical sense. The chiral monomer has specific optical rotation of only -0.04° (neat), but conformationally chiral helical polymer has a much larger specific optical rotation of +302° (hexane). The polymer, based on this idea, serves as an amplifier of the monomeric chirality.

1.3.3. Cooperativity

The fact that a very small energy difference per deuterium between diasteromers produces a significant helical excess was attributed to the cooperativity effect. Cooperativity refers to interaction between monomer units that allow single chiral perturbation in the polymer to influence the regional conformation of the polymer. This means that when one repeat unit is perturbed by incorporating additional stereo-centers into

the side chain, the information carried by the asymmetric carbon could be extended along the polymer chain (Figure 1.9). The cooperativity depends on the effectiveness of the interaction of the repeat units along the polymer chain. The interaction on long length scales corresponds to the high degrees of cooperativity. Highly cooperative systems undergo large changes with relatively simple/subtle structural changes in the monomers.

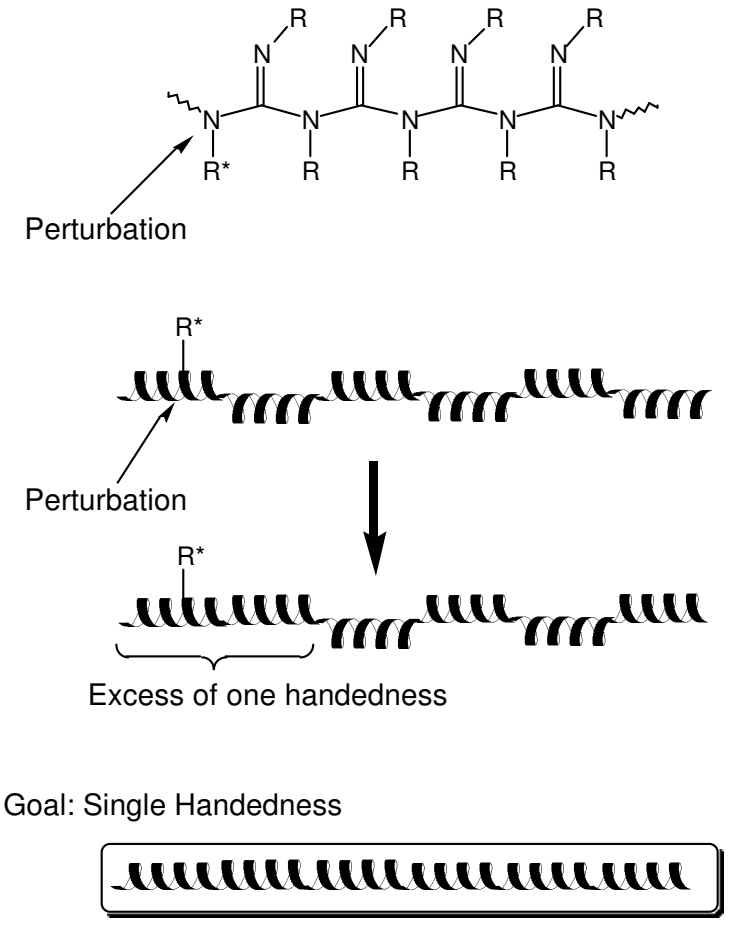

Figure 1.9. Cooperativity within a helical polymer chain.

The effectiveness of cooperativity is influenced by the stiffness of the polymer backbone and the sterics of the pendant groups. When the side chain is too small or the backbone is flexible, the bond rotation along the backbone occurs freely and results in a large number of helical reversals. Such results are observed for poly(α-olefins).

Several strategies have been designed to exploit cooperativity and these are illustrated in Figure 1.10. Each of these methods can be used for the preparation of single-handed helical polymers. These experiments could be conveniently expressed on a pyramid according to the different length scales. From the bottom of pyramid to the top, as the number of chiral centers decrease, the interactions are probed from the local scale (nearest neighbor) to the long range (many repeat units).

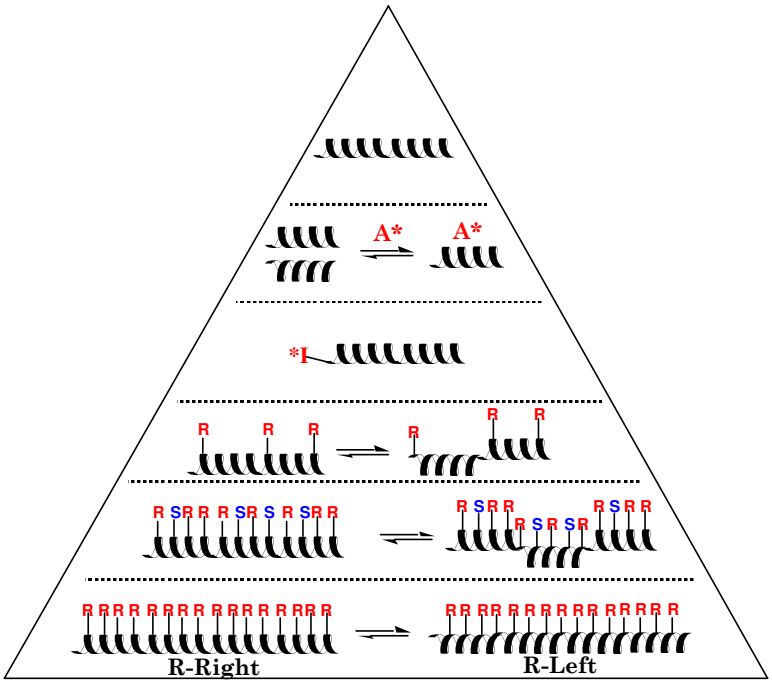

Figure 1.10. The pyramid of cooperativity.

1.4. Polyguandines

In our previous discussion, we have indicated the polyguanidines possess many attractive properties resulting from their particular structure and these have broad appeal in several applications. In the past several years, our group has investigated the synthesis and polymerization of the carbodiimide monomers, their characterization, and the relationship between the structure and properties of the polymers.

1.4.1. Carbodiimide monomer

From a structure standpoint, carbodiimides are similar to allenes. However, unlike symmetrically substituted allenes, the *N*,*N'*-di-substituted carbodiimides are not linear based on X-ray diffraction studies. The NCN bond angles vary from about 166 to 170°. The dihedral angle of the cumulenic π bond system is nearly 90° and therefore they can exist in optically active forms (Figure 1.11).[85] Application of molecular orbital theory to

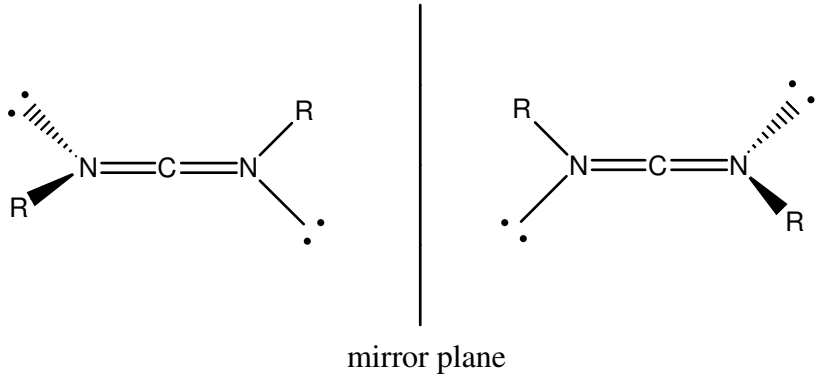

Figure 1.11. The enantiomeric conformers of carbodiimides.

carbodiimides indicates that the inversion barrier for these two enantiomers is 8.4 kcal/mol, which is in agreement with the value of 6-9 kcal/mol obtained by NMR. Due to the low barrier of isomerization, only carbodiimides with either bulky groups or in ring structures have been partially resolved.[88, 89]

Among the several synthetic routes to carbodiimides, three in particular are typically employed. These include the dehydration of ureas and thioureas with reagents such as metal oxides,[90, 91] sodium hypochloride,[92] phosgene,[93] or phosphorus halides,[94] catalytic decarboxylation of isocyanates with phosphorus oxides,[95] or utilization of the Tiemann Rearrangement.[96] In our work, the dehydration procedure using triphenyl phosphine, bromine, and triethyl amine was commonly used.

1.4.2. Living polymerization of carbodiimides

Living polymerizations are polymerizations that proceed without significant chain transfer or terminating steps.

The polymerization of carbodiimide monomers was first reported by Robinson and co-workers in 1964.[97] Although numerous initiating agents, including Na/DMF, CH_3I, $AlBr_3$, $Zn(Et)_2$, allyl lithium, $Hg(Et)_2$, and different reaction conditions were explored, the polymers produced were found to be of similar molecular weight and independent of the monomer to initiators ratio, and molecular weights were too low to make polymer characterization efforts possible.

Our group had a long-standing interest in designing polymerization catalysts that would allow control over the molecular weight. This is typically performed by stabilizing the propagating ionic chain end using transition metal complexes. This approach often

manifests itself as an attenuation in the rate of polymerization. The ability to control the target molecular weight can then be achieved by changing the monomer to catalyst ratio.

On the basis of our work on the living polymerization of the polyisocyanides [98-103] and polyisocyanates,[104-107] Goodwin used titanium(IV) based catalysts to achieve the living polymerization of many different carbodiimide monomers.[108] Subsequent work by Shibayama showed that Cu(I/II) based catalysts also initiated living polymerization of carbodiimide monomers (Figure 1.12).[109] These new living systems enable the synthesis of polyguanidines having uniform chain-end groups, precisely controlled molecular weights, and narrow molecular weight distributions.

The metal complex acts to stabilize the propagating anionic chain end resulting in a reduction in the rate of polymerization but better control. According to the proposed mechanism of the polymerization (Figure 1.13), the polymerization is initiated by insertion of the monomer into a titanium-nitrogen or oxygen bond to form an intermediate amidinate complex. Propagation proceeds through monomer coordination to titanium and insertions into titanium-amidinate bond. All the steps are fully reversible. The ceiling temperature of polymerization of carbodiimides depends on the side chains (i.e., 80°C for *N,N'*-di-*n*-hexylcarbodiimide, and 156°C for *N*-(*R/S*)–(±)-(1-phenylethyl)-*N'*-methylguanidine). Since polymerization proceeds through consecutive equilibrium reactions, polymerization in minimum amount of solvent or in bulk is favored to achieve high yield.

1.4.3. Liquid crystalline properties of polyguanidines

The polyguanidines display rigid rod properties due to the restricted bond rotations along their backbones. In keeping with their intramolecular characteristics, including high

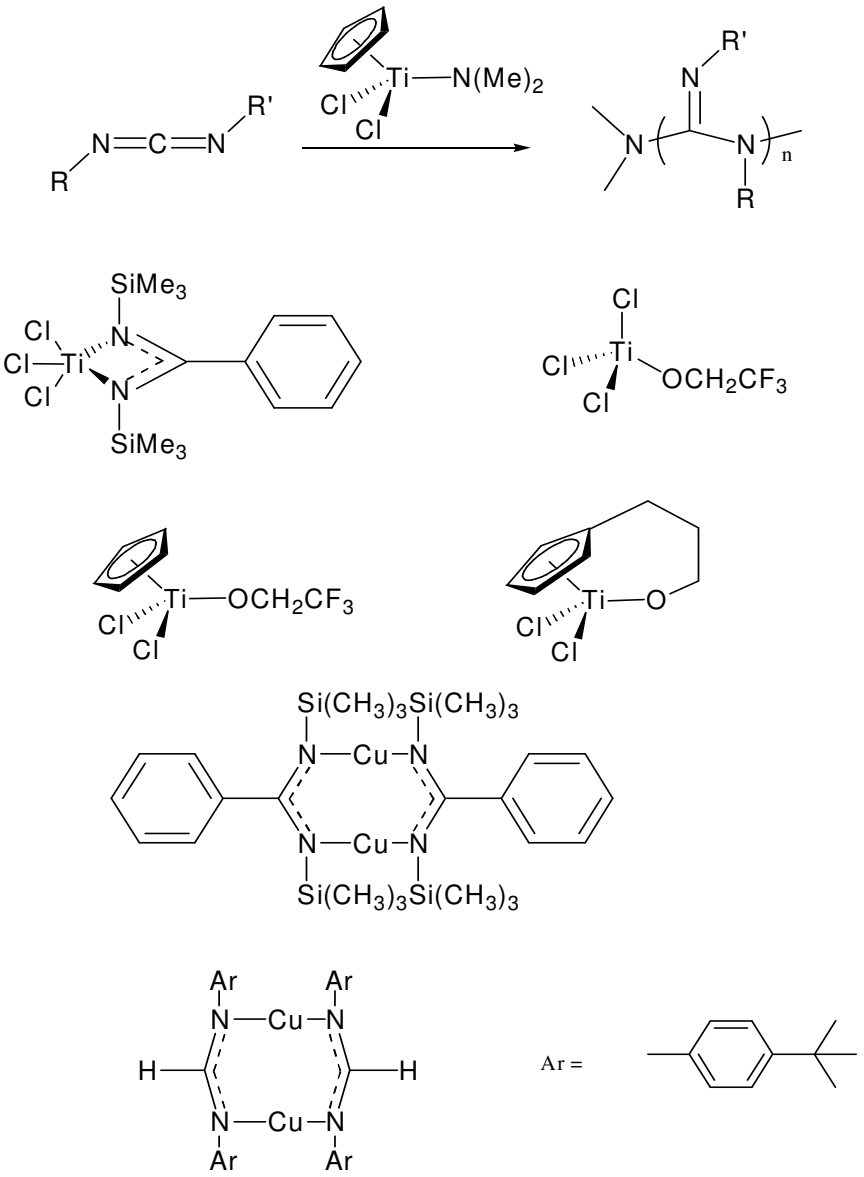

Figure 1.12. Effective catalysts for the polymerization of carbodiimides.

Initiation step:

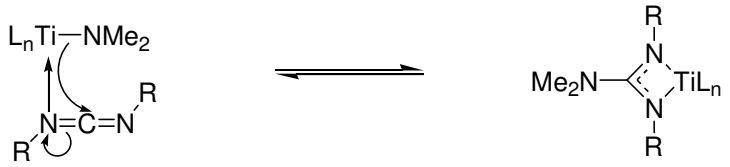

Propagation step:

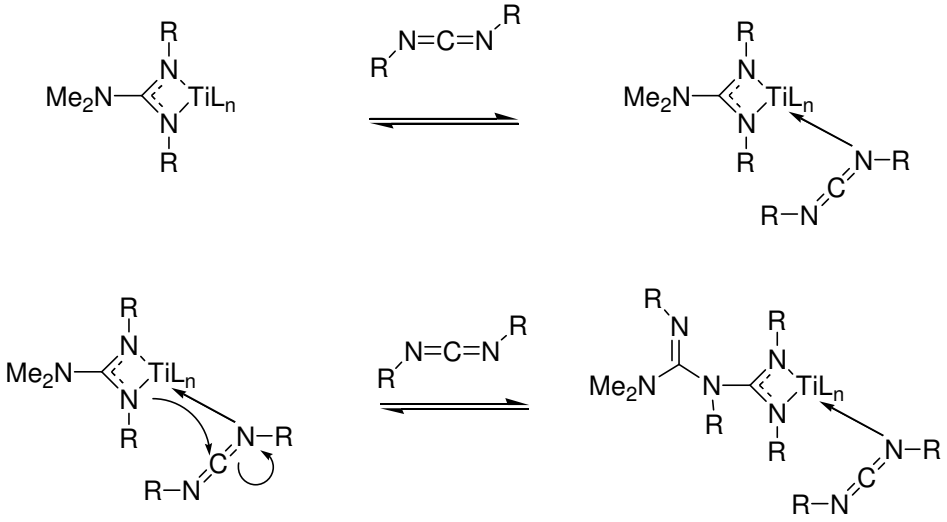

Figure 1.13. The mechanism of polymerization of carbodiimide monomer using a Ti(IV) catalyst.

inversion barriers and long persistence lengths, these polymers were found to display a range of liquid crystalline phases. When the two side chains of polyguanidines are identical, like poly(*N,N'*-di-*n*-hexylguanidine) and poly(*N,N'*-di-*n*-dodecylguanidine) (Figure 1.14), these polymers display a lyotropic layered structure. The higher level of ordering is believed to arise from the formation of a dense corona barrier that effectively acts to uniformly separate the helical backbones. When the side chains differ in length, e.g., poly [*N*-methyl-*N'*-(±)-(*α*)-methylbenzylguanidine] and poly{*N*-6-[4-(4-methoxyphenylazo)phenyloxy]hexyl-*N'*-*n*-hexylguanidine}, the uniform layering breaks down and a simplier nematic structure arises. Chirality also plays a very important role. Fixed, homochiral side chains, e.g., poly[*N*-methyl-*N'*-(*R*)-(+)-(*α*)-methylbenzylguanidine], force all of the chains to adopt a preferred helical sense, and these screws now pack in a cholesteric mesophase. Furthermore, the dilute solution studies along with these liquid crystalline studies demonstrate that the polymers with chiral side chains are stiffer than their racemic counterparts.[110-112]

1.4.4. The cooperativity of polyguanidines

Like the previously discussed polymers, polyguanidines can be induced to form biased helical senses through chiral groups in their side chains.[113,114] Chiral catalysts have also been successfully used to induce a biased helical sense in the polyguanidines.[86,115] Unlike the polyisocyanates which racemize quickly, the stability of the polyguanidine helix formed is highly dependent upon the side chains of the polymer. In many cases a slow racemization is observed; however, bulky side chains can lead to a stable biased helical conformation even when those side chains are achiral.[86]

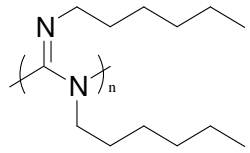

poly(*N,N'*-di-*n*-hexylguanidine)

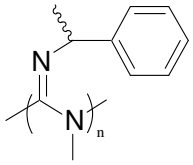

poly [*N*-methyl-*N'*-(±)-(*α*)-methylbenzylguanidine]

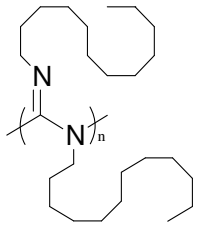

poly(*N,N'*-di-*n*-dodecylguanidine)

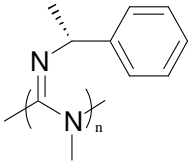

poly[*N*-methyl-*N'*-(*R*)-(+)-(α)-methylbenzylguanidine]

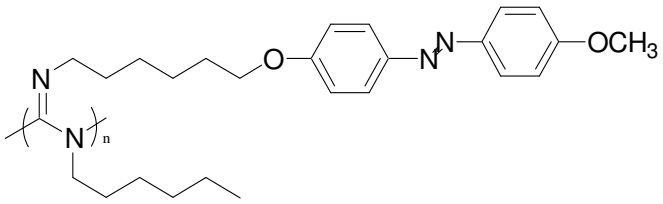

poly {*N*-6-[4-(4-methoxyphenylazo)phenyloxy]hexyl-*N'*-*n*-hexylguanidine}

Figure 1.14. Structures of some of the liquid crystalline polyguanidines.

The cooperativity of polyguanidines has been shown through both majority rules experiments and molecular chaperoning.[113,116] In the molecular chaperone experiment, when a chiral acid was added to a solution of a racemic polyguanidine, a biased helix was induced. The extent of bias in that helix was dependent upon the ratio of chiral acid to monomer repeat unit. This relationship was non-linear suggesting cooperativity among the monomer units in the polymer backbone. This experiment showed that the helical conformation of a polyguanidine can be manipulated by an external influence. This molecular chaperone effect piqued our interest and led to the current goals in our ongoing studies of polyguanidines.

1.4.5. Characterization of polyguanidines

Since the polymerizations of the carbodiimide monomers are carried out through a living route, the molecular weight can be controlled stoichiometically by the ratio of monomer to initiator. Characterization of polymer includes IR, ^{1}H NMR, solid state ^{13}C NMR, and elemental analysis. Especially useful are the IR bands at 1640 (stretching of -C=N-), 1360, and 1250cm^{-1}, which are consistent with a guanidine structure.

Tandem GPC/LS has been used to determine molecular weights of the polyguanidines. Unfortunately, the molecular weight analysis of these polymers could not be successfully performed using a GPC equipped with a light scattering detector, since they elute over unusually large elution volume. This large elution volume is indicative of an interaction between the polymer and the column packing. Many of the polyguanidines are isorefractive with toluene and the change in refractive index, ($\partial n/\partial c$), is very small in THF. To overcome this interaction, displacing solvents blended with THF were evaluated. A

sharp unimodal over a short elution volume were obtained in the mixture of acetonnitrile-THF (20:80).[117]

1.5. Reference and notes

1. Eliel, E. L.; Wilen, S H.; Doyle, M. P. *Basic Organic Stereochemistry*. New York. New York,
2. Solomons, T. W. G. *Fundamentals of Organic Chemistry*, *Fifth Edition;* John Wiley & Sons, New York, 1992
3. Carey, F. A. *Organic Chemistry*, *Fourth Edition;* McGraw-Hill Higher Education, 2000
4. Challener, C. A. *Chiral Drugs*; Ashgate, Burlington, 2001.
5. Edin, M.; Backvall, J-E.; Cordova, A. *Tetrahedron Letters* **2004**, *45*, 7697.
6. Schirier, P.; Bernreuther, A.; Huffer, M. *Analysis of Chiral Organic Molecules: methodology and applications,* Walter de Gruyter, New York, 1995
7. Carey, F. A.; Sunberg, J. Advanced Organic Chemistry, Fourth Edition, Kluwer Academic Plenum Publisher, New York, 2001
8. March, J. Advanced Organic Chemistry; Wiley-Interscience: new York, 1992
9. Cornelissen, J. J. L. M.; Rowan, A. E.; Nolte, R. J. M.; Sommerdijk, N. A. J. M. *Chem. Rev.* 2001, 101, 4039-4070.
10. Morino, K.; Maeda, K.; Yashima, E. *Macromolecules*, 2003, 36, 1480-1486.
11. Meurer, K. P.; Vogtle, F. *In Topics in Curent Chemistry*; Boschke, F.L., Ed. Springer-Verlag: New York, 1985.
12. Volhardt, K. P. C. Organic Chemistry; Freeman: New York, 1987.
13. Newman, M. S.; Lednicer, D. *J. Am. Chem. Soc.* **1956**, 78, 4765-4770.
14. Stevens, M. P. Polymer Chemistry; Oxford Unviersity: New York, 1990
15. Pauling, L.; Corey, R. B.; Branson, H. R. *Proc. Natl. Acad. Sci. U.S.A*. 1951, 378, 205
16. Watson, J. D.; Crick, F. H. C. *Nature*, **1953,** *171*, 737.
17. Cantor, C. R.; Schimmel, P. R. *Biophysical Chemistry, Part I: The Comformation of Biological Macromolecule*; W. H. Freeman and Co.: New York, 1980.
18. Kreil, G. *Annu. Rev. Biochem*. **1997**, *66*, 337.
19. Lorenzi, G. P.; Jackle, H.; Tomasic, L.; Rizzo, V.; Pedone, C. *J. Am. Chem. Soc*, **1982**, *104*, 1728
20. Dappen, R.; Arm, H.; Meyer, V. R. *J. Chromatogr*, **1986**, *373*, 1
21. Nakano, T.; Okamoto, Y.; Hatada, K. *J. Am. Chem. Soc*. **1992**, *114*, 1318
22. Okamoto, Y.; Honda, S.; Okamoto, I.; Yuki, H. *J. Am. Chem. Soc*. **1981**, *103*, 6791.

23. Okamoto, Y.; Honda, S.; Hatada, K.; Okamoto, I.; Toga, Y.; Kobayashi, S. *Bull. Chem. Soc. Jpn*. **1984**, *57*, 1681

24. Okamoto, Y.; Yashima, E.; Hatada, K.; Mislow, K. *J. Org. Chem*. **1984**, *49*, 557.

25. Okamoto, Y.; Honda, S.; Hatada, K.; Yuki, H. *Bull. Chem, Soc. Jpn*. **1985**, *58*, 3053.

26. Okamoto, Y.; Kawashima, M.; Hatada, K. *J. Chromatogr*, **1986**, *373*, 173.

27. Okamoto, Y.; Yashima, E.; Ishikura, M. Hatada, K. *Bull. Chem, Soc. Jpn*. **1988**, *61*, 255.

28. Parker, C. E.; Levy, L. A.; Smith, R. W.;Yamaguchi, K.; Gaskell, S. J. *J. Chromatogr*, **1985**, *344*, 378.

29. Yuki, H.; Okamoto, Y.; Okamoto, I. *J. Am. Chem. Soc*. **1980**, *102*, 6356

30. Evbrahim, S.; Wills, M. *Tetrahedron: Asymmetry*. **1997**, *8*, 3163

31. Sugimoto, T.; Matsumura, Y.; Tanimoto, S.; Okano, M. *J. Chem. Soc., Chem. Commun.* **1978**, 926

32. Baba, N.; Matsumura, Y.; Sugimoto, T. *Tetrahedron Lett*. **1978**, 4281

33. Gamez, P.; Dunjic, B.; Fache, F.; Lemaire, M. *J. Chem. Soc., Chem. Commun.* **1994,** 1417

34. Ma, L.; Hu, Q.-S.; Musick, K.; Vitharana, D.; Wu, C.; Kwan, C. M. S.; Pu, L. Macromolecules, 1996, 29, 5083

35. Ma, L.; Hu, Q.-S.; Vitharana, D.; Wu, C.; Kwan, C. M. S.; Pu, L. Macromolecules, 1997, 30, 204

36. Pu, L. *Tetrahedron: Asymmetry*. **1998**, *9*, 1457

37. Buckley, G. S.; Roland, C. M. *Polym. Eng. Sci*. **1997**, *37*, 138

38. Pham, V. P.; Manivannan, G.; Lessard, R. A.; Bornengo, G.; Po, R. *Applied Physics Science & Processing*, **1995**, *A60(3)*, 239.

39. Ciferri, A.; Ed. Liquid Crystallinity in Polymers; VCH Publisher: New York, 1991

40. Muller, M.; Zentel, R. *Macromolecules* **1996**, *29*, 1609.

41. Lifson, S.; Andreola, C.; Peterson, N. C.; Green, M. M. *J. Am. Chem Soc*. **1989**, *111*, 8850

42. Beredjick, N. and Schuerch, C. *J. Chem. Soc*. **1956**, *78*, 2646.

43. Pino, P., Ciardelli, F. and Zandomeneghi, M. *Ann. Rev. Phys. Chem*. **1970**, *21*, 561.

44. Zambelli, A., Grassi, A., Galimberti, M. and Perego, M. *Makromol. Chem. Rapid Commun.* **1992**, *13*, 407.

45. Lorenzi, G. P., Benedetti, E. and Chiellini, E. *Chim. Ind. Milan*. **1964**, *46*, 1474.

46. Coates, G. W. and Waymout, R. M. *J. Am. Chem. Soc*. **1991**, *113*, 6270.

47. Coates, G. W. and Waymout, R. M. *J. Am. Chem. Soc*. **1993**. *115*. 91.

48. Kurokawa, M. and Minoura, Y. *Makromol. Chem*. **1980**, *181*, 707.

49. De, B. B., Sivaram, S. and Dhal, P. K. *Polymer*, **1992**, *33*, 1756.

50. Batistini, A., Consiglio, G. and Suter, U. W. *Angew. Chem. Int. Ed. Engl*. **1992**, *31*, 303.

51. Sen, A. *Acc. Chem. Res*. **1993**, *26*, 306.

52. Pino, P., Ciardelli, F., Lorentzi, G. P. and Natta, G. *J. Am. Che,. Soc.* **1962**, *84*, 1487.

53. Pino, P., Montagnoli, G., Ciardelli, F. and Benedetti, E. *Makmol. Chem.* **1966**, *93*, 158.

54. Montagnoli, G., Pini, D., Lucherini, A., Ciardelli, F. and Pino, P. *Macromolecules*, **1969**, *2*, 684.

55. Furukawa, J., Akutu, S. and Saegusa, T. *Makomol. Chem*, **1966**, *94*, 68.

56. Cahn, R. S.; Ingold, C.; Prelog, V. *Angew. Chem., Int. Edn. Engl*. **1966**, *5*, 385

57. West, R. *J. Organomet. Chem*, **1986**, *300*, 327

58. Miller, R. D.; Michl, J. *Chem. Rev*. **1989**, *89*, 1359.

59. Sen, A. *Acc. Chem. Res*. **1993**, *26*, 306

60. Pino, P.; Ciardelli, F.; Lorentzi, G. P.; Natta, G. *J. Am. Chem. Soc*. **1962**, *84*, 1487.

61. Fujiki, M. *J. Am. Chem. Soc.* **1994**, *116*, 6017.

62. Fujiki, M. *J. Am. Chem. Soc*. **1994**, *116*, 11976.

63. Fujiki, M. *Appl. Phy. Lett*. **1994**, *65*, 3251.

64. Fujiki, M. *Macromol. Rapid Commun*. **2001**, *22*, 539

65. Okamoto, Y.; Suzuki, K.; Ohta, K.; Hatada, K.; Yuki, H. *J. Am. Chem. Soc*. **1979**, *101*, 4763.

66. Nakano, T.; Okamoto, Y.; Hatada, K. *J. Am. Chem. Soc*. **1992**, *114*, 1318.

67. Okamoto, Y.; SHohi, H.; Yuki, H.; J. *Polym. Sci., Polym. Lett. Ed*. **1983**, *21*, 601.

68. Nakano, T.; Mori, M.; Okamoto, Y. *Macromolecules*, **1993**, *26*, 867.

69. Yuki, H.; Okamoto, Y.; Okamoto, I. *J. Am. Chem. Soc*. **1980**, *101*, 6356.

70. Deming, P. J.; Novak, B. M. *J. Am. Chem. Soc*. **1992**, *114*, 7926.

71. Nolte, R. J. M.; Beijnen, A. J. M.; Drench, W. *J. Am. Chem. Soc*. **1974**, *96*, 5932.

72. Drench, W.; Nolte, R. J. M. *Acc. Chem. Res*. **1979**, *12*, 30.

73. Green, M. M.; Andreola, C.; Munoz, B.; Reidy, M. P.; Zero, K. *J. Am. Chem, Soc*. **1988**, *110*, 4063.

74. Green, M. M.; Reidy, M. P.; Johnson, R. D.; Darling, G.; O'Leary, D. J.; Willson, G. *J. Am, Chem. Soc.* **1989**, *111*, 6452.

75. Troxell, T. C.; Scheraga, H. A. *Macromelcules*, **1971**, *1*, 528.

76. Itou, T.; Chikiri, H.; Teramoto, A.; Aharoni, S. M. *Polym. J*. **1988**, *20*, 143.

77. Lifson, S.; Andreola, C.; Peterson, N. C.; Green, M. M. *J. Am. Chem. Soc*. **1989**, *111*, 8850.

78. Maxein, G.; Keller, H.; Novak, B. M.; Zentel, R. *Adv. Mater*, **1988**, *3*, 341.

79. Green, M. M.; Zanella, S.; Gu, H.; Sato, T.; Gottarelli, G.; Jha, S. K.; Spada, J. P.; Schoevaars, A. M.; Feringa, B.; Teramoto, A. *J. Am. Chem. Soc*. **1998**, *120*. 9810.

80. Tang, K.; Green, M. M.; Cheon, K. S.; Selinger, J.V.; Garetz, B. A. *J. Am. Chem. Soc*. **2003**, *125*, 7313.

81. Green, M; Gross, R.; Schilling, F.; Zero, K.; Crosby, C. *Macromolecules*, **1988**, *21*, 1839.

82. Roks, M.; Nolte, R. *Macromolecules*, **1992**, *25*, 5398.

83. van Esch, J.; Roks, M.; Nolte, R. *J. Am. Chem.Soc*. **1986**, *108*, 6093.

84. Visser, H.; Nolte, R.; Drenth, W. *Macromolecules*, **1985**, *18*, 1818.

85. Goodwin, A. Ph.D. Thesis, University of California at Berkeley, 1996.

86. Tang, H. Z.; Lu, Y. J.; Tian, G, L.; Capracotta, M. D. ; Novak, B. M. *J. Am. Chem. Soc*. **2004**, *126*, 3722.

87. Goodman, M.; Chen, S. *Macromolecules*, **1970**, *3*, 398.

88. Anet, F.; Jochims, J.; Bradley, C. *J. Am. Chem. Soc*. **1970**, *92*, 2557.

89. Schlogl, K.; Mechtler, H. *Angew. Chem., Int. Ed. Eng*. **1966**, *5*, 596.

90. Hiatt, R., Shaio, M. and Georges, F. *J. Org. Chem*. **1979**, *44*, 3265.

91. Tomsdchewski, G., Breifeld, B. and Zanke, D. *Tetrahedron Lett*. **1969**, 3191.

92. Iwakura, I., Tsuzuki, R. and Noguchi, K. *Makromol. Chem*. **1966**, *98*, 21.

93. Gupta, R. and Stammer, C. *J. Org. Chem*. **1969**, *33*, 4368.

94. (a) Moeita, T., Okamoto, Y. and Sakurai, H. *Chem. Lett*. **1980**,435. (b) Palomo, C. and Mestres, R. *Synthesis,* **1981**, 373.

95. Monagle, J., Cambell, T. and McShane, H. *J. Am. Chem. Soc*. **1962**, *84*, 4288.

96. Richer, R.; Tucker, B.; Ulrich, H. *J. Org. Chem*. **1983**, *48*, 1694.

97. (a) Robinson, G. *J. Polym. Sci. A* **1964**, *2*, 3901. (b) Robinson, G. U. S. Patent 3,200,087 (1965).

98. Deming, T. J.; Novak, B. M. *J. Am. Chem. Soc*. **1992**, *114*, 4400.

99. Deming, T. J.; Novak, B. M.; Ziller, J. W. *J. Am. Chem. Soc*. **1994**, *116*, 2366.
100. Deming, T. J.; Novak, B. M. *J. Am. Chem. Soc*. **1993,** *115*, 9101.
101. Deming, T. J.; Novak, B. M. *Macromolecules*, **1993**, *26*, 7092.
102. Deming, T. J.; Novak, B. M. *Macromolecules*, **1993**, *26*, 7089.
103. Deming, T, J.; Novak, B. M. *J. Am. Chem. Soc*. **1993**, *114*, 7426.
104. Patten, T. E.; Novak, B. M. *Macromolecules*, **1996**, *29*, 5882.
105. Hoff, S. M.; Novak, B. M. *Macromolecules*, **1993**, *26*, 4067.
106. Patten, T. E.; Novak, B. M. *J. Am. Chem. Soc*. **1996**, *118*, 1906.
107. Patten, T. E.; Novak, B. M. *Macromolecules*, **1993**, *26*, 436.
108. Goodwin, A.; Novak, B. M. *Macromolecules*, **1993**, *26*, 436.
109. Shibayama, K.; Seidel, S. W.; Novak, B. M. *Macromolecules*, **1997**, *30*, 3159.
110. Kim, J.; Novak, B. M.; Waddon, A. J. *Macromolecules*, **2004**, *37*, 1660.
111. Kim, J.; Novak, B. M.; Waddon, A. J. *Macromolecules*, **2004**, *37*, 8286.
112. Kim, J. Ph.D. thesis. North Carolina State University, 2003
113. Schlitzer, D. S.; Novak, B. M. J. Am. Chem. Soc. 1998, 120, 2196.
114. Nieh, M. P.; Goodwin, A. A.; Stewart, J. R.; Novak, B. M.; Hoagland, D. A. *Macromolecules*, **1998**, *31*, 3151.
115. Tian, G. L.; Lu, Y. J.; Novak, B. M. *J. Am. Chem. Soc*. **2004**, *126*, 4082.
116. Schlitzer, D. S. Ph.D. thesis. Univerisity of Massachusetts, 1998.
117. Larson, R. J. Ph.D. thesis. Univerisity of Massachusetts, 2000.
118. http://www.chembio.uoguelph.ca/educmat/phy456/456lec01.htm
119. Edin, M.; Backvall, J-E.; Cordova, A. *Tetrahedron Letters* **2004**, *45*, 7697.
120. Maeda, K.; Morino, K.; Okamato, Y.; Sato, T.; Yashima, E. *J. Am. Chem. Soc.* **2004**, *126*, 4329.
121. Tabei, J.; Nomura, R.; Sanda, F.; Masuda, T. *Macromolecules* **2003**, *36*, 8603.

Chapter II: Influencing Macromolecular Chirality in Subtle Ways

2.1. Introduction

2.1.1. Helical reversals and inversion barriers

There are two directions screw senses for a helix, left- and right-handed. These conformations are enantiomers, have equivalent free energies and neither conformation is thermodynamic preferred. When helical polymers, like polyisocyanates and polyguanidines, are formed from achiral monomers, the left- and right-handed helical senses are mirror images related, and therefore, of equal energy and probability. If one looks at a single chain, it can exist as a series of blocks of right and left-handed regions separated by kinked and mobile helical reversals. The helix reversal is defined as a defect region spanning several repeat units in which the dihedral angle defining the helical sense changes sign. Helix reversals can introduce bends within otherwise straight chains. Higher population of helical reversals would result in a change of the conformation and a shorter persistence length, i.e., worm-like polymers. In the poly(*n*-hexylisocyanate), the low population of these reversals leads to such an extreme sensitivity of these polymers to chiral information that even minute chiral forces give rise to a large excess of one helical sense and therefore to large optical activity.[1] The energy of a helical reversal is a high energy state in the helical polyisocyanates chains, which was calculated by statistical methods to be 19 kcal/mol in hydrocarbon solvents. This data could be translated to about one reversal every 800 chain units at nearly ambient temperature.[2-6]

Inversion barrier is an important parameter in characterizing the helical structure. It is defined as the activation energy required to switch one-handed helix to the other helix

sense (Figure 2.1). The barrier depends on several factors, including the size and steric nature of the side chain and the inherent stiffness of the polymer backbone. The polymer with a high inversion barrier will racemize slowly, while a low inversion barrier leads to faster racemization.

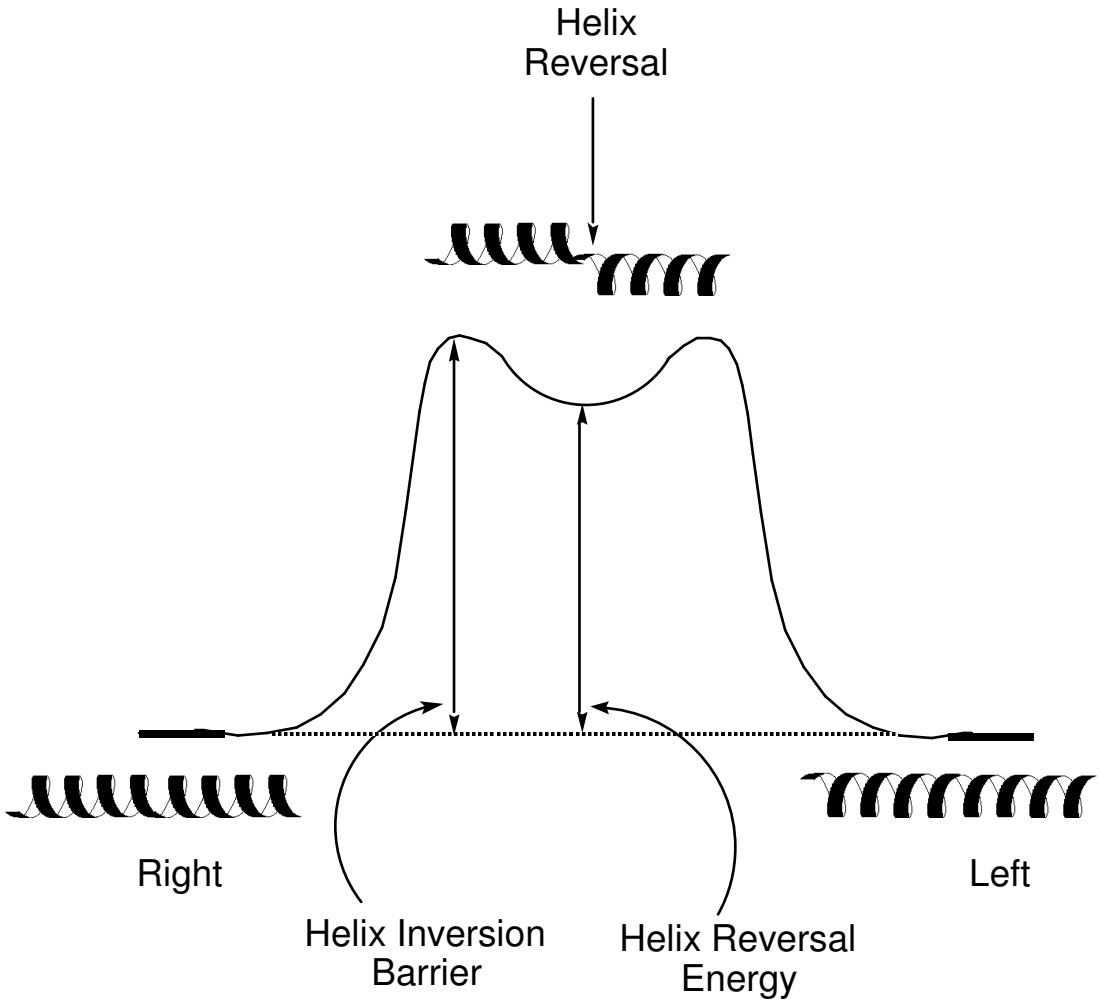

Figure 2.1. An energy diagram of helical inversion.

2.1.2. Regioselectivity in carbodiimide polymerizations

Each carbodiimide monomer has two substituents, which can be identical or different. Unlike poly(*N,N'*-di-*n*-hexylguanidine), poly-**1**, polyguanidines produced from unsymmetrical carbodiimides have two possible pathways in the coordination-insertion step (Figure 2.2), which results in two potential polyguanidine structures (Figure 2.3). The regioselectivity will depend on the nature of the two substituents on the nitrogens, including both steric and electronic effects. If the structures of two substituents are similar, the polymer chain would be expected to be non-regiospecific due to the poor regioselectivity in the propagation steps. However, if the difference between their structures is significant,

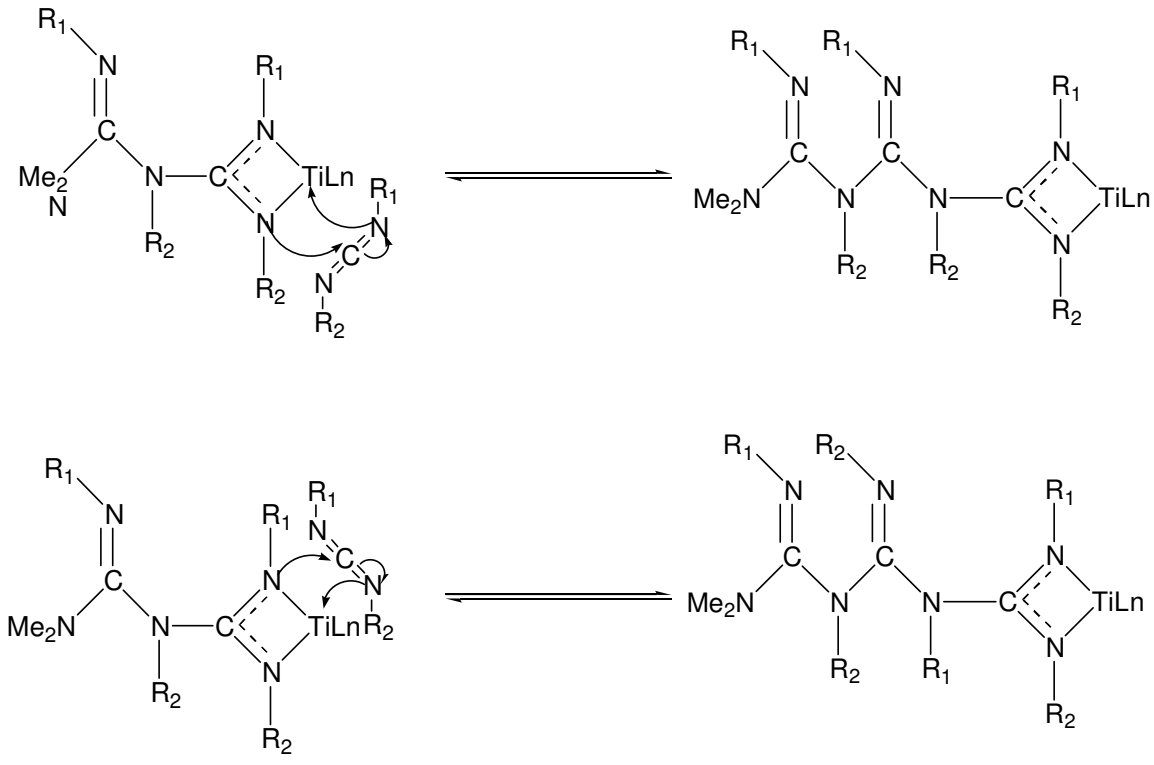

Figure 2.2. Two possible insertion pathways in the polymerization of unsymmetrical carbodiimides.

then regiospecific polymer chains could be obtained, and that should lead to high-order conformations.

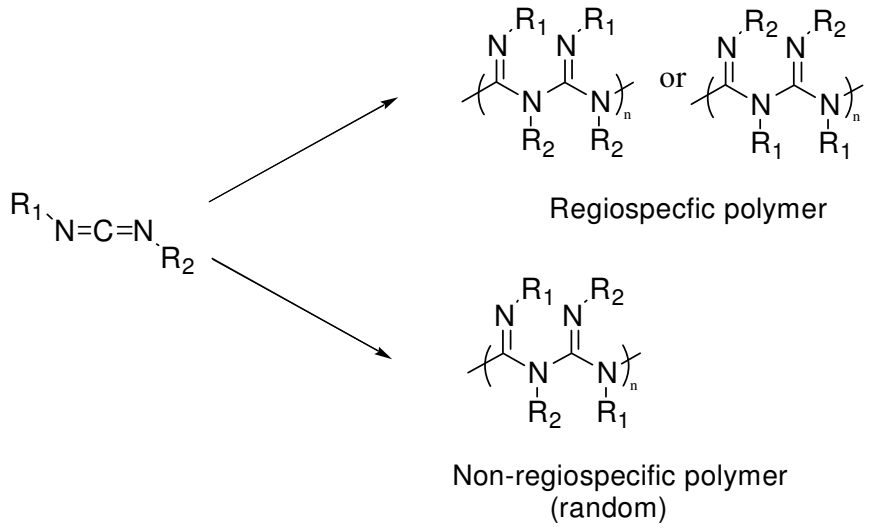

Figure 2.3. Regiospecificities which may arise upon polymerization of asymmetric carbodiimides.

2.1.3. Motivation: highly ordered helical polyguanidines

We have previously prepared an optically active polyguanidine from *N*-(*R*)-2,6-dimethylheptyl)-*N'*-hexylcarbodiimide, possessing a chiral pendant group. This polymer displayed a specific rotation essentially identical to its monomer ([α] = +7.5º), but after the dilute polymer solution was annealed at higher temperatures (30-85 ºC), the specific optical rotation changed in sign and increased in magnitude to –157.5º (Scheme 2.1).[12] This is interpreted to be the formation of a dominant screw sense diastereomer from a non-equilibrium population of conformations.

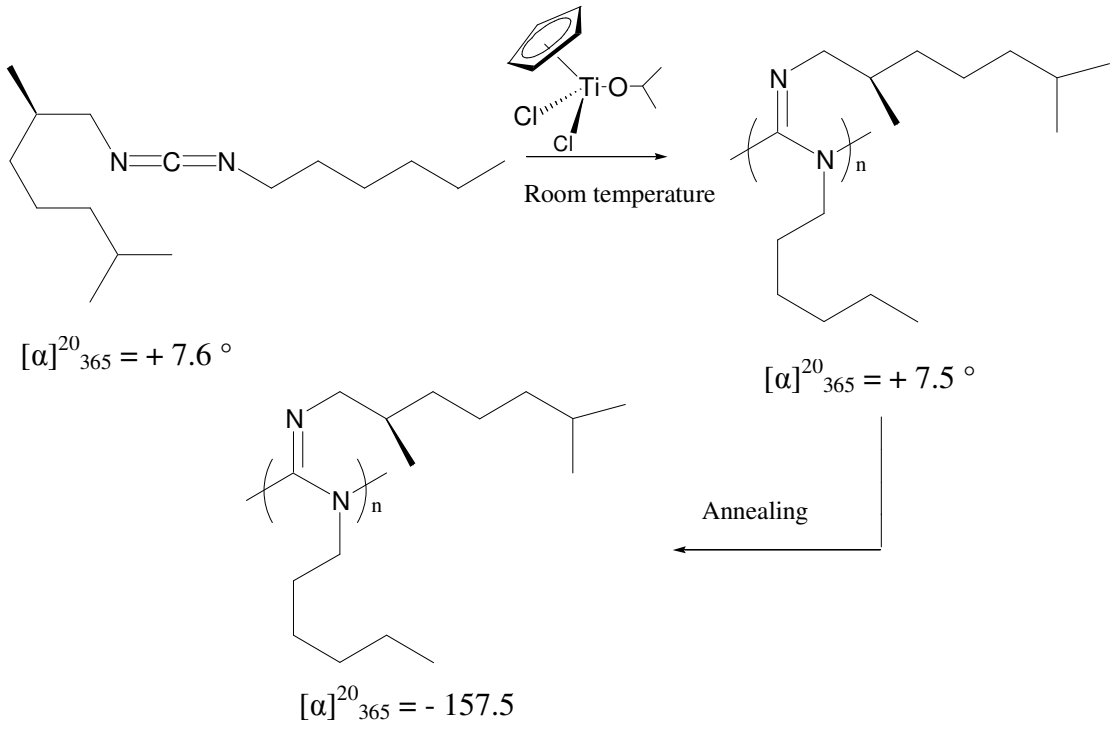

Scheme 2.1. The previous works on the polyguanidine prepared from homo-chiral monomer and its annealing behavior.

Structure and order are important in determining the properties of polymeric systems. Restricting the conformational degrees of freedom within a polymer's backbone can have the effect of extending the chain and endows the materials with order and exactitude in their structures. As a result, they can display many of interesting, higher-order properties of macromolecules, such as high strength and modulus, piezoelectric, nonlinear optical, and liquid crystallinity, etc. Moving from achiral to homochiral materials can induce further alteration and improvement of properties. Examples include solid state properties (thermal properties), dilute solution properties (rod vs. coil conformations), concentrated solution properties (lyotropic liquid crystalline behavior), and surface

adsorption properties.[7] As discussed, in order to access materials with these attributes, we have been interested in developing living, chain growth routes into extended-chain, helical polymers. Furthermore, we have been interested in discovering ways of capturing the benefits of chiral materials from essentially "achiral" materials through the concepts of induction and amplification. For the purposes of this study, the chiral element of interest is the helix. In order to get the "perfect" single-handed helix excluding helical reversals, asymmetric pendant groups are incorporated in the structure and one helical sense is biased. Because enantiomeric relationship between left- and right-handed screw senses is broken when the polymer is prepared by a monomer with an asymmetric center on the side chain, a diastereomeric relationship is introduced into the system. Therefore, the free energies of the left and right-helix are no longer equal and one of them would be energetically favored over the other in the polymerization (Figure 2.4). The placement of the asymmetric unit is responsible for the cooperativity. Chiral centers placed close to the polymer backbone have a greater effect on the cooperativity than those placed more remotely.[13]

Toward this end, we have been studying the helical polyguanidines possessing high inversion barriers, which are prepared by living polymerizations from chiral carbodiimide monomers with different substituents. [8-11]

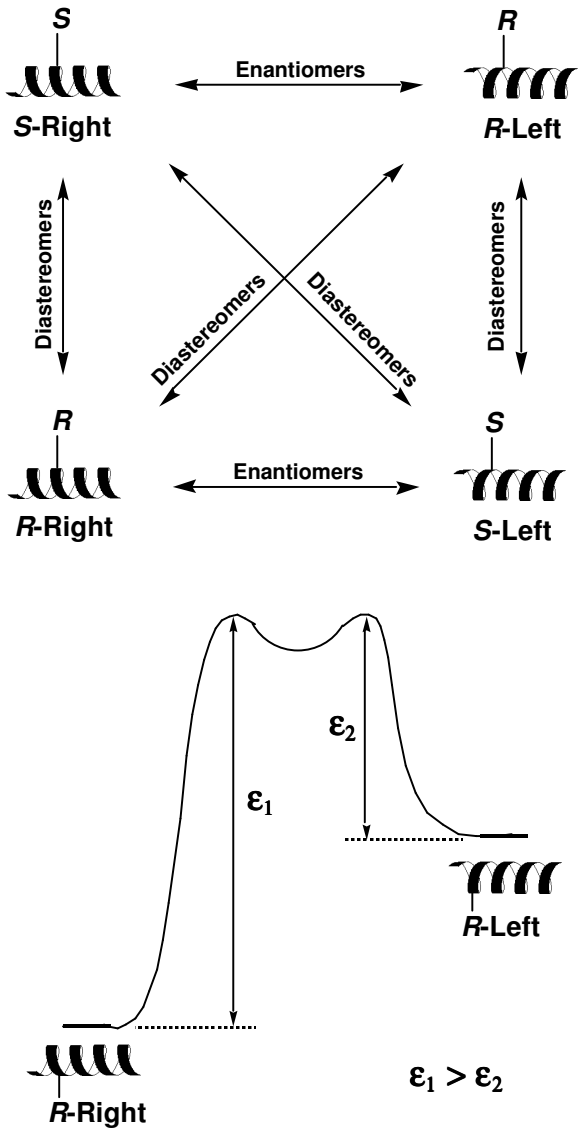

Figure 2.4. Diastereomeric nature between right and left handed helices for polymers composed of chiral monomers.

2.2. Amplification of chirality

2.2.1. Preparation of materials

Monomers

Carbodiimides are typically synthesized by the dehydration of a urea. A variety of dehydration agents have been reported in the literature; bromotriphenylphosphonium bromide works well for most dehydrations. Typically, one can easily obtain a yield of 70-80% with alkyl substituents; aryl substituents tend to show slightly reduced rates of the reaction and lower yields.[8,14] We generally use distillation to purify the monomer products. However, carbodiimides with low vapor pressures (high boiling points) co-distill with triphenylphosphine oxide (100 °C at 1 mTorr). This is usually a problem when the substituents contain more than a combined 12 carbon atoms, but currently, this is the best approach we have found to synthesize carbodiimide.

As discussed earlier, the different nature of substituents on the carbodiimide monomers leads to different regioselectivity in the polymerization. So unlike the monomer, *N*-(*R*)-2,6-dimethylheptyl-*N'*-hexylcarbodiimide, used in our previous work, we synthesized enantiomerically pure *N*-(*R*)-2,6-dimethylheptyl-*N'*-isopropylcarbodiimide, **2**, and *N*-(*R*)-2,6-dimethylheptyl-*N'*-phenylcarbodiimide, **3**. The isopropyl group was chosen due to its steric hindrance. Monomer **3** varies in both the steric and electronic environment around the carbodiimide functionality due to its aromatic substituent.

As seen in Scheme 2.2, the synthesis starts with the commercially available (*R*)-pulegone. The ring opening reaction was carried out and produced the (*R*)-citronellic acid. The unsaturation was hydrogenated over Pd-C to obtain (*R*)-2,6-dimethylheptanoic acid.

The acid chloride was generated from the addition of oxalyl chloride and catalytic amount of *N,N*'-dimethylformamide. This was converted to the isocyanate via a Curtius rearrangement of the acyl azide which was generated from reaction of azidotrimethylsilane with the acid chloride. The (*R*)-2,6-dimethylheptylisocyanate was allowed to react with isopropyl amine or aniline to generate the urea which was subsequently dehydrated with bromotriphenylphosphonium bromide to give the carbodiimide monomer.

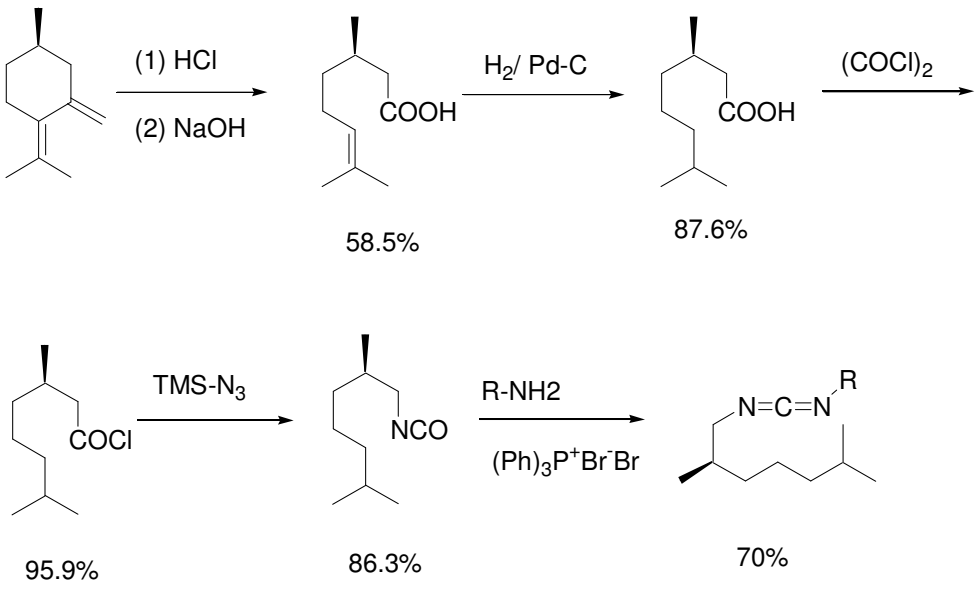

Scheme 2.2. Synthetic route of the chiral monomer of **2** (R=isopropyl) and **3** (R=phenyl).

Polymers

The living polymerization of carbodiimides with titanium(IV) catalysts can be carried out as neat reactions or run in solvents, for example, toluene or chloroform. Typical polymerizations take a few hours at room temperature and are run under an inert atmosphere. A number of catalysts for the polymerization of carbodiimides have been developed in our group that show a range of reactivities. The reactivity of this polymerization is largely determined by the steric demands of the monomer,[8] where large substituents inhibit or prevent polymerization. Both monomers **2** and **3** have bulky groups, therefore, catalysts with high reactivity are necessary.

To date, the titanium(IV) catalysts **I** and **II** have been used in this project (Figure 2.5). They have different reactivity because of the different ligands. Catalyst **I** is moderately active for the polymerization of carbodiimides and catalyzes a living polymerization with good control. Catalyst **II** is more active and works very well when the monomers have sterically bulky side chains. The molecular weight in both cases is controlled stoichiometrically by the monomer: initiator ratio.

I **II**

Figure 2.5. Catalysts used in this work.

2.2.2. Amplification of chirality

We tried the polymerization with monomer **2** using catalyst **II**, but due to the bulky isopropyl group, the reaction was longer and the yield was lower than that of a typical carbodiimide polymerization (Scheme 2.3). During latter annealing experiments, the optical rotation went to 0˚ after heating for several hours, and, polymer decomposition was detected by FT-IR spectroscopy. The carbodiimide monomer absorption at 2130 cm^{-1} was found in the annealed poly-**2** solution, which implies that the chirality decay of poly-**2** was caused, partially or completely, by polymer decomposition (Figure 2.6).

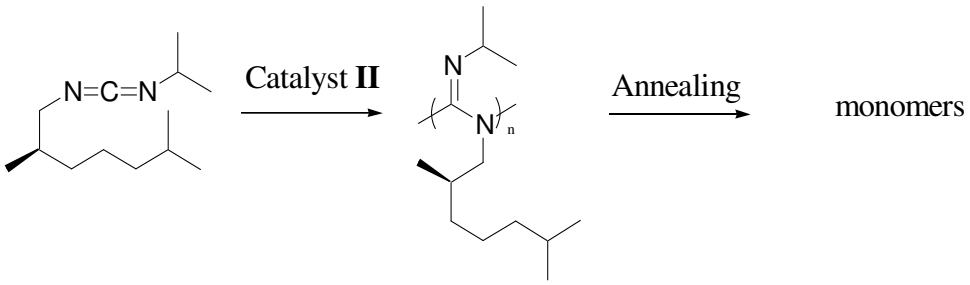

2 poly-**2**

$[\alpha]_{435}^{20} = +7.11°$ $[\alpha]_{435}^{20} = -49.3°$ $[\alpha]_{435}^{20} \approx 0$

Scheme 2.3. Polymerization of carbodiimide **2**.

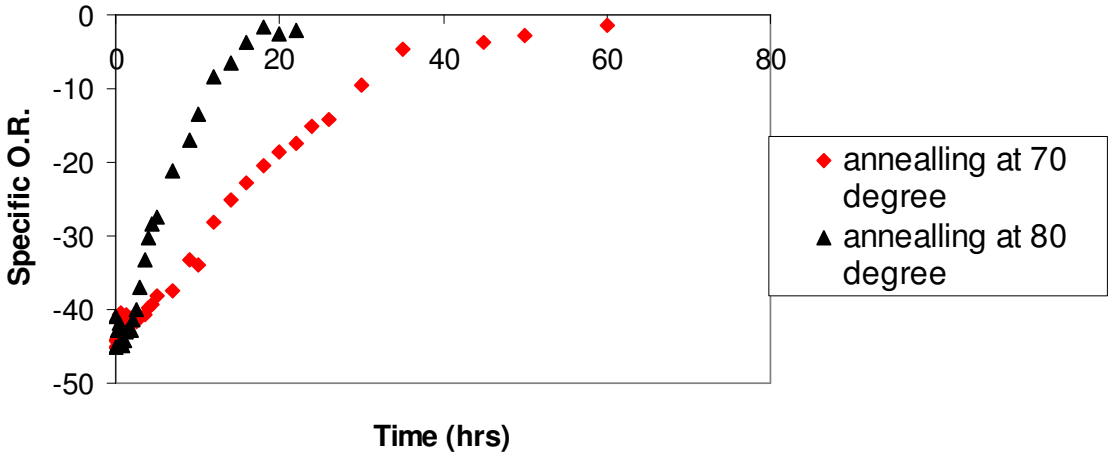

Figure 2.6. Annealing behavior of Poly-**2**.

Table 2.1. The specific optical rotation of monomers and polymers.

	Previous results[(1)]		**2**		**3**	
	monomer	polymer	monomer	polymer	monomer	polymer
[α]	7.6˚ ($CHCl_3$, λ=365nm)	7.5˚ ($CHCl_3$, λ=365nm)	7.11˚	-49.3˚	-0.32˚	-209˚

(1) Refer to Scheme 2.1 for the structure of the samples in previous works.
(2) Refer to Scheme 2.2 for the structures of the samples **2** and **3**.
(3) Unless otherwise noted, all optical rotation were measured at 435 nm, room temperature and C = 0.2 g/ 100mL in toluene.

Because of these problems, we then tried monomer **3** and found it was easily polymerized using catalyst **II**. As shown in Table 2.1, we can see that both poly-**2**, and especially poly-**3**, show very large specific optical rotation values, compared to their monomers, whose specific optical rotations were so small as to be almost unmeasurable - a characteristic of small molecular chirality which impeded the acceptance of "chirality" for many years. Clearly, the optical activity of the polymer can not arise simply from the intrinsic chirality of the monomeric units. However, there is an energy difference between the left- and right-handed helical senses of these chains, and even if this is extremely small, this energy difference may cause an uneven distribution of the two screw senses.

This is possible because of a cumulative effect where the distribution is determined by the energy difference per sequence rather than per monomer. In other words, the energy difference per monomer unit is multiplied by the large number of monomer units between helix reversals. Such cooperativity results in the fact that a very small energy difference per stereo center between diastereomers produces a significant helical excess in the polymer chains, which leads to a large specific rotation in polymers.

Therefore, the large increase in optical rotation in going from the monomer to the polymer is interpreted as arising from the formation of a stereo-regular structure which is very probably a helix with an excess of one handedness. However, one cannot, simply from the optical rotation, assign a quantitative preference to this helical sense or assign which handedness is in excess.

The helical chromophore in the polyguanidines absorbs UV light, and if one sense of the helix predominates, there will be a differential absorption of the left- and right-

handed circularly polarized light. This can be measured using circular dichroism. The circular dichroism (CD) and ultraviolet (UV) spectra in hexane at room temperature for poly-**3** are presented on the same scale in Figure 2.7. The optical rotation, α, in the visible region arises from the tail of a Cotton effect centered in the UV region of the spectrum at about 247 nm. This strong negative CD band is followed by a small band around 210 nm where solvent absorption precludes measurement. The fact that the UV absorption is lower than the CD band could suggest exciton coupling, a phenomenon associated with a helical polymer conformation.[16,17] The polyguanidines synthesized from the homo-chiral monomers lead to the large CD intensity, which is caused by a large excess of one helical sense.

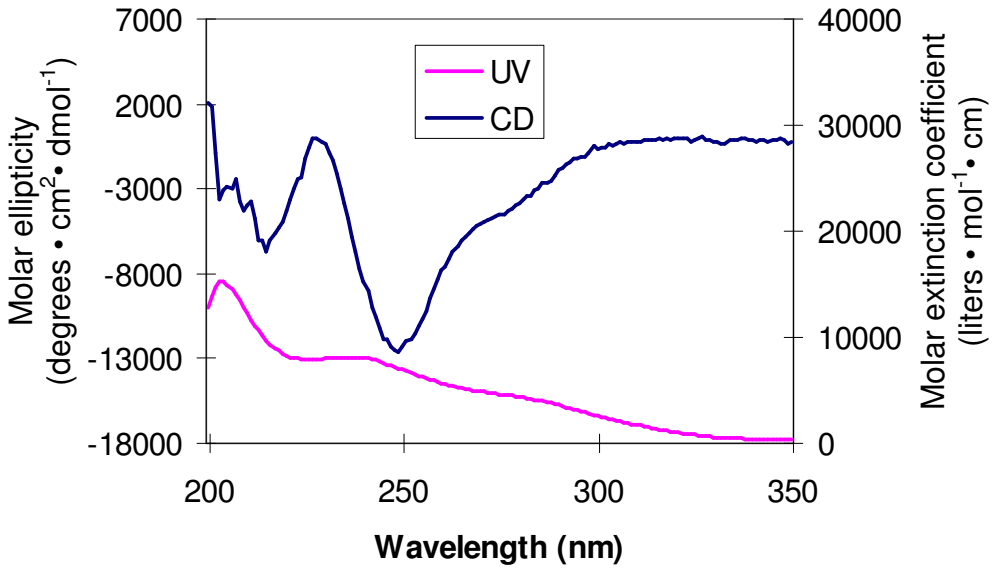

Figure 2.7. Circular dichroism and UV spectra for Poly-**3** in hexane at room temperature.

In our more recent work,[18] in order to stabilize the helix, the phenyl group in the chiral monomer **3** was replaced by the more bulky anthracyl groups to get monomer **4**. The enantiomer of **4**, i.e. **5**, was also prepared. The monomers **4** and **5** could be polymerized using catalyst **II** to get reasonable yields (Scheme 2.4). The specific optical rotation of poly-**4** ($[\alpha]^{25}_{D}$= + 791°, toluene) and poly-**5** ($[\alpha]^{25}_{D}$= - 778°, toluene) are opposite in sign and much greater in magnitude as compared to their corresponding monomers of **4** ($[\alpha]^{25}_{577}$= - 2.7°, toluene) and **5** ($[\alpha]^{25}_{577}$= + 2.6°, toluene). Furthermore, poly-**4** and poly-**5** show a mirror-image intense CD signal in THF (Figure 2.8), chloroform, and toluene, which corresponds to their UV-vis absorptions. Both the data of the optical rotation and CD spectra imply that poly-**4** and poly-**5** adopt a regular one-handed helical conformation with the opposite screw sense in solution, and further confirms our conclusion that the asymmetric carbon in the monomer unit can cause tiny differences in energy between the two screw senses. When all of such small forces are combined, the polymer chains would show a bias favoring one particular helical sense, which results in a large specific rotation in the polymers.

2.3. Regioselectivity

As we discussed before, there are two kinds of possible pathways in the coordination-insertion step when non-asymmetrical carbodiimides are polymerized. In order to determine the regioselectivity, our group has established a method of analyzing the resultant monomer products after decomposition to determine the orientation of monomers along the polymer backbone by GC-MS. For example, consider a polymer composed of an asymmetric monomer in which a strong regiochemical preference is displayed. Because of

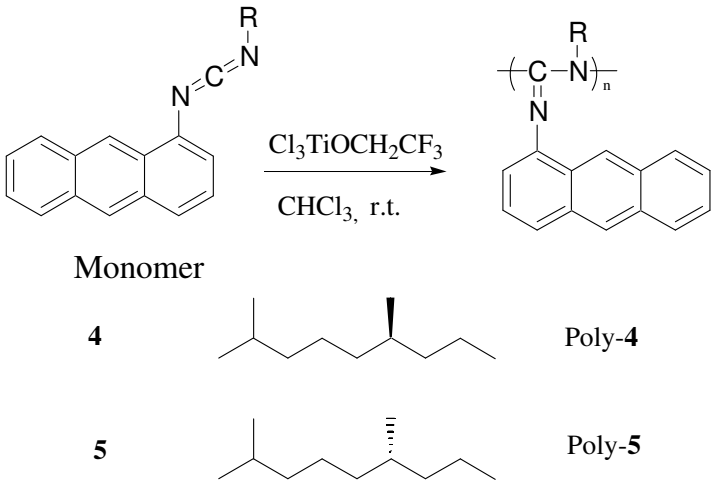

Scheme 2.4. Polymerization of carbodiimides **4** and **5**.

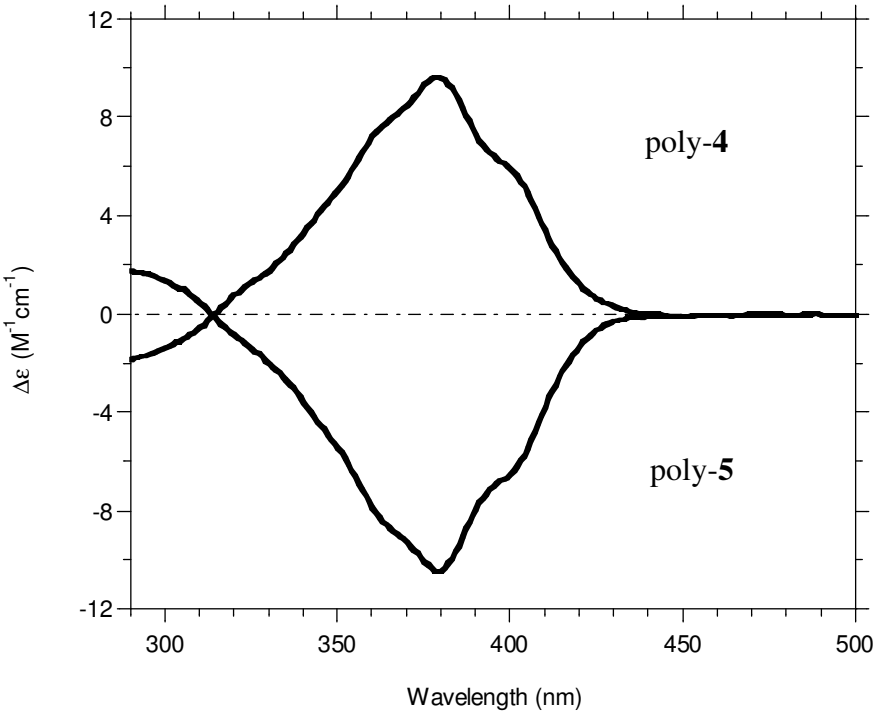

Figure 2.8. CD spectra of poly-**4** and poly-**5**.

the equality of all bonds in the polymer backbone, chain scission would be expected to be random, and polymer decomposition would occur by two pathways, either across (i.e., breaking C-N bonds original monomer) or between original monomers (i.e., breaking C-N bonds that were formed during polymerization). The products of these two pathways would be identical. However, the consequences of these two pathways are strikingly difference for a polymer composed of an asymmetrical monomer that has no regiochemical preference. Chain scission between the original monomers would yield only one product: the original monomer. Decomposition across the original monomer, however, would yield two new metathesis monomers. As long as no regiochemical preference exists, the decomposition products would be composed of three monomers: the original and two metathesis monomers. An assumption in this analysis is that backbone bond cleavage is random and there exists no preference for bond cleavage based on the sterics or electronics of the substituents (Figure 2.9). From our previous studies, the original monomers make up the majority (up to 90-100%) of the resultant monomers after decomposition for most of the polyguanidines. For some polymers formed by monomers with substituents possessing big difference, like poly[*N*-methyl-*N'*-(*R*)-(+)-α-phenylethylguanidine], the degree of regioselectivity can reach 100%. However, these studies do not tell us which group is in which position.

Herein, we developed a simple method to detect the regiochemical orientation of the poly-**4**. Since in the monomer **4**, the phenyl substituent has significantly different steric effects and electronic properties from the chiral alkyl chain on the other side, it is

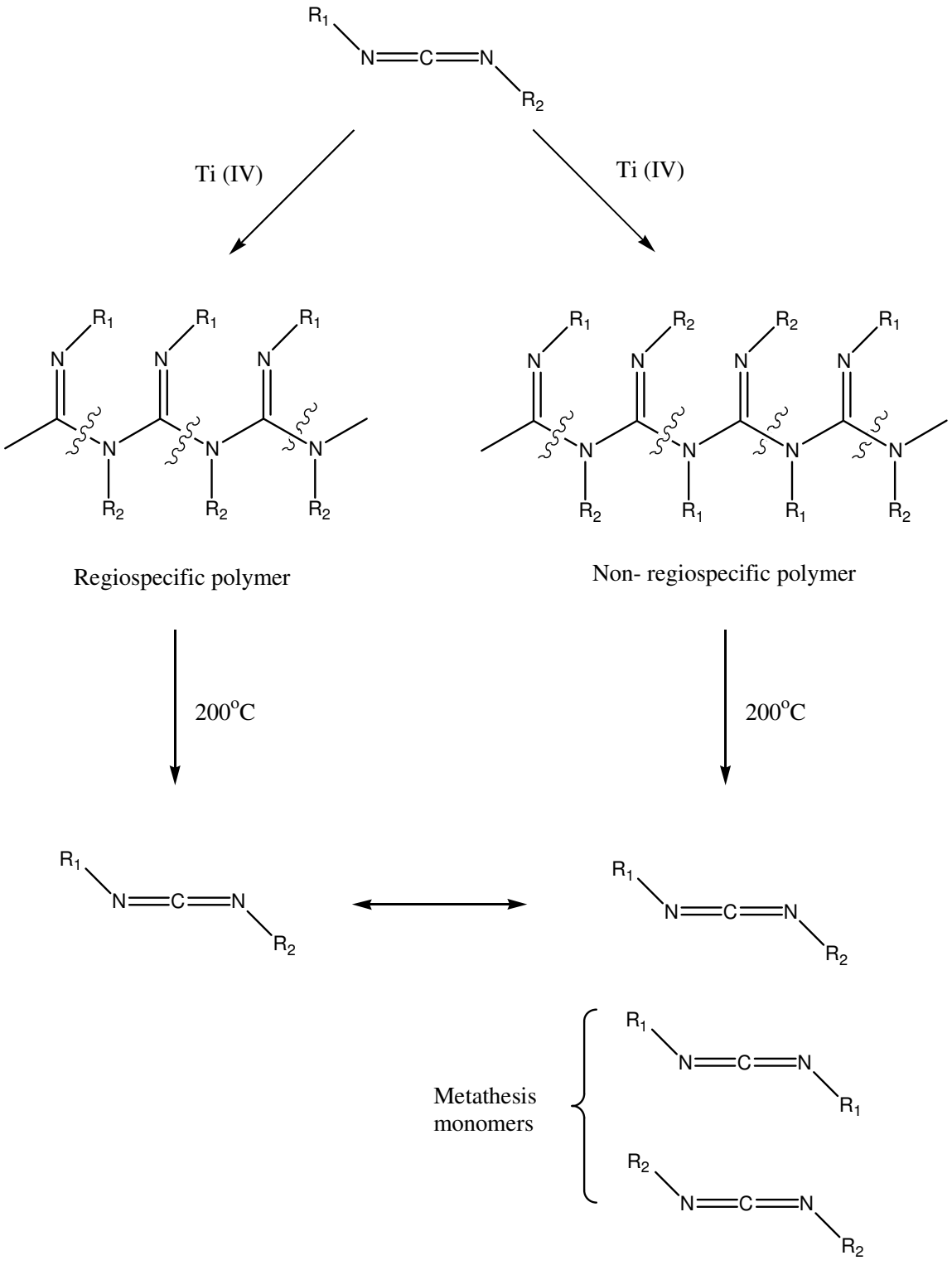

Figure 2.9. Possible decomposition products for polyguanidines.

reasonable to believe the degree of the regioselectivity of the polymerization of **4** is high. As a result of these chemical differences, the carbon in the alkyl chain connected directly with nitrogen in the imine or amine should show a different chemical shift in the ^{13}C NMR. Also, the absorbance of imine functional group would occur at different wavenumbers when nitrogen in the imine is connected to an aromatic ring or an aliphatic chain due to the conjugation (Figure 2.10).

For each repeat unit in the poly-**1**, there are two alkyl carbons connected with the nitrogen. One connects with imine and the other connects with amine, and their ^{13}C NMR chemical shifts are 48.7 and 32.3, respectively, with the one connected with the amine nitrogen shifted to lower frequency (high field). Comparing the ^{13}C NMR chemical shift of the alkyl α-carbons in poly-**3** and poly(*N*-hexyl-*N'*-phenylguanidines) (poly-**6)**, at 47.3 and 52.6, respectively, we could determine that the alkyl chain is connected with imine group nitrogen. This conclusion is further confirmed by the band position of the imine functional group stretching mode, which is the most significant absorbance of the guanidine repeat unit in the infrared. The observed C=N stretching frequency for the poly-**1** is 1644 cm^{-1}. If the aromatic ring is connected to the N on the imine group, the *n*-π conjugation between phenyl LUMO and nitrogen lone pair electrons increases the C=N stretching force constant and leads to an increase in frequency. For the poly[*N*,*N'*-bis(4-*n*-butlphenyl)guanidines] (poly-**7**), the band is approximately 1665 cm^{-1}, and in poly-**3**, poly-**5** and poly-**6**, the imine show strong stretching frequency at 1636, 1641 and 1624 cm^{-1}. From the ^{13}C NMR and IR, we can qualitatively determine that the phenyl group connects with nitrogen on the amine

		^{13}C (ppm)	IR (cm^{-1}) (C=N stretch mode)
poly-**1**	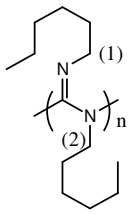	(1) 48.7 (2) 32.3	1644
poly-**3**	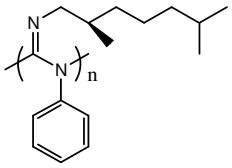	53.6	1637
poly-**4**	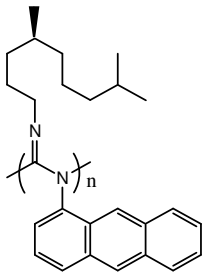		1641
poly-**6**	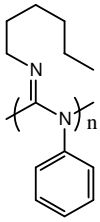	47.3	1624
poly-**7**	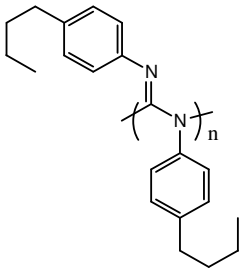		1665

Figure 2.10. ^{13}C NMR and IR data for polyguanidines.

group, rather than the imine position. Here, we need to say this conclusion requires more direct evidence for support, such as an isotopic experiment.

To account for the observation phenyl group takes the amine position, we propose a regioregular insertion mechanism. In the propagation step of carbodiimide polymerization by Ti(IV) catalyst, both titanium-amidinate bonds are susceptible to be break when the monomer is non-symmetric (Figure 2.11). The aromatic rings can delocalize the electrons on the nitrogen thereby stabilizing the species with the alkyl-imine group. This would result in the microstructure having the phenyl group connected with the amine nitrogen.

2.4. Annealing behaviors

The first isolated polymer produced from *N*-[(*R*)-(+)-2,6-dimethylheptyl]-*N'*-hexyl carbodiimide has a low specific optical rotation, which might be because this polymer has a highly disordered structures, or large number of defects (i.e., helical reversals) and does not adopt a helical structure. By annealing, the existing defects and/or helical reversals are extruded, and the polymer adopts a more orderly conformation. Herein, we employed optical rotation, circular dichroism spectrum and ^{19}F NMR to monitor the conformation changes during the annealing process.

2.4.1. Optical Rotation

When dilute solutions of poly-**3** are annealed at higher temperatures, 50 - 85˚C, we discovered that the optical rotation of the polymers dramatically changed in magnitude with time and also changed in sign (Figure 2.12). At 70˚C, it takes about 80 hours to reach a plateau value of +255˚, from the original value of –209˚. Higher temperatures accelerated

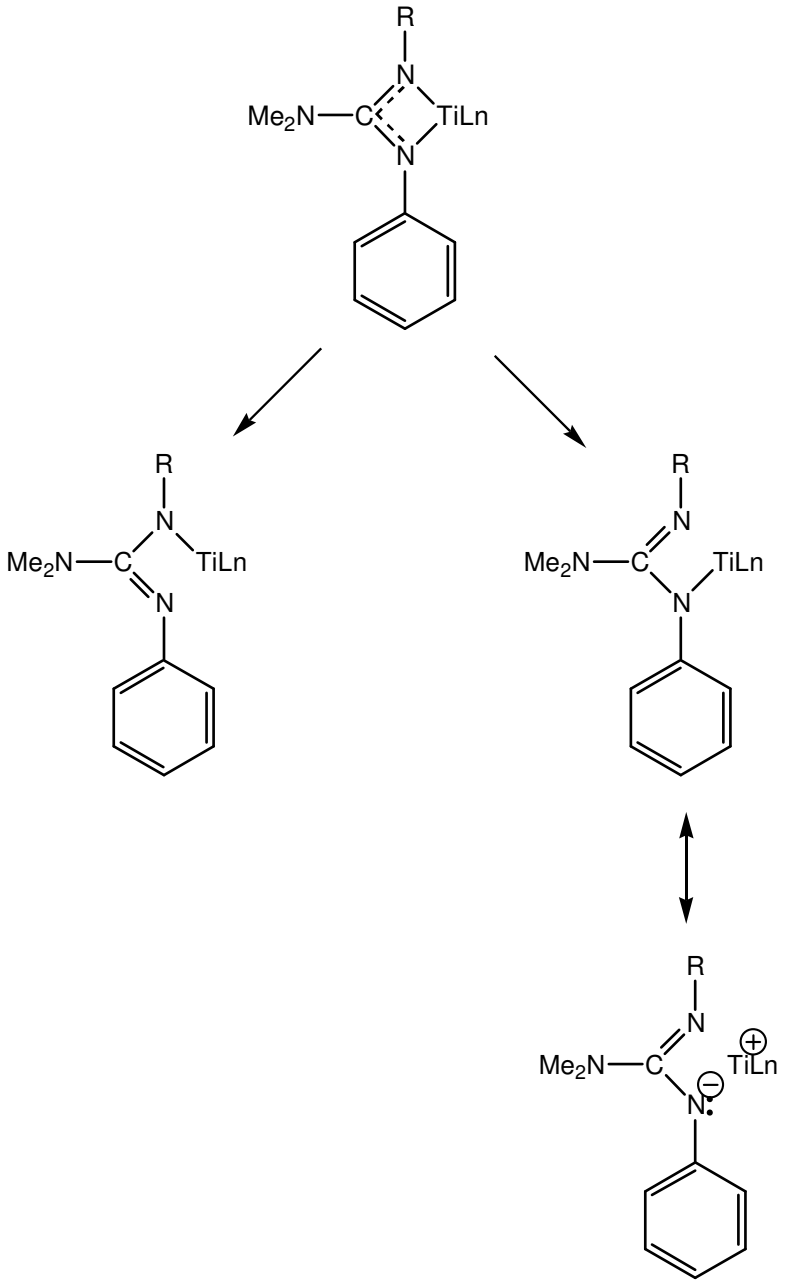

Figure 2.11. Proposed mechanism for regioselective polymerization of non-symmetric aryl carbodiimides.

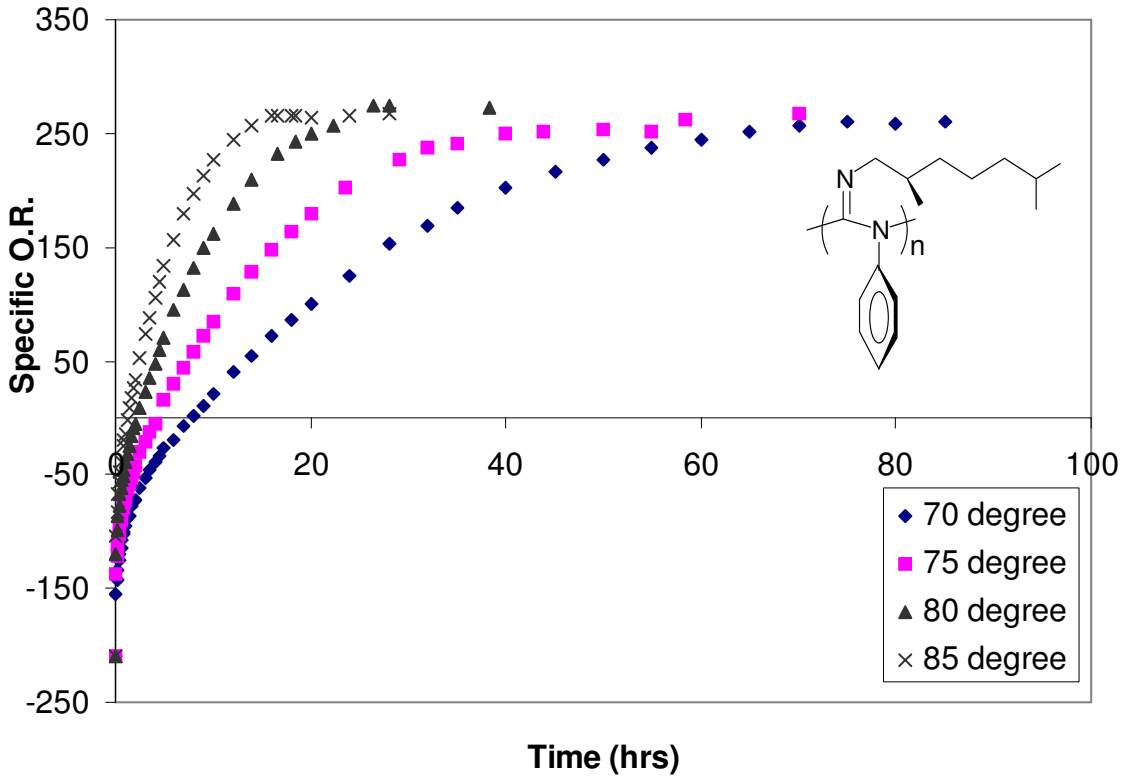

Figure 2.12. Specific optical rotation of poly-**3** as the function of time at different annealing temperatures.

this process: a toluene solution of poly-**3** at 85˚C only requires 16 h to reach the plateau value.

The unannealed polymer conformation is unique; it is a conformation which is not at its thermodynamic energy minimum. We believe this kinetically controlled conformation (KCC) arises during the polymerization and is thought to be either a high energy state or a state with the introduction of the defects, helix reversals, along the polymer chain. The activation energy for the extrusion of these reversals is sufficiently high that they cannot be removed at room temperature over a reasonable period of time. Annealing the polymer in solution allows the high energy helix reversals to move toward the chain ends or each other

(resulting in annihilation); this manifests itself as an increase in the optical rotation for the system. The KCC has unique optical properties which cannot be obtained once the system has been annealed. After annealing poly-**3**, a thermodynamically controlled conformation (TCC) is obtained. Base on the magnitude of the optical rotation of the KCC, we believe its conformation is not fundamentally different from the KCC. The polymers switch from a disordered conformation or high energy helical diastereomer to the low energy diastereomer.

The changes in the specific rotation for annealed poly-**3** with respect to temperature are linear over the observed range. If this linear relationship holds over a lightly wider temperature range than that measured, the conformation possessed by virgin poly-**3** should theoretically be accessible to the annealed sample at elevated temperatures; however, due to polymer decomposition (ca. 180 ˚C), this is not possible. Once annealed, poly-**3** irreversibly adopts a new conformation with a characteristic optical rotation; thus, both the conformational and optical properties of the virgin material are unique.

2.4.2. Circular Dichroism

The irreversible conformational change with temperature is common in biological systems (e.g., polypeptides), rather than in synthetic analogs when polymerization occurs at room temperature. The effect has been observed in some methacrylate polymers when the polymers were synthesized at low temperature. Circular dichroic spectroscopy can be used to probe the conformation of the polymer chain.

To further understand the conformations of the helical polyguanidines, variable temperature CD spectra were recorded. As seen in Figure 2.13, the poly-**3** at 0 °C shows the

strongest Cotton effect and the intensities decrease as the temperature goes up. These results support our hypothesis that the conformation initially obtained from the polymerization is kinetically favored, rather than thermodynamically favored.

Monitoring CD spectra of the samples allows us to determine if there are large conformational changes occurring during this annealing process. Figure 2.14 shows the

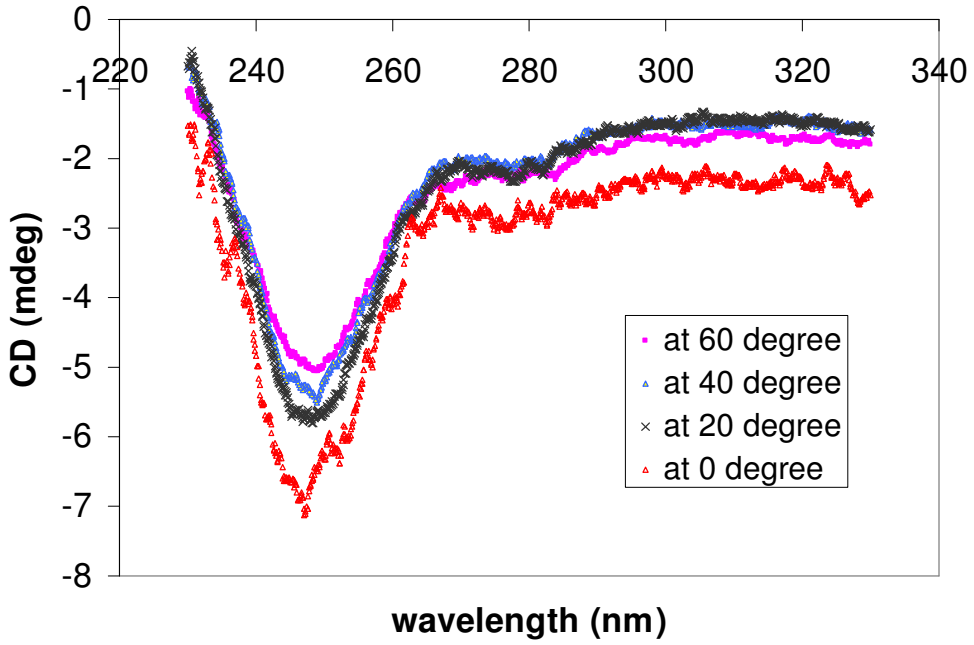

Figure 2.13. Variable temperature CD spectra of poly-**3** in hexane (c = 4.1 x 10^{-5} M, path length = 1.0 cm).

unannealed poly-**3** shows a negative Cotton effect with the maximum at 250 nm. When Poly-**3** is heated in the octane solution at 80 °C for 36 hrs, the Cotton effect gradually changes in sign from negative to positive and the intensity of the annealed polymer is weaker than that of virgin with maximum absorbance shifting from the 250 nm to 261 nm.

These results provide further evidence that supports our conclusion about the origin of this chiroptical switching phenomenon. The bathochromic shift of the UV maximum might be due to the different orientation of phenyl rings in the two screw senses.

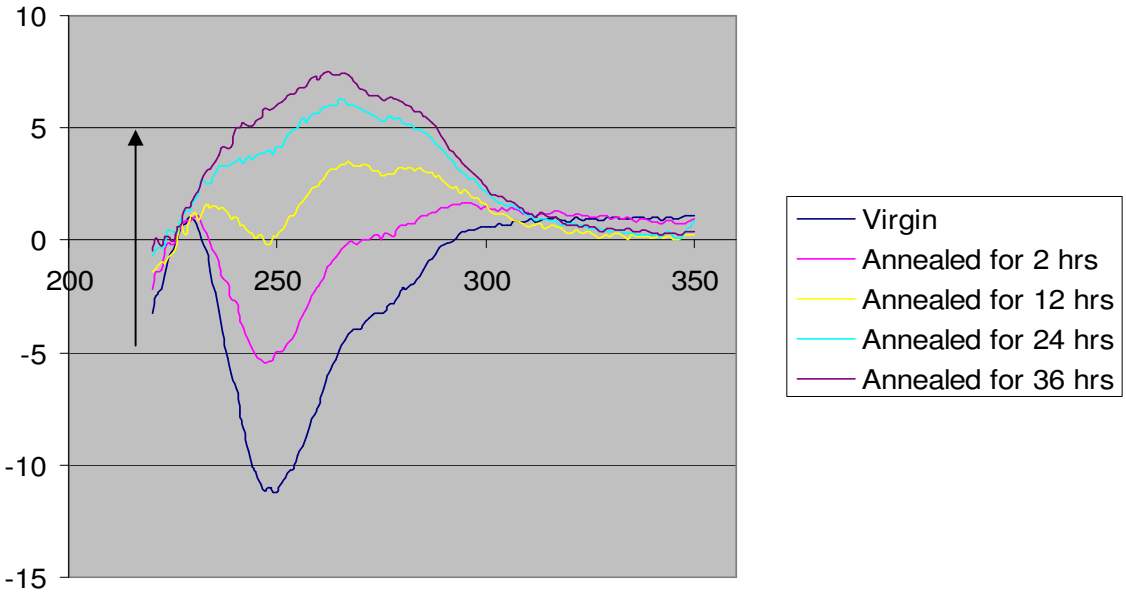

Figure 2.14. The CD spectra of poly-**3** in the octane solution during the annealing process (c = 7.38 x 10^{-5} M, path length = 1.0 cm).

2.4.3. ^{19}F NMR

Although the optical rotation and CD spectra have provided useful information about the conformation changes in the annealing process, NMR offers an interesting approach because movement of the reversal will interconvert a left- and right-handed helical segment, causing all constitutionally identical groups in the side chain to exchange their diastereotopic positions. If such diastereotopic groups have distinguishable chemical

shift properties in the NMR, the conformation change could be detected by the appearance of new peaks or disappearance of the existing peaks.

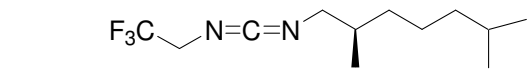

Monomer **8**

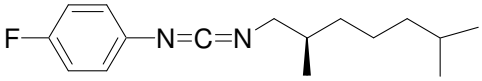

Monomer **9**

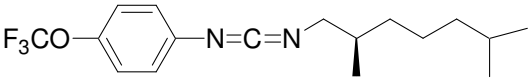

Monomer **10**

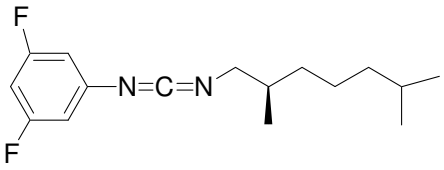

Monomer **11**

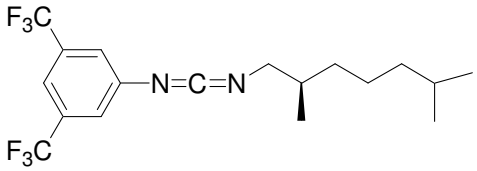

Monomer **12**

Figure 2.15. Fluorinated carbodiimide monomers.

Because of the abundant carbon and hydrogen atoms in the polyguanidines, the overlaps of those peaks in the NMR spectrum are unavoidable, which precludes us from using these nuclei to investigate the conformation switching process. However, ^{19}F NMR provides a practical approach, because the fluorinated groups are very sensitive to chemical

environments, appearing in significantly different regions of the spectrum, making quantitative measurement possible. To get the better probes, a family of fluorinated derivatives of monomer-**10** has been prepared (Figure 2.15). These differ in the bulkiness and position of the fluorinated groups on the aromatic ring. Poly-**10** gave the better results due to its relative higher reactivity in the polymerization, better solubility, and stronger peaks in the ^{19}F NMR spectrum.

The ^{19}F NMR spectra were monitored at 50 °C as a function of time. We observed that a sharp peak building up from a broad peak as the sample was annealed over a long times (Figure 2.16). Since the left- and right-handed helical senses are diastereomers, the atoms on the two screw senses are not equivalent due to different environments. Initially, the broad peak indicates the multiple environments of the fluorines, possibly corresponding to the left- and right-handed helices, helical reversals, or disordered structures. No single conformation appears dominant in the polymer chains. As the sample is annealed, a sharp peak grows, which corresponds to adoption of the thermodynamically preferred helical sense. Monitoring the optical rotation changes when the sample was annealed provided further confirmation (Figure 2.17). The specific optical rotation increases in the absolute value (ca. 450°) and changes the signs (negative to positive) as the sample was annealed longer.

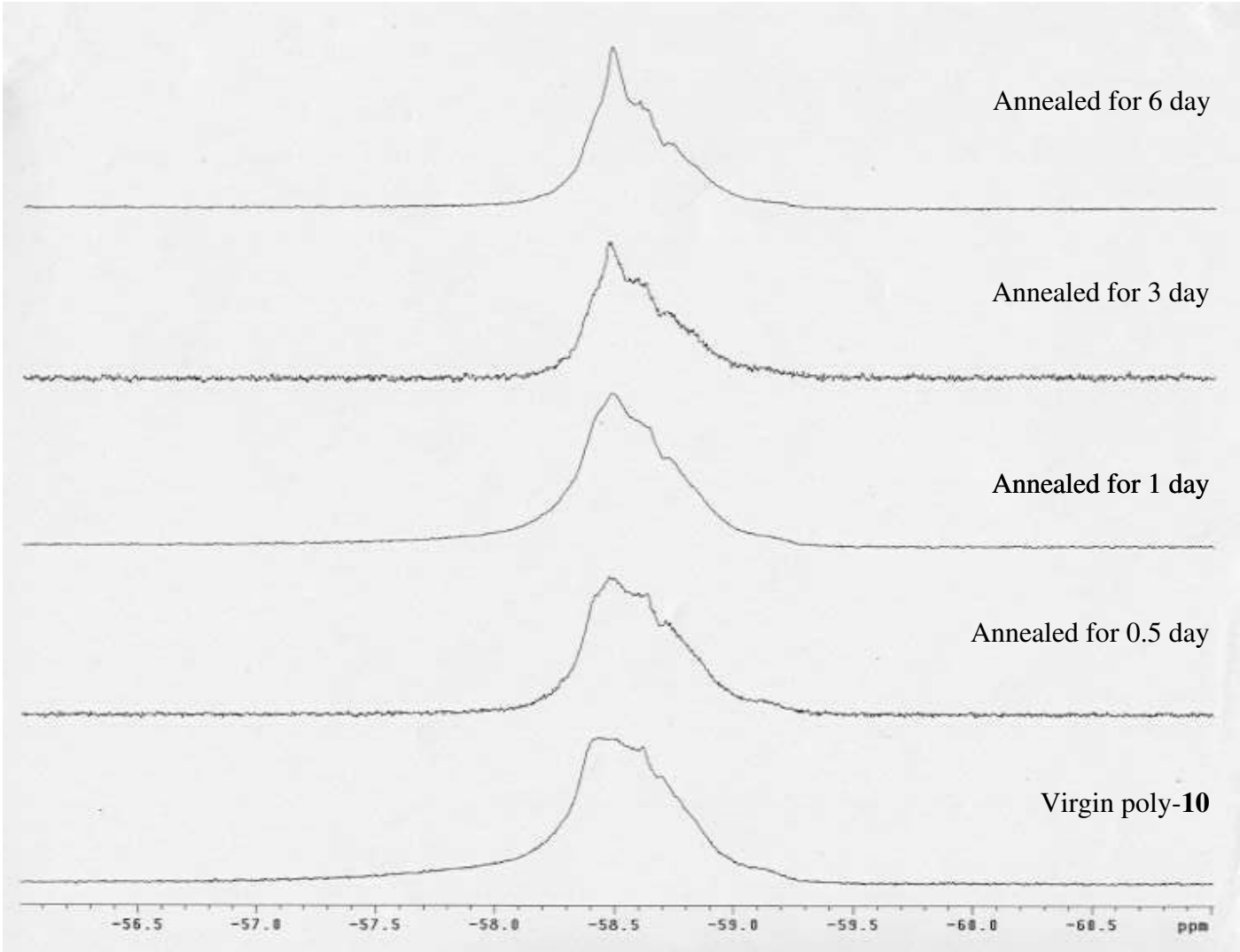

Figure 2.16. ^{19}F NMR spectra of Poly-**10** in the solution of $CDCl_3$ annealed at 50 °C.

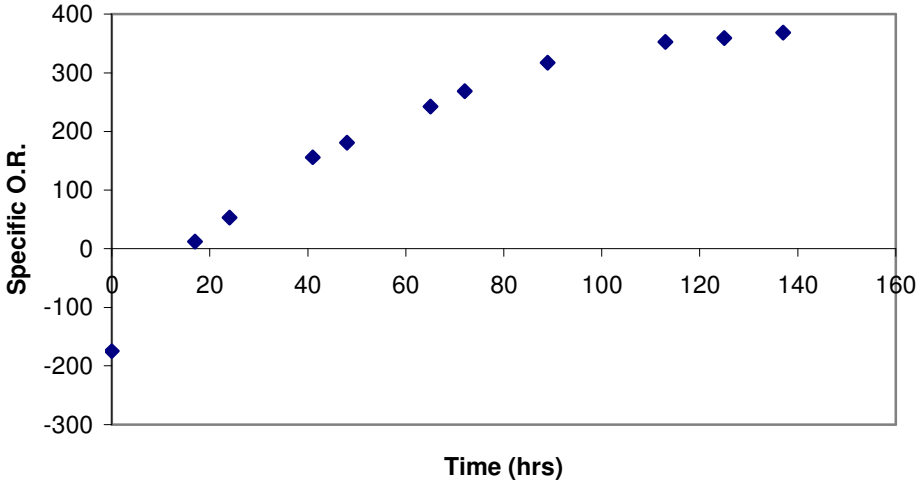

Figure 2.17. Specific optical rotation of poly-**10** as the function of time annealing at 50°C.

2.5. Activation energy for the polymer reorganizaion

An energy diagram for this system is shown in Figure 2.18. The KCC, a non-equilibrium state, is a local energy minimum. The activation energy for the transformation from the KCC to TCC was determined by monitoring the rotational changes as a function of time at different temperatures. This system was modeled as two states (helical senses) in a reversible equilibrium.

$$\ln\left(\frac{([M]_o - [M]_{eq})}{([M] - [M]_{eq})}\right) = k_{obs}\ t \qquad (1)$$

The variables $[M]_o$, $[M]_{eq}$, and $[M]_t$ refer to the concentration excess of one particular handedness: initially, at equilibrium, and at time "t". Since concentrations were not directly measurable, optical rotations were substituted. The rate constant, k_{obs}, and time, t, were calculated and measured, respectively. The rate constants at several temperatures

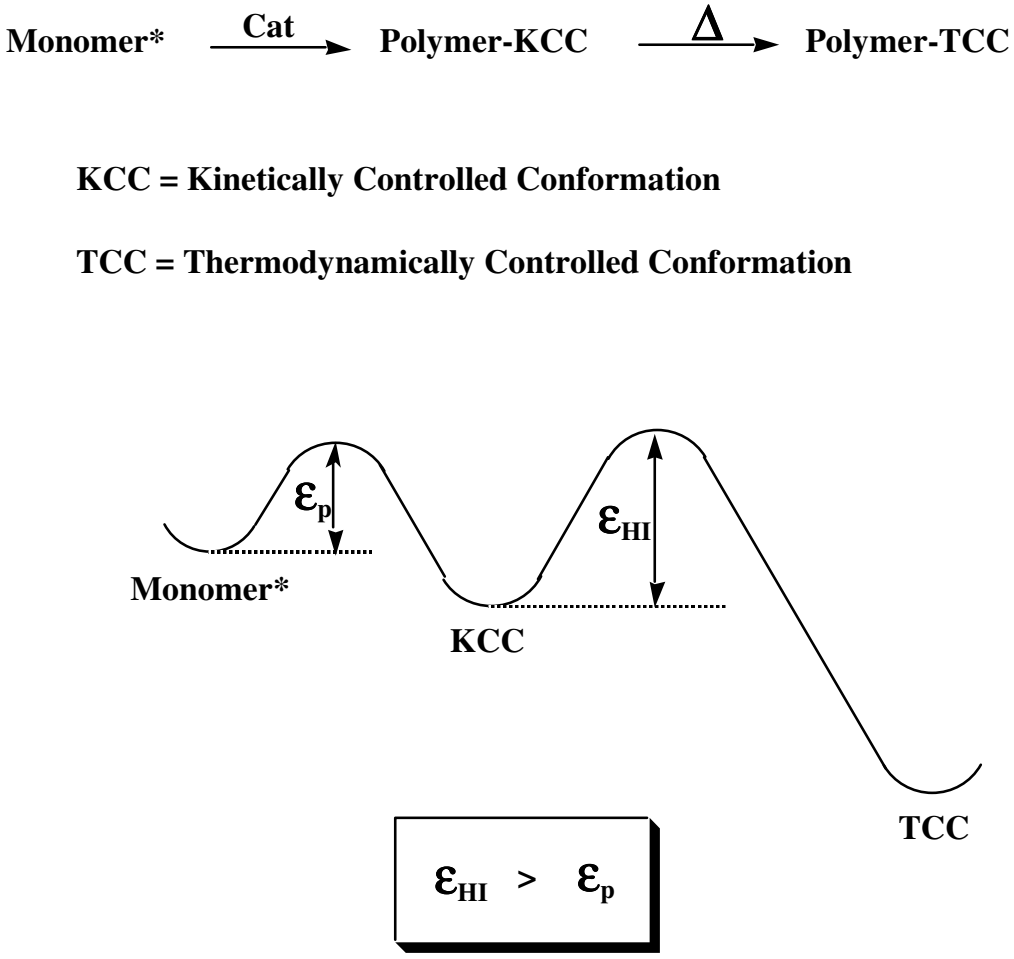

Figure 2.18. Kinetic vs. thermodynamic control over helical conformation.

were determined from the annealing curves, Figure 2.19. From the slope of the Arrhenius plot we obtained an apparent activation energy of 29.2 kcal/mol for poly-**3** (Figure 2.20). Compared to the polymer reorganization of poly{[*N*-(*R*)-2,6-dimethylheptyl]-*N*'-hexylcarbodiimide}, 21.6 kcal/mol, poly-**3** requires higher energy to undergo such conformation changes.

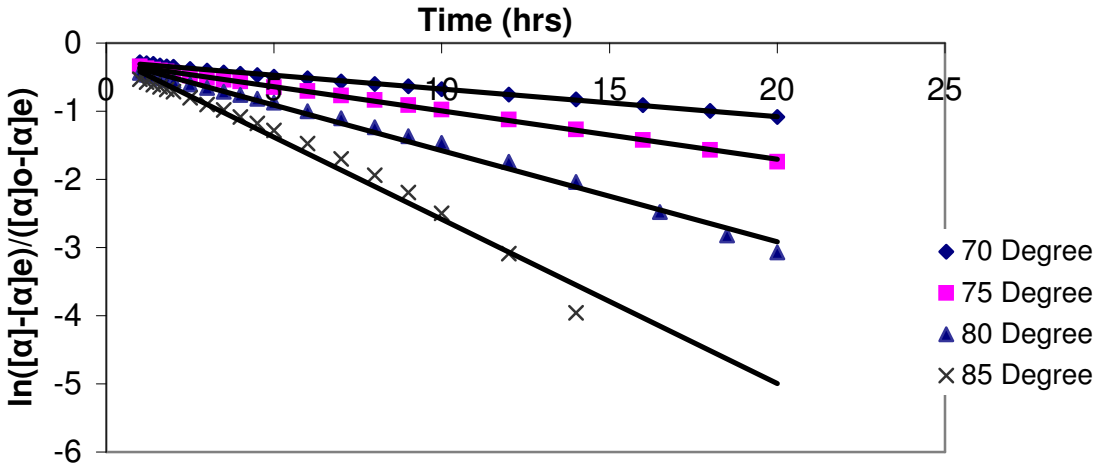

Figure 2.19. The rate of helix inversion of poly-**3**.

Linear least squares fit:

70 ˚C:	Y = -0.0406X - 0.2701	R^2 = 0.9967
75 ˚C:	Y = -0.0712X - 0.2834	R^2 = 0.999
80 ˚C:	Y = -0.1337X - 0.2434	R^2 = 0.9917
85 ˚C:	Y = -0.2409X - 0.1756	R^2 = 0.9786

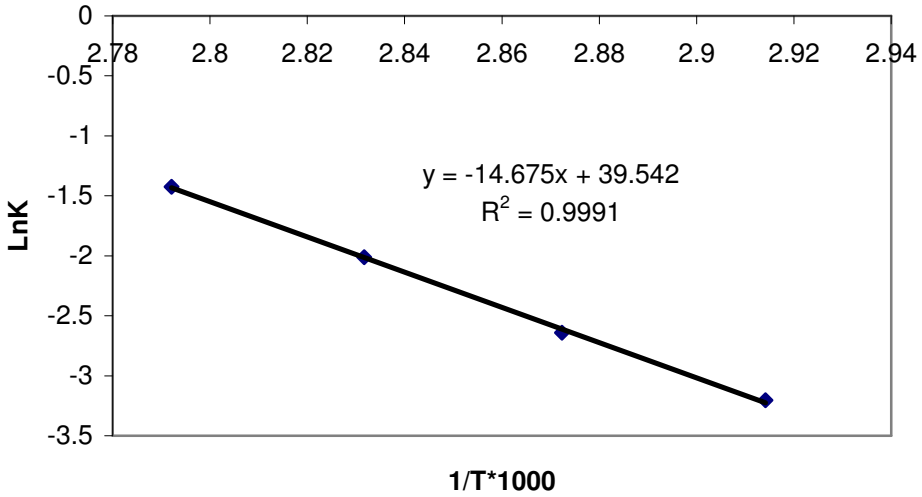

Figure 2.20. Arrhenius plot for annealing poly-**3.** The activation energy is determined to be 29.2 kcal/mol.

These annealing experiments support the hypothesis that these polymers adopt conformations that are kinetically controlled, rather than thermodynamically controlled. Furthermore, the kinetic barrier of approximately 30 kcal/mol makes the isolation of these KCC possible and therefore, the conformations after annealing is irreversible and stable at room temperature.

Since the poly-**3** possesses a high activation energy, its racemization at room temperature is negligible. Hence, the KCC could be kept in the solid state at room temperature for long times. The observation was made when a solid sample of poly-**3** was stored at room temperature over a 24 month period, the change of the specific optical rotation was found to be negligible.

2.6. Molecular weight dependence of optical rotation of polyguanidines

Helix reversals can migrate up and down the chains by a series of bond rotations along the backbone. There are two possible mechanisms for loosing helical reversals (Figure 2.21). The reversals can rotate off the end of the polymer chains or disappear by moving together and annihilating one another. Whatever the mechanism, the rate is proportional to the concentration of the reversals.

The molecular weights (measured by monomer/initiator ratio) in the Table 2.2 is relative since the polymers tend to adhere to the GPC columns, and hence, it is difficult to get the exact molecular weights. However, due to the advantages of living polymerization, the molecular weight can be controlled stoichiometrically by the ratio of monomer and initiator.

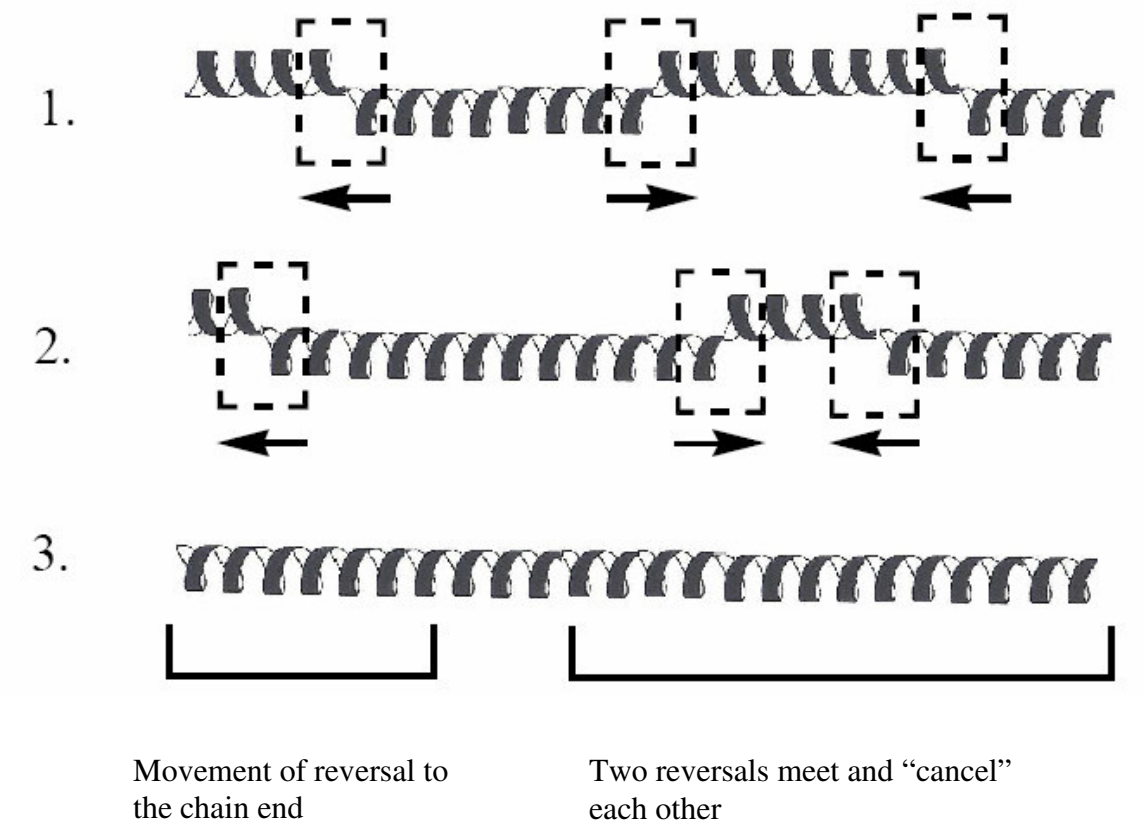

Figure 2.21. Two possible mechanisms for lose helical reversals.

From the data in Table 2.2, it can be seen that the polymers with shorter chains have larger (more positive) optical rotations. The reason might be that there are fewer helix reversals in the shorter polymers, which results in the higher orderliness and in most of the chains adopting the preferred single-handed screw sense. The annealing behavior in Figure 2.22 also supports the aforementioned hypothesis. The longer the polymer chain is, the more helical reversals present, and the longer it takes to reach the TCC from the KCC.

Table 2.2. The specific optical rotation of poly-**3** (virgin) with different molecular weights.

	1	2	3	4	5
Monomer/ Initiator	100	200	400	600	1000
[α] *	333	-126	-169	-164	-174

* The measurement is in chloroform at room temperature.

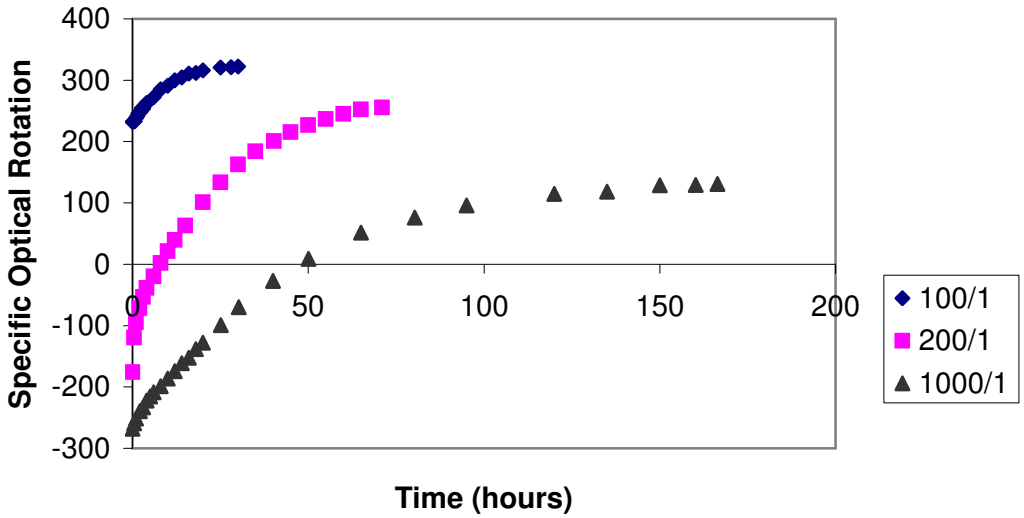

Figure 2.22. The evolution of the optical rotation of poly-**3** of different molecular weights at 70 ºC.

2.7. Cooperativity through chiral seeding

Pedant chiral centers on helical polymers introduce a diastreomeric relationship between the right- and left-handed senses, which can result in an excess of a particular helix sense. The homopolymerization of chiral monomers is a classic example of this

phenomenon. However, this approach is usually limited by high costs, the small number of viable monomers, and frequently long synthetic routes. Hence, other methods for generating these diastereomeric polymers are of interest. Two such approaches are: 1. helix-sense selective polymerization of achiral monomers using chiral catalysts; and 2. the incorporation of small amounts of optically active monomers. In the latter, the cooperativity still relies on the presence of chiral monomers to force a preferred handedness, but the quantity is reduced considerably.

Incorporation of chiral monomer units into achiral polymers can induce remarkable optical activities in the copolymers, which changes disproportionately with the mole fraction of the chiral monomer. This is due to the chiral perturbation of the chiral units that force the achiral units to adopt the helical conformation with the same sense as itself. The chiral unit is referred to as a sergeant because it forces the achiral unit, a soldier, to adopt a particular helical conformation, thus the resulting polymer is referred to as a sergeant and soldier copolymer. In the present model, the two monomer units share the same backbone with different side chains for each monomer type. The chain consists of an alternating sequence of left- and right-handed helices separated by helical reversals with one helical sense in excess.

Results obtained by Green and coworkers have shown that as the amount of chiral units was increased in helical polyisocyanates, a linear increase in the optical activity is followed by a plateau. They concluded that the optical rotation of the copolymer will increase as the number of chiral monomers increases and a copolyisocyanate containing

15% sergeant is nearly indistinguishable from that of a polymer composed purely of the chiral monomer (Figure 2.23).[1,19-21]

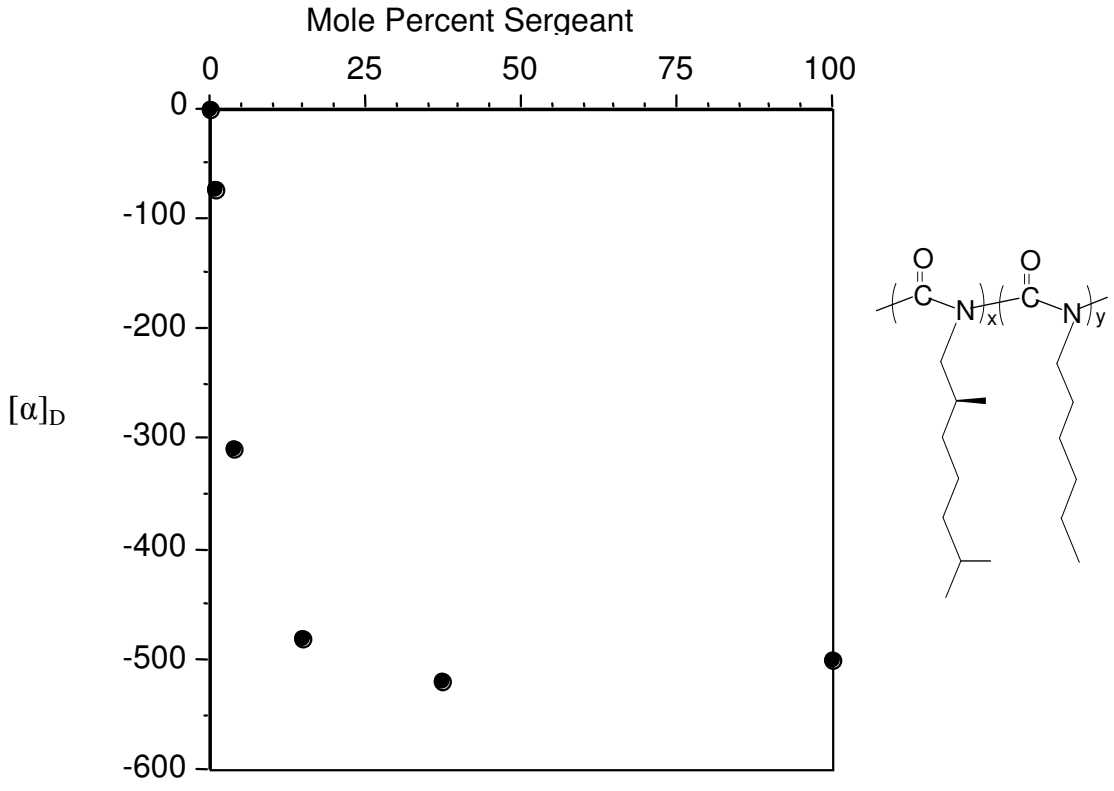

Figure 2.23. Optical rotation for a series of polyisocyanates containing different amount of of (R)-2,6- dimethylheptyl isocyanate (sergeant) and n-hexyl isocyanate (solider).[1,20]

Our present study is concerned with the random copolymers of *N*-(*R)*-2,6-dimethylheptyl-*N'*-phenylcarbodiimide (**3**) and *N*-hexyl-*N'*-phenylcarbodiimide (**6**). These copolymers show remarkable optical rotations, which originates from the conformational perturbations induced by the chiral monomers. This is due to an imbalance in the stability between left- and right-handed helices of the monomer, which is greatly amplified along the

long chain assisted by the difficulty of introducing helical reversals. However, to our surprise, we found that the optical rotation increases for the virgin copolymers as the percent of the chiral monomer decreases (Figure 2.24). Furthermore, in the annealing studies at 70°C, the copolymers containing more chiral units have lower optical rotations after reaching their plateau values, take longer to reach the TCC, and the absolute value of the change is smaller (Figure 2.25). These results show the cooperativity of polyguandines is different from that observed for the polyisocyanates.

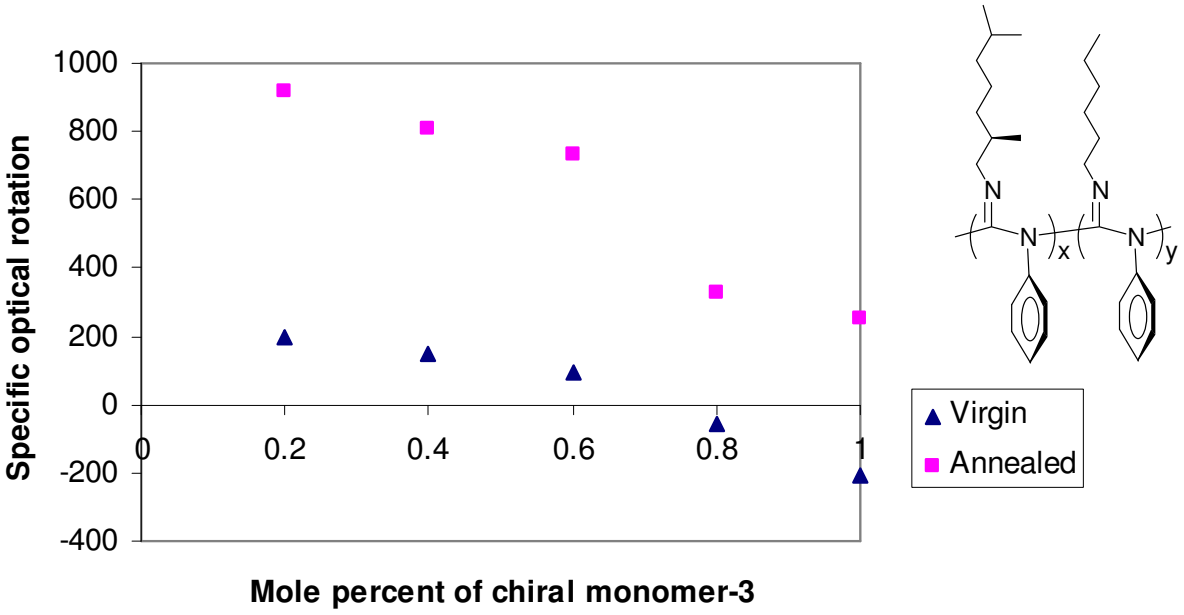

Figure 2.24. Optical rotation for a series of poly (**3**-*co*-**6**) containing different amounts of sergeant and soldier monomers.

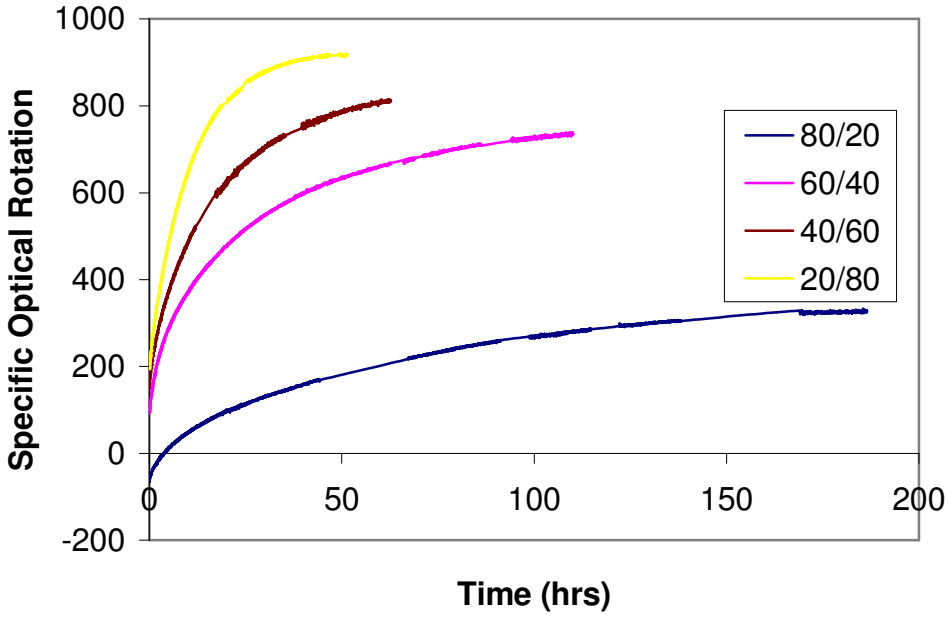

Figure 2.25. The specific optical rotation of the poly (**3**-*co*-**6**) as a function of time .

The reason for these differences may be the difference and variations of the conformations and inversion barrier energies between these two kinds of polymers. The structure of polymers, and many materials, is commonly represented on two dimensional media with the third dimension implied in some fashion (e.g., dashes/wedges). Many times this two-dimensional representation is mistakenly assumed to be the conformation of the material, when in fact, many more complex conformations are usually possible in the true three dimensional environment. Polyisocyantes and polyguanidines are no exception to this rule. Research has indicated the structures of those polymers more likely exists as that shown in Figure 2.26.[16,22] The interactions between the chiral side chains and the backbone carbonyl or imine groups of the adjacent repeat unit become more obvious in these conformations. The interaction not only forces the carbonyl oxygen or imine nitrogen

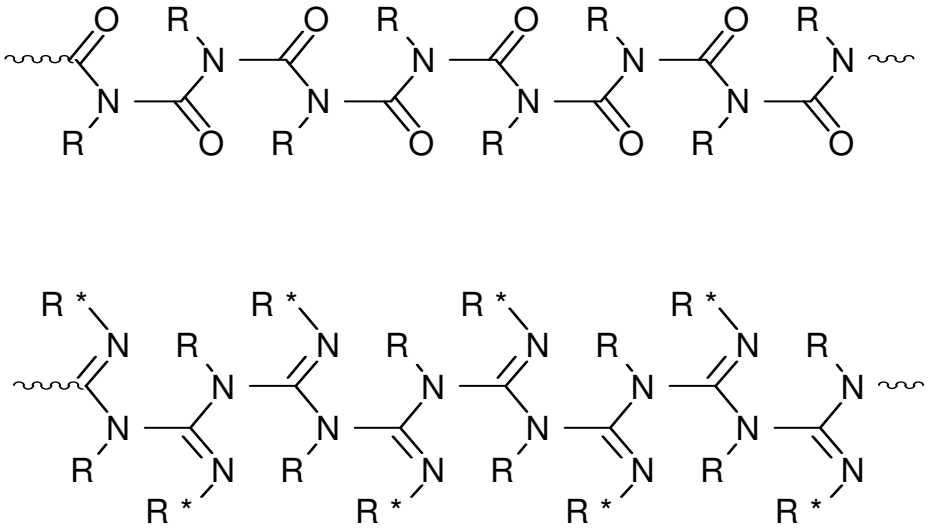

Figure 2.26. The more realistic two-dimensional depictions of the polyisocyanate chain (upper) and polyguanidines (lower).

out of the planar structure, which leads to the helical nature of those polymers, but is responsible for the cooperativity in the copolymers. For polyisocyanates, the lower helix inversion barrier of approximately 19 kcal/mol, does not appear to be dependant on the identity of the adjacent monomers, and allows inter-conversion of left- and right-handed helical conformation at nearly ambient temperature.[3] Therefore the 'soldiers' take the 'sergeants' preferred screw sense which is the thermodynamically controlled preference. The effectiveness of relatively small amounts of chiral units to the optical activity is comparable to that obtained from the pure chiral monomers. While in polyguanidines, the barrier appears to depend heavily on the branching of the side chains. In poly (**3**-*co*-**6**), adjacent units of monomer **3** increase the inversion barrier due to steric interactions of the methyl branches in the *β*–positions. The more chiral units present, the higher the reversal

energy, and the more disorder that will be present, thus necessitating the longer annealing times.

To support this hypothesis we measured the activation energy for the annealing of poly-**3** to be 29.2 kcal/mol (*vide supra*). And the activation barrier for poly-**6** has been measured independently and was found it to be lower at 25.6 kcal /mol.

As the homochiral units are dominating in the copolymer with a high content of **3**, the properties associated with these units such as the biased helix conformation and the character of the copolymers is similar as that of an enantiomerically pure sample. When the percentage of chiral units is decreased, the achiral units are induced to be one particular screw sense by the interaction with chiral units. Such cooperativity could be extended over long length scales since the majority of the chain is made up of the same monomer. Thus, there is less disorder and reversals along the chains, and the orderliness of the polymers is higher. When such copolymers are heated and compared with the copolymer with more chiral units, it is easier to get to the TCC from the KCC due to the lower activation energy barriers.

2.8. Helix-sense-selective polymerization of carbodiimides from achiral monomers

The preparation of optically active polymer from a chiral monomer is sometimes inconvenient, because it requires a large amount of expensive chiral starting materials. A more attractive strategy is to polymerize achiral monomers with a catalytic amount of initiator/catalyst. However, only a very few attempts have been found to be successful in this regard.[25,26] Herein, we present an example of helix-sense-selective polymerization of

carbodiimides: the synthesis of optically active polyguanidines from achiral carbodiimides using chiral catalysts.

We focused on a chiral titanium catalyst system. Our group has discovered that titanium(IV) alkoxide, amidinate, and amide complexes catalyze the living polymerization of carbodiimides.[7] Modification of the catalyst by attaching chiral ligands, such as (*S*)-binaphthnol (BINOL) and (*R*)-binaphthnol (BINOL), to the titanium center affords potential catalysts ((*S*)-BINOL-Ti) (**III**) and ((*R*)-BINOL-Ti) (**IV**) (Scheme 2.5).[27] Presumably, initiation of the polymerization proceeds through insertion of a carbodiimide into the isopropoxyl-titanium bond to afford an amidinate complex, which could then act as the propagation species in the polymerization process. Meanwhile, the chiral BINOL ligand affects the stereochemistry at the active catalytic site and subsequently controls the conformation of polymer chain to form optically active polyguanidines.

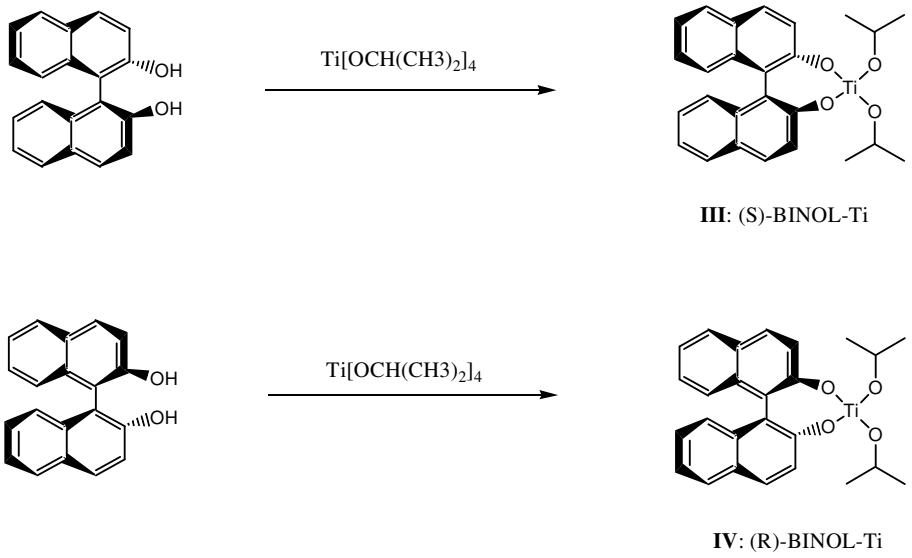

Scheme 2.5. Preparation of optically active catalysts **III** and **IV**.

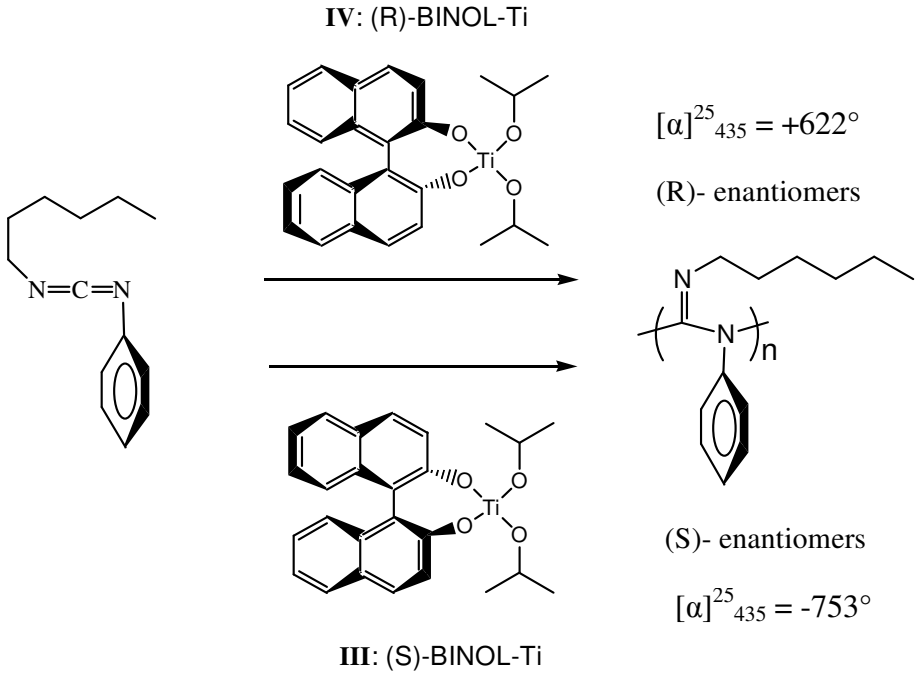

Scheme 2.6. Polymerization of achiral carbodiimide monomer-**6** with the chiral titanium catalysts.

The carbodiimide monomer **6** was polymerized with the catalysts **III** and **IV** (Scheme 2.6). High reaction yields were achieved in reasonable reaction times and showed varying degrees of asymmetric induction. Furthermore, the polymers produced were found to be optically active, verifying that the chiral ligand indeed affected the conformation of the polymer chains. The optical rotations of the polymers catalyzed with **III** and **IV** were measured to be $[\alpha]^{25}_{435}$ = -753° and +622°, (*c* = 0.2 in toluene), respectively. Furthermore, they show essentially mirror images in the CD spectra (Figure 2.27). Both of the results indicate chiral catalysts could produce helical polymers with one dominant screw sense and

the helix-sense-selective polymerization of carbodiimides was achieved. Another achiral carbodiimide monomer **1** also was polymerized by **III** and the optical rotation, $[\alpha]^{25}_{435}$ = -44° (*c* = 0.2 in toluene), is smaller than poly-**6** in absolute value.

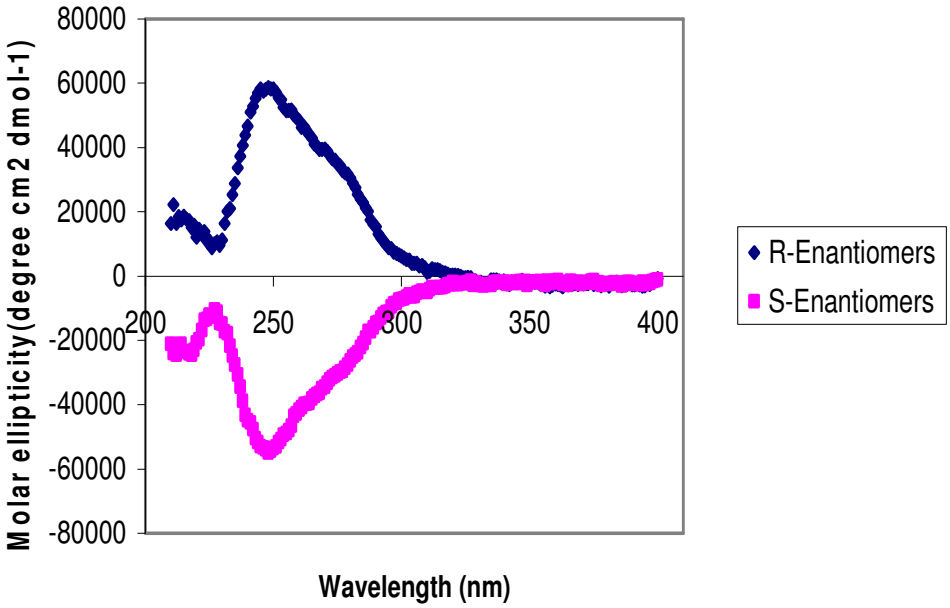

Figure 2.27. CD spectra of enantiotopic poly-**6**.

By measuring optical rotations as a function of time, we discovered that the optical activity stabilities of poly-**1** and poly-**6** were temperature dependent. Figure 2.28 shows the change in optical activity of poly-**6** as a function of time at different temperatures. The optical activity was relatively stable at 25 °C (k_{obs} = 3.96 s^{-1}, $t_{1/2}$ = 1578 hrs). However, the optical rotation decreased rapidly and approached 0° after 15 hour when the toluene polymer solution was heated at 70 °C (k_{obs} = 920 s^{-1}, $t_{1/2}$ = 2.7 hrs). We ascribe this behavior to the conversion of the chains with predominated screw sense to the racemic

mixture of chains through a helix inversion process. At the same annealing temperature, the racemization rate of poly-**1** is faster than that of poly-**6**, which indicates that helix inversion rates of polymers were affected by the size of side chains. Bulky groups slow the inversion of the helix conformation.

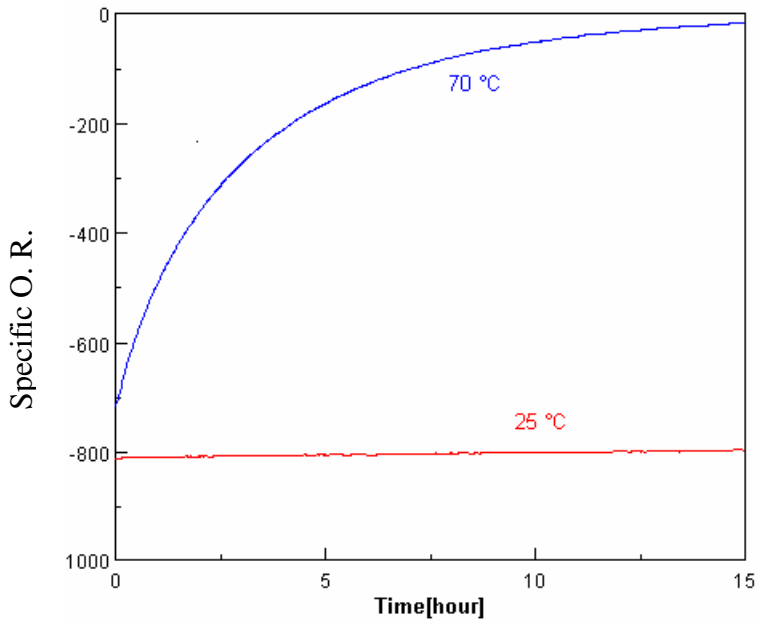

Figure 2.28. The specific rotation of poly-**6** as a function of time and annealing temperature.

The mutarotation of poly-**1** and poly-**6** provided opportunities for kinetic studies in great detail. Plots of $\ln\{([\alpha]-[\alpha]_\infty/([\alpha]_0-[\alpha]_\infty)$ versus time yielded linear lines at different temperatures, which suggested that the helix inversion is the first order with respect to polymer concentration. From Arrhenius plots, the apparent activation energy barriers for racemization were calculated to be 22.8 kcal and 25.6 kcal/mol for poly-**1** and poly-**6**, respectively.

Recently, our group also reported some stable polyguanidine helices in the solution, for example, poly[*N*-methyl-*N'*-(2-methyl-6-isopropylphenyl)guanidines] and Poly{*N*-(1-anthryl)-*N'*-[(*R*)- and/or (*S*)-3,7-dimethyloctyl]guanidines},[18,28] even after they were annealed at higher temperature. Such extremely stable helical polyguanidines will offer utility potential, for example, in applications such as chiral HPLC stationary phase and novel liquid crystalline materials.

2.9. Conclusion

The polymerization of *N*-(*R*)-2,6-dimethylheptyl-*N'*-phenylcarbodiimide, **3**, with titanium(IV) trifluoroethoxide, catalyst **II**, produces a polymer, which possesses predominant one handed helical sense which results from the amplification of optical activity by induction of asymmetric center into the polymer chains. Annealing the polymer solution at elevated temperature resulted in the change in the magnitude and sign of the optical rotation. This phenomenon was also characterized by the CD and ^{19}F NMR. We ascribe such change to an evolution of the polymer chains from kinetically controlled conformations (KCC) to thermodynamically controlled conformations (TCC). The apparent activation barrier for reorganization was calculated to be 29.2 kcal/mol. The kinetic barrier of nearly 30 kcal/mol makes the isolation of these KCC possible and therefore, the conformation after annealing is irreversible and is stable at room temperature.

Random copolyguanidines of chiral and achiral monomers show remarkable optical rotations, which originates from conformational perturbations of the chiral carbodiimide monomers that display good cooperativity. Due to its different structure, the polyguanidines show different cooperativity than the polyisocyanate.

Predominant single handed helical polyguanidines were also achieved by helix-sense-selective polymerization with chiral catalysts. The polymers produced by the enantiotopic catalysts show essential mirror images resulting from adopting an opposite screw sense.

2.10. Experimental section

2.10.1. General procedures and characterization

Instruments

Air and moisture sensitive procedures were carried out using standard Schlenk techniques or in a Unilab glove box under an atmosphere of nitrogen. All glassware was either flame dried or oven dried overnight. All infrared spectra (cm^{-1}) were recorded in on NaCl plates and were acquired on a JASCO FT/IR-410 spectrometer. Wavenumbers in cm^{-1} are reported for characteristic peaks. The ^{1}H and ^{13}C NMR spectra were measured in $CDCl_3$ on a Mercury 300 or 400 spectrometers. Chemical shifts are reported in δ (ppm) relative to tetramethylsilane as internal standard. ^{19}F NMR spectra were measured at 376.46 MHz using a Varian-Mercury NMR spectrometer in $CDCl_3$. Except for the result in the Figure 2.16, ^{19}F NMR spectra are referenced to C_6F_6 used as an external 0 ppm reference. UV-vis/CD spectra were recorded on a JASCO J-600 spectropolarimeter. A NESLAB RTE-210 circulating water bath was used to vary the temperatures of the samples. The path length of cell is 10 mm. UV-vis spectra were recorded on a JASCO V-550 spectrophotometer. Optical rotation measurements were taken on a JASCO P-1010 polarimeter at 435 or 589 nm in a thermostatted 50 mm the cell at 25 °C unless noted otherwise. All solution for optical rotation measurements were 0.2 g/100 mL prepared in volumetric flasks at room temperature. The polymers were allowed to be dissolved (several hours to overnight) at room temperature. Annealing experiments were conducted on polymers dissolved in solution in the sealed cell with water jacket to eliminate any concentration changes. The

temperature of the sample was controlled by utilizing a NESLAB RTE-140 circulating water system in conjunction with a water jacket surrounding the cell.

Reagents

Unless otherwise noted all reagents used were obtained from a commercial supplier and were used without further purification. The solvents used for air and water sensitive procedures were purified via chromatography except for the THF, which were distilled from a Na/benzophenone ketyl under nitrogen. The solvents used for the measurement of optical rotation and CD are A.C.S. spectrophotometic grade. Unless otherwise noted, all other solvents were reagent grade and used without further purification.

2.10.2. Experimental procedures and characterizations

(*R*)-(+)-citronellic acid

(*R*)-Pulegone (83.73g, 0.55mol, vacuum distilled) was added to a 3-neck round bottom flask containing a gas inlet, suitable for submersing in the solution, and a gas outlet. The reaction flask was cooled to 0 °C and anhydrous HCl (g) was bubbled through the pulegone for 3.5 h. HCl (g) was produced by adding concentrated hydrochloride acid dropwise to the concentrated sulfuric acid and purified by passing the gas through concentrated sulfuric acid again. The color of reaction solution changed from light yellow to dark red. The dark red mixture was poured into aqueous NaOH (5% (w/w), 1.6 L) and stirred for 5 h. A white precipitate formed in the aqueous layers followed by becoming light yellow milky solution. The mixture was separated and the aqueous layer was extracted with ether (3 x 100 mL). The combined ether aliquots were extracted with aqueous NaOH (15% (w/w), 2 x 60 mL); these aqueous fractions were acidified with cold hydrochloride acid and

extracted the aqueous phase with ether (2 x 100 mL). All of the ether fractions were combined and extracted with water (2 x 50 mL) followed by brine (2 x 50 mL). The ether fraction was dried over anhydrous magnesium sulfate. The solvent was removed by rotary evaporator, and light yellow liquid was vacuum distilled (0.1 Torr, 102 °C) to give a clear colorless liquid (54.44g, 58.2%). IR (neat): 3624-2167 (s, br), 2966 (s), 2920 (s), 2677 (s), 1712 (s), 1437 (s), 1410 (s), 1379 (s), 1300 (s), 1230 (s), 1164 (m), 1111 (m), 1081 (m), 941 (s), 826 (m). ^{1}H NMR: 5.09 (1H, t), [2.40 (d) and 2.35 (d), 1H], 2.16 (1H, m), 1.98 (3H, m), 1.68 (3H, s), 1.60 (3H, s), 1.37 (1H, m), 1.26 (1H, m), 0.99 (3H, d). ^{13}C NMR {^{1}H}: 179.8, 131.6, 124.1, 41.5, 36.7, 29.8, 25.7, 19.6, 17.6. Specific rotation: (neat) $[\alpha]_D = 8.71°$.

(*R*)-(+)-5,6-dihydrocitronellic acid

To a high pressure hydrogenation bottle was added (*R*)-(+)-citronellic acid (28 g, 0.166 mol) in methanol (100 mL). The bottle was briefly purged with nitrogen and 10% palladium on activated carbon (Pd/C, 1.0 g) was added. The bottle was placed under hydrogen (60 psi) and stirred overnight. The Pd/C was removed via filtration. The methanol was removed on a rotary evaporator and the material was vacuum distilled (85 mTorr, 75 °C) to give a clear colorless liquid (24.8 g, 87.6%). IR: 3500-2500 (m, br), 3059 (m), 2958 (s), 2679 (m), 1703 (s), 1463 (s), 1410 (s), 1384 (m), 1366 (m), 1295 (s), 1216 (s), 1184 (m), 909 (s). ^{1}H NMR: 2.34 (1H, dd), 2.14 (1H, dd), 1.95 (1H, br), 1.57, (1H, m), 1.31-1.16 (6H, m), 0.97 (3H, d), 0.87 (6H, d). ^{13}C NMR {^{1}H}: 180.3, 41.7, 39.0, 36.9, 30.1, 27.9, 24.6, 22.6, 22.5, 19.6. Specific rotation: (neat) $[\alpha]_D = 5.16°$.

(*R*)-(+)-5, 6-dihydrocitronellic acid chloride

To a 100 mL 3-neck flask was added oxyle chloride (14.97 mL, 0.172 mol, 1.2 eq). *N,N'*-dimethylformamide (5 drops) was added to the flask and a white precipitate formed. The flask was cooled to 0° C and (*R*)-(+)-5,6-dihydrocitronellic acid (24.6 g, 0.143 mol) was added dropwise over 30 min. The mixture was stirred for 2.5 h at 0 °C followed by heating at 80 °C for 2 h. The yellow liquid was then vacuum distilled (0.1 Torr, 40 °C). A clear color liquid (24.75 g, 95.9%) was obtained. IR: 2957 (s), 2930 (s), 2869 (m), 1799 (s), 1466 (m), 1401 (w), 1384 (m), 1366 (w), 1216 (m), 1135 (w), 986 (m), 929 (m). ^{1}H NMR: 2.86 (1H, dd), 2.71 (1H, dd), 2.08 (1H, br), 1.52, (1H, m), 1.33-1.14 (6H, m), 0.99 (3H, d), 0.88 (6H, d). ^{13}C NMR {^{1}H}: 173.5, 54.6, 39.2, 36.7, 31.1, 28.2, 24.9, 23.0, 22.9, 19.6. Specific rotation: $[\alpha]_D = 5.16°$. (chloroform, c = 4.4).

(*R*)-(+)-2,6-dimethylheptylisocyanate

To a 100 mL Schlenk flask equipped with a condenser and nitrogen inlet was added (*R*)-(+)-5,6-dihydrocitronellic acid chloride (24.29g, 0.128 mol) followed by toluene (15 mL). Azidotrimethlysilane (18.6 mL, 0.14 mol, 1.1 eq) was added to the mixture and stirred at room temperature for 30 min and then refluxed for 20 h. The yellow liquid was vacuum distilled (90 mTorr, 41 °C) to give a clear colorless liquid (18.67 g, 86.3%). IR: 2957 (s), 2929 (s), 2870 (s), 2266 (s), 1466 (m), 1384 (m), 1366 (m), 1216 (m). ^{1}H NMR: 3.19 (2H, m), 1.71 (1H, br), 1.54 (1H, m), 1.4-1.15 (6H, m), 0.97 (3H, d), 0.88 (6H, d). ^{13}C NMR {^{1}H}: 124.0, 119.9, 47.0, 37.2, 32.8, 32.1, 26.0, 22.7, 20.7, 15.5. Specific rotation: (neat) $[\alpha]_D = 0.5482°$.

***N*-(*R*)-2,6-dimethylheptyl-*N'*-phenylurea**

A 100 mL round bottom flask was charged with 1.73 g (*R*)-(+)-2,6-dimethylheptyl isocyanate (10.2 mmol), a magnetic stir bar and 20 mL reagent grade chloroform. The resulting solution was cooled to 0 °C by the use of an ice bath. Over the next 30 min, the solution of 0.93 mL aniline (10.2 mmol (distilled before using)) in 10 mL chloroform was added to the cooled solution. The resultant solution was stirred overnight at room temperature after the addition of the aniline. The solvent was removed on a rotary evaporator. The unisolated urea was used directly for the subsequently condensation to the carbodiimide.

_N_-(_R_)-2,6-dimethylheptyl-_N'_-phenylcarbodiimide

Most carbodiimides were prepared similarly with a slight modification of literature procedures.[29] The following description of the preparation of *N*-(*R*)-2,6-dimethylheptyl-*N'*-phenylcarbodiimide serves as a typical example. A dry 200 mL three neck flask was charged with 20 mL CH_2Cl_2, 2.63 g triphnylphosphine (10 mmol, 1.25 eq). A dry pressure equalizing addition funnel was charged with 10 mL CH_2Cl_2 and 0.52 mL bromine (10 mmol, 1.25 eq) and was then placed on the 3-neck flask. The whole apparatus was placed under a dry nitrogen atmosphere and the triphenylphosphine solution was cooled by an ice bath and stirred vigorously. The bromine solution was added dropwise over the course of 30 min. The mixture turned yellow and was allowed to stir for an additional 10 min. 2.78 mL of triethylamine (20 mmol, 2.5 eq) was added to the resulting suspension of dibromotriphenylphosphorane. The unisolated *N*-(*R*)-2,6-dimethylheptyl-*N'*-phenyl urea (ca. 2.10 g, 8.0 mmol, 1.0 eq) was added as a viscous liquid in 20 mL CH_2Cl_2 under a nitrogen flow in three potions at 0 °C over 15 min. The cooling bath was removed after the reaction

mixture stirred over 1 h, then it was allowed to stir at room temperature for additional 1 h. The reaction could be monitored by infrared spectroscopy. Strong adsorption of 2130 cm^{-1} N=C=N antisymmetric stretch suggests that the reaction is nearing completion and can be stopped within an additional 30 min of stirring. The CH_2Cl_2 was removed by rotary evaporation. The orange precipitate was extracted with 200 mL hexane followed by filtration to remove the triphenylphosphine oxide. The solvent was removed to leave an oil material. Distillation of the extracts from CaH_2 using a short path distillation head at 87 °C and 40 mTorr afforded a clear, colorless liquid (1.77 g, 90.7%). IR: 2134 (s, N=C=N). ^{1}H NMR: 7.29 (m, 3H), 7.01 (m, 2H), 3.33 (m, 2H), 1.75 (m, 1H), 1.53 (m, 1H), 1.43-1.15, (m, 6H), 1.01 (d, 3H), 0.88 (d, 6H). ^{13}C NMR {^{1}H}: 141.0, 134.0, 129.5, 128.9, 124.6, 124.4, 123.7, 53.0, 39.3, 35.0, 34.4, 28.1, 24.8, 22.9, 22.8, 18.0. $[\alpha]_{435}^{25}$ = -0.32° (toluene, C= 0.20)

***N,N'*-di-*n*-hexylcarbodiimide**

The same procedure for the preparation of *N*-(*R*)-2,6-dimethylheptyl-*N'*-phenylcarbodiimide was employed. The quantities of reagents used were 7.4 g hexylisocyanate (58 mmol), 5.84 g hexylamine (58 mmol), 19.01 g triphenylphosphine (72.5 mmol, 1.25 eq), 3.73 mL bromine (72.5 mmol, 1.25 eq) and 20.0 mL triethylamine (145 mmol, 2.5 eq). Distillation: 60-65 °C, 0.15 Torr. Yield: 11.8 g, (96.9%). IR: 2131 (s, N=C=N). ^{1}H NMR (400 MHz, $CDCl_3$) δ: 3.14 (t, 4H), 1.50 (tt, 4H), 1.23 (m, 12H), 0.82 (t, 6H). ^{13}C NMR {^{1}H} (100 MHz, $CDCl_3$) δ: 144.4, 46.09, 41.06, 31.34, 31.23, 26.44, 22.51, 13.93.

***N*-(*n*-hexyl)-*N'*-isopropylcarbodiimide**

The same procedure for the preparation of *N*-(*R*)-2,6-dimethylheptyl-*N'*-phenylcarbodiimide was employed. The quantities of reagents used were 6.36 g hexylisocyanate (50 mmol), 2.95 g isopropylamine (50 mmol), 16 g triphenylphosphine (60 mmol, 1.2 eq), 3.25 mL bromine (60 mmol, 1.2 eq) and 17.5 mL triethylamine (120 mmol, 2.4 eq). Distillation: 55-60 °C, 0.5 Torr. Yield: 7.2 g, (85.7 %). IR: 2119 (s, N=C=N).^{1}H NMR (400 MHz, $CDCl_3$) δ: 3.54 (heptet, 1H), 3.18 (t, 2H), 1.55 (m, 2H), 1.30 (m, 6H), 1.20 (d, 6H), 0.87 (t, 3H); ^{13}C NMR {^{1}H} (100 MHz, $CDCl_3$) δ: 140.31, 48.93, 46.85, 31.39, 31.34, 26.53, 24.61, 22.56, 13.98.

_N_-(_R_)-2,6-dimethylheptyl-_N'_-isopropylcarbodiimide

The same procedure for the preparation of *N*-(*R*)-2,6-dimethylheptyl-*N'*-phenylcarbodiimide was employed. The quantities of reagents used were 6.16 g (*R*)-(+)-2, 6-dimethylheptyl isocyanate (36.4 mmol), 2.15 g isopropylamine (36.4 mmol), 11.9 g triphenylphosphine (45.5 mmol, 1.25 eq), 2.34 mL bromine (45.5 mmol, 1.25 eq) and 12.65 mL triethylamine (91 mmol, 2.5 eq). Distillation: 65 °C, 0.14 Torr. Yield: 1.82 g, (23.8 %). IR: 2123 (s, N=C=N).^{1}H NMR (400 MHz, $CDCl_3$) δ: 3.55 (m, 1H), 3.11 (m, 2H), 1.65 (m, 2H), 1.22-1.12 (m, 12H), 0.93 (t, 3H), 0.87 (d, 6H); ^{13}C NMR {^{1}H} (100 MHz, $CDCl_3$) δ: 140.31, 53.21, 49.03, 39.28, 34.95, 34.46, 28.04, 24,79, 24.70, 22.80, 22.74, 22.69, 17.89. $[\alpha]_{435}^{25}$ = 3.48° (chloroform, c = 2.16).

_N_-(_n_-hexyl)-_N'_-phenylcarbodiimide

The same procedure for the preparation of *N*-(*R*)-2,6-dimethylheptyl-*N'*-phenylcarbodiimide was employed. The quantities of reagents used were 24.11 g phenyl isocyanate (0.2 mol), 20.2 g hexylamine (0.2 mol), 65 g triphenylphosphine (0.25 mol, 1.25

eq), 13 mL bromine (0.25 mol, 1.25 eq) and 70 mL triethylamine (0.5 mol, 2.5 eq). Distillation: 90 °C, 0.1 Torr. Yield: 35 g, (69.2 %). IR: 2131 (s, N=C=N). ^{1}H NMR (400 MHz, $CDCl_3$) δ: 7.28 (m, 3H), 7.07 (m, 2H), 3.40 (t, 2H), 1.67 (m, 2H), 1.41 (m, 2H), 1.31 (m, 4H), 0.88 (t, 3H). ^{13}C NMR {^{1}H} (100 MHz, $CDCl_3$) δ: 140.8, 136.0, 129.3, 124.5, 123.5, 46.85, 31.34, 31.28, 26.46, 22.51, 13.94.

***N, N'*-di-4-butylphenylcarbodiimide**

The same procedure for the preparation of *N*-(*R*)-2,6-dimethylheptyl-*N'*-phenylcarbodiimide was employed. The quantities of reagents used were 5.0 g 4-butylphenyl isocyanate (28.5 mmol), 4.26 g 4-butylphenyl amine (28.5 mmol), 9.0 g triphenylphosphine (34 mmol, 1.25 eq), 1.75 mL bromine (34 mmol, 1.25 eq) and 9.2 mL triethylamine (68 mmol, 2.5 eq). Distillation: 175-180 °C, 0.03 Torr. Yield: 7.82 g, (93 %). IR: 2112 (s, N=C=N). ^{1}H NMR (400 MHz, $CDCl_3$) δ: 7.11 (m, 8H), 2.61 (t, 4H), 1.60 (m, 4H), 1.38 (m, 4H), 0.95 (t, 6H). ^{13}C NMR {^{1}H} (100 MHz, $CDCl_3$) δ: 140.6, 136.3, 129.6, 124.1, 35.3, 33.9, 22.5, 14.2.

***N*-(*R*)-2,6-dimethylheptyl-*N'*-2, 2, 2-trifluoroethylcarbodiimide**

The same procedure for the preparation of *N*-(*R*)-2,6-dimethylheptyl-*N'*-phenylcarbodiimide was employed. The quantities of reagents used were 3.71 g (*R*)-(+)-2,6-dimethylheptyl isocyanate (22 mmol), 2.17 g isopropylamine (22 mmol), 7.25 g triphenylphosphine (27.5 mmol, 1.25 eq), 1.41 mL bromine (27.5 mmol, 1.25 eq) and 7.66 mL triethylamine (55 mmol, 2.5 eq). Distillation: 60 °C, 0.15 Torr. Yield: 2.24 g, (38.0 %). IR: 2147 (s, N=C=N).^{1}H NMR (400 MHz, $CDCl_3$) δ: 3.72 (q, 2H), 3.19 (m, 2H), 1.72-1.48 (m, 2H), 1.34-1.14 (m, 6H), 0.95 (d, 3H), 0.87 (d, 6H). ^{13}C NMR {^{1}H} (100 MHz, $CDCl_3$)

δ: 138, 126, 52.4, 48.3, 39.3, 34.7, 34.4, 28.1, 24.8, 22.75, 22.66, 17.7. $[\alpha]_{435}^{25}$ = 4.89° (chloroform, c = 1.5).

_N_-(_R_)-2,6-dimethylheptyl-_N'_-4-fluoro-phenylcarbodiimide

The same procedure for the preparation of _N_-(_R_)-2,6-dimethylheptyl-_N'_-phenylcarbodiimide was employed. The quantities of reagents used were 1.54 g (_R_) - (+)-2, 6-dimethylheptyl isocyanate (9.1 mmol), 1.01 g 4-fluorophenylamine (9.1 mmol), (the addition of urea is 2.2 g, 7.9 mmol), 2.52 g triphenylphosphine (9.8 mmol, 1.25 eq), 0.49 mL bromine (9.8 mmol, 1.25 eq) and 2.73 mL triethylamine (19.6 mmol, 2.5 eq). Distillation: 85 °C, 80 mTorr. Yield: 1.81 g, (87.4 %). IR: 2135 (s, N=C=N). ^{1}H NMR (400 MHz, $CDCl_3$) δ: 7.04-6.95 (m, 4H), 3.33 (m, 2H), 1.75 (m, 1H), 1.54 (m, 1H), 1.33 (m, 6H), 1.00 (d, 3H), 0.87 (d, 6H). ^{13}C NMR {^{1}H} (100 MHz, $CDCl_3$) δ: 161.2, 134.1, 128.9, 124.8, 116.4, 53.0, 39.3, 35.0, 34.5, 28.1, 24.8, 22.9, 22.8, 18.0. ^{19}F NMR ($CDCl_3$) δ: 43.6.

_N_-(_R_)-2,6-dimethylheptyl-_N'_-4-trifluoromethoxy-phenylcarbodiimide

The same procedure for the preparation of _N_-(_R_)-2,6-dimethylheptyl-_N'_-phenylcarbodiimide was employed. The quantities of reagents used were 1.6 g (_R_)-(+)-2, 6-dimethylheptyl isocyanate (9.5 mmol), 1.01 g 4-trifluoromethoxy-aniline (9.5 mmol), 3.05 g triphenylphosphine (11.88 mmol, 1.25 eq), 0.59 mL bromine (11.88 mmol, 1.25 eq) and 3.25 mL triethylamine (23.75 mmol, 2.5 eq). Distillation: 87 °C, 85 mTorr. Yield: 2.02 g, (64.8 %). IR: 2139 (s, N=C=N). ^{1}H NMR (400 MHz, $CDCl_3$) δ: 7.19-7.06 (m, 4H), 3.34 (m, 2H), 1.75 (m, 1H), 1.54 (m, 1H), 1.41-1.14 (b, 6H), 1.00 (d, 3H), 0.87 (d, 6H). ^{13}C NMR {^{1}H} (100 MHz, $CDCl_3$) δ: 140.1, 134.5, 124.6, 122.3, 122.0, 119.4, 52.9, 39.3, 34.9, 34.4, 28.1, 22.8, 22.7, 18.0. ^{19}F NMR ($CDCl_3$) δ: 103.8.

_N_-(_R_)-2,6-dimethylheptyl-_N'_-3, 5-bis-trifluoromethyl-phenylcarbodiimide

The same procedure for the preparation of _N_-(_R_)-2,6-dimethylheptyl-_N'_-phenylcarbodiimide was employed. The quantities of reagents used were 2.01 g (_R_)-(+)-2, 6-dimethylheptylisocyanate (11.9 mmol), 2.73 g 3,5-bis(trifluoromethyl)aniline (11.9 mmol), (the reaction of producing urea is slower and the yield was lower), 3.05 g triphenylphosphine (11.88 mmol, 1.25 eq), 0.59 mL bromine (11.88 mmol, 1.25 eq) and 3.25 mL triethylamine (23.75 mmol, 2.5 eq). Distillation: 85-90 °C, 85 mTorr. Yield: 1.8 g, (39.5 %). IR: 2162 (s, N=C=N). ^{1}H NMR (300 MHz, $CDCl_3$) δ: 7.56 (s, 1H), 7.46 (s, 2H), 3.41 (m, 2H), 1.80 (m, 1H), 1.53 (m, 1H), 1.41-1.12 (b, 6H), 1.03 (d, 3H), 0.87 (d, 6H). ^{13}C NMR {^{1}H} (100 MHz, $CDCl_3$) δ: 143.9, 134.1, 132.7, 128.9, 123.6, 117.7, 52.8, 39.2, 34.9, 34.4, 28.1, 24.8, 22.8, 22.7, 17.9. ^{19}F NMR ($CDCl_3$) δ: 99.0.

(2,2,2-trifluoroethoxy)trichlorotitanium(IV)

This compound was synthesized similarly with a slight modification of literature procedures.[30, 31] To a 50 mL Schlenk flask containing the mixture of 5 mL of dry benzene and 1.0 mL 2,2,2-trifluoroethnol (1.37g, 13.7 mmol) was added dropwise via syringe 1.65 mL titanium chloride (2.86 g, 15.1 mmol, 1.1 eq). The solution was stirred for 1 h at 0 °C by ice bath. The volatile materials were removed under vacuum. Then 5 mL dry hexane was added by syringe to wash the solid followed filtration under anhydrous condition. The white powder was obtained (1.64 g, 47.5%).

(S-BINOL)Ti(OiPr)$_2$

This compound was synthesized similarly with a slight modification of literature procedures.[32] To a suspension of dried (_R_)-1,1'-bi-2-naphthol (0.50 g, 1.7 mmol) in

toluene (10 mL) was added distilled $Ti(OPri)_4$ (0.51 mL, 1.7 mmol) at room temperature. After stirring for 1 h at room temperature, azeotropic distillation was carried on until the volume of the solution was reduced to 2 mL. Further concentration was continued under reduced pressure. The resulting orange residue was dissolved into ether (10 mL) and left to stand for 4 hours at -20 °C. The resulting needle–crystalline material was obtained by removing the supernatant solution with a syringe. The remaining ether solvent was removed under reduced pressure to give yellowish–orange crystals in 78% yield (0.6 g).

(R-BINOL)Ti(OiPr)$_2$

The same procedure used for the preparation of (S-BINOL)$Ti(OiPr)_2$ was employed, but with R-BINOL ligand.

General Method for the polymerization of carbodiimides

The following description serves as a general method for the polymerization of carbodiimides. All manipulations were performed in a glove box. A volumetric solution of the catalyst, depending upon the monomer-to-initiator ratio, was prepared using the appropriate solvent (toluene for **II**.) To a 20 mL vial with a magnetic stir bar, a measured amount of this solution was added followed by addition of the appropriate amount of carbodiimide monomer, and the vial was tightly capped with a rubber septum. The reaction was then stirred at room temperature. The color of the polymerization serves as an indicator: a persistent red-rust color indicates an active polymerization; white color indicates the Ti(IV) species has been deactivated, for example, by reaction with water. Over the course of several hours to several days, successful polymerizations would always become increasingly viscous, yet clear, until the solutions would cease to flow, or in the

case of an insoluble polymer, become cloudy and deposit the polymer as a white or light red solid, at which time the polymerization was assumed to be complete.

In the case of a copolymerization the comonomers were mixed well before the addition of any catalyst. In the cases where the polymerization was done in a solvent a stock solution of catalyst was prepared in either dry chloroform or dry toluene and a small amount of that solution was added to the monomer mixture.

After the polymerization was complete, the cap was removed from the vial and some toluene or chloroform was added to dissolve the solid dark red mass. The contents were stirred until dissolution was complete. The solution was then poured into about 100 mL of methanol resulting in a white solid precipitated. The concentration of the polymer solution prior to precipitation is critical. Solutions which are too concentrated will not precipitate well; they will form insoluble beads of polymer. Solutions which are too dilute will form a milky precipitate, which is very difficult to filter. The ideal concentration is one in which the polymer forms a string-like texture when added the methanol. After the precipitation is complete, centrifugation and filtration yielded the polymer as white mass which was placed in a second scintillation flask and dissolved in benzene. The benzene solution was frozen in liquid nitrogen and lyophilized yielding the polymer as fluffy, solid white plug. The general yield is about 70-90%.

Poly (*N,N'*-di-*n*-hexylcarbodiimide)

IR: 1648 (s, guanidine stretching). ^{1}H NMR (400 MHz, $CDCl_3$) δ: 4.00-4.20 (br), 2.80-3.20 (br), 1.00-1.47 (br), 0.60-1.00 (br). ^{13}C NMR (100 MHz, $CDCl_3$) δ: 48.76, 32.34, 31.92, 29.17, 27.73, 22.92, 14.14.

Poly [*N*-(*n*-hexyl)-*N'*-isopropylcarbodiimide]

IR: 1639 (s, guanidine stretching). ^{1}H NMR (400 MHz, $CDCl_3$) δ: 3.05-3.25 (br), 1.35-1.80 (br), 1.20-1.35 (br), 0.60-1.20 (br).

Poly [*N*-(*R*)–2,6-(dimethylheptyl)-*N'*-phenylcarbodiimide]

IR: 1643 (s, guanidine stretching).^{1}H NMR (400 MHz, $CDCl_3$) δ: 7.28 (br), 6.93 (br), 3.07 (br), 1.57 (br), 1.38 (br), 0.87 (br), 0.79 (br). ^{13}C NMR (100 MHz, $CDCl_3$) δ: 128.4, 122.3, 53.6, 39.4, 34.8, 28.4, 28.1, 24.9, 22.9,17.9. $[\alpha]_{435}^{25}$ = -209° (toluene, C= 0.20).

Poly [*N*-(*n*-hexyl)-*N'*-phenylcarbodiimide]

IR: 1624 (s, guanidine stretching). ^{1}H NMR (400 MHz, $CDCl_3$) δ: 7.2-6.4 (br), 2.8-3.6(br), 1.2-0.2 (br). ^{13}C NMR (100 MHz, $CDCl_3$) δ: 148.5, 148.2, 128.3, 122.1, 47.3, 31.8, 28.3, 26.3, 23.0, 14.4.

Poly [*N*-(*R*)-2,6-dimethylheptyl-*N'*-4-trifluoromethoxy-phenylcarbodiimide]

IR: 1632 (s, guanidine stretching).^{1}H NMR (400 MHz, $CDCl_3$) δ: 7.2-6.4 (br), 2.9 (br), 1.55 (br), 1.34 (br), 0.8 (br).

2.11. References and notes

1. Green, M. M.; Peterson, N. C.; Sato, T.; Teramoto, A.; Cook, R.; Lifson, S. *Science*, **1995**, *268*, 1860.
2. Lifson, S.; Andreola, C.; Peterson, N. C.; Green, M. M. *J. Am. Chem. Soc*. **1989**, *111*, 8850.
3. Ute, K.; Fukunishi, Y.; Jha, S. K.; Cheon, K. S.; Munoz, B.; Hatada, K.; Green, M. M. *Macromolecules*, **1999**, *32*, 1304.
4. Gu, H.; Nakamura, Y.; Sato, Teramoto, A.; Green, M. M.; Androela, C.; Peterson, N. C.; Lifson, S. *Macromolecules*, **1995**, *28*, 1016.
5. Okamoto, N.; Mukaida, F.; Gu, H.; Nakamura, Y.; Sato, T.; Teramoto, A.; Green, M. M.; Andreola, C.; Peterson, N. C.; Lifson, S. *Macromolecules*, **1996**, *29*, 2878.
6. Green, M. M; Cheon, K. S.; Yang, S. Y.; Park, J. W.; Swansburg, S.; Liu, W. H. *Acc. Chem. Res*. **2001**, *34*, 672.
7. Goodwin, A.; Novak, B. M. *Macromolecules*, **1994**, *27*, 5520.
8. Goodwin, A. Ph. D. thesis, University of California at Berkley, 1996.
9. Novak, B. M.; Goodwin, A.; Seery, T. *Polymer Preprints*, **1994**, *35*, 678.
10. Deming, T. J.; Novak, B. M. *Polymer Preprints*, **1991**, *32*, 641.
11. Novak, B. M.; Goodwin, A. *Polymer Preprints*, **1995**, *36*, 611.
12. Schlitzer, D. S.; Novak, B. M. *J. Am. Chem. Soc*. **1998**, *120*, 2196.
13. Pino, P. *Adv. Polym. Sci*. **1965**, *4*, 393.
14. Sanler, S. R.; karo, W. *Organic Functional Group Preparations*; Academic Press: New York, 1971.
15. Green, M. M.; Andreola, C.; Muńoz, B.; Reidy, M. P.; Zero, K. *J. Am. Chem. Soc*. **1988**, *110*, 4063.
16. Green, M. M.; Gross, R. A.; Crosby, C.; Schilling, F. C. *Macromolecules*, **1987**, *20*, 992.
17. Sears, D. W.; Beychok, S. *Physical Principles and Techniques and Protein Chemistry*; Part C; Leach, S. J., Ed., Academic: New York, 1973, Chapter 23.
18. Tang, H. Z.; Lu, Y. J.; Tian, G. L.; Capracotta, M. D.; Novak, B. M. *J. Am. Chem. Soc*. **2004**, *126*, 3722.
19. Gu, H.; Nakamura, Y.; Sato, T.; Teramoto, A.; Green, M. M.; Jha, S. K.; Andreola, C.; Reidy, M. P. *Macromolecules*, **1998**, *31*, 6362.
20. Green, M. M.; Reidy, M. P.; Johnson, R. J.; Draling, G.; O'Leary, D. J.; Willson, G. *J. Am. Chem. Soc*. **1989**, *111*, 6452.

21. Green, M. M.; Park, J. W.; Sato, T.; Teramoto, A.; Lifson, S.; Selinger, R. L. B.; Selinger, J. V. *Angew, Chem. Int. Ed*. **1999**, *38*, 3138.

22. Green, M. M.; Peterson, N. C.; Lifson, S.; Sato, T.; Teramoto, A. *Makromol. Chem., Macromol. Symp.* **1993**, *70/71*, 23.

23. Doty, P. Bradbury, J. H.; holtzer, A. M. *J. Am. Chem. Soc*. **1956**, *78*, 947.

24. Okamoto, Y.; Nakano, T.; Asakura, T.; Mohri, H.; Hatada, K. *J. Polym. Sci., Polym. Chem. Ed.* **1991**, *29*, 287.

25. Nakano, T.; Okamoto, Y. *Chem. Rev*. **2001**, *101*, 4013.

26. Okamoto, Y.; Nakano, T. *Chem. Rev*. **1994**, *94*, 349.

27. The BINOL-Ti catalyst system has been used in small molecule asymmetric synthesis. See ref. (a) Terada, M.; Matsumoto, Y.; Nakamura, Y.; Mikami, K. *Inorg. Chim. Acta*. **1999**, *296*, 267. (b). Keck, G. E.; Krishnaurthy, D. *J. Am. Chem. Soc*. **1995**, *117*, 2363.

28. Tian, G. L.; Lu, Y. J.; Novak, B. M. *J. Am. Chem. Soc*. **2004**, *126*, 4082.

29. (a) Bestmann, H. J. ; Lienert, J. ; Mott, L. *Lieb. Ann. Chem*. **1968**, *718*, 24. (b) Palomo, C.; Mestres, R. *Synthesis.* **1981**, 373.

30. Paul, Ram Chand; Sharma, Pratibha; Gupta, P. K.; Chadha, S. L. *Inorganica Chimica Acta*.**1976**, *20(1)*, 7.

31. Patten, Timothy E.; Novak, Bruce M. *J. Am. Chem. Soc*. **1996**, *118*, 1906.

32. Terada, M.; Matsumoto, Y.; Nakamura, Y.; Mikami, K. *Inorg. Chim. Acta* **1999**, *296*, 267-272

Chapter III: The Adsorption of Thiol Terminated Rod-like Polyguanidines on Gold Surface

3.1. Introduction to ultrathin organic films

Thin organic films of a thickness of a few nanometers (a monolayer) are expected to be useful components in many practical and commercial applications such as sensors, detectors, displays and electronic circuit components.[1-3] The possibility of synthesizing organic molecules, almost without limitations, with desired structure and functionality in conjunction with sophisticated thin film deposition technology will enable the production of electrically, optically and biologically active components on a nanometer scale.

An organic thin film can be deposited on a solid substrate by various techniques, such as thermal evaporation, sputtering, electrodeposition, molecular beam epitaxy, adsorption from solution, Langmuir-Blodgett (LB) techniques, and self-assembly.[4] These films represent a particularly flexible means of surface modification and are believed to hold promise in a variety of technologies, including corrosion resistance, prevention of bio-fouling, chemical sensing, and microelectronics.

3.1.1. Langmuir-Blodgett films

Origin

The origin of the oil-on-water subject began quite early. It was in the 19th century that Agnes Pockels prepared the first monolayers at the water-air interface,[5,6] which was an ingenious work, especially in view of the computer-controlled, expensive instrumentation in today's modern laboratories. Irwing Langmuir was the first to perform

systematic studies on floating monolayers of amphiphilic molecules at water-air interface in the late 1910's and early 1920's.[7] These studies led to him being awarded the Nobel Prize. As early as 1920, he reported the transfer of fatty acid molecules from water surfaces onto solid supports. However, the first detailed description of sequential monolayer transfer was given several years later by Katherine Blodgett.[8,9] These built-up monolayer assemblies, which are transferred from the water-air interface (or liquid-gas interface in general) onto a solid substrate, are therefore referred to as Langmuir-Blodgett (LB) films. The term "Langmuir film" is normally reserved for a floating monolayer at the water-vapor surface.

The formation of LB films

LB was, indeed, the first technique to provide the chemists with the practical capability to construct ordered molecular assemblies.[10, 11] The manipulation of LB films is accomplished by successively dipping a solid substrate up and down through the monolayer while simultaneously keeping the surface pressure constant by a computer controlled feedback system between the electrobalance measuring the surface pressure and the barrier moving mechanism. Consequently the floating monolayer is adsorbed to the solid substrate. In the way, multilayer structures of hundreds of layers can be produced.[1,12] The process can be visualized as taking place as illustrated in Figure 3.1. When the solid substrate is hydrophilic (glass, SiO_2, etc.), the first layer is deposited by raising the solid substrate from the subphase through the monolayer, where if the solid substrate is hydrophobic (silanized SiO_2, etc.), the first layer is deposited by lowering the substrate into the subphase through the monolayer.[13,14]

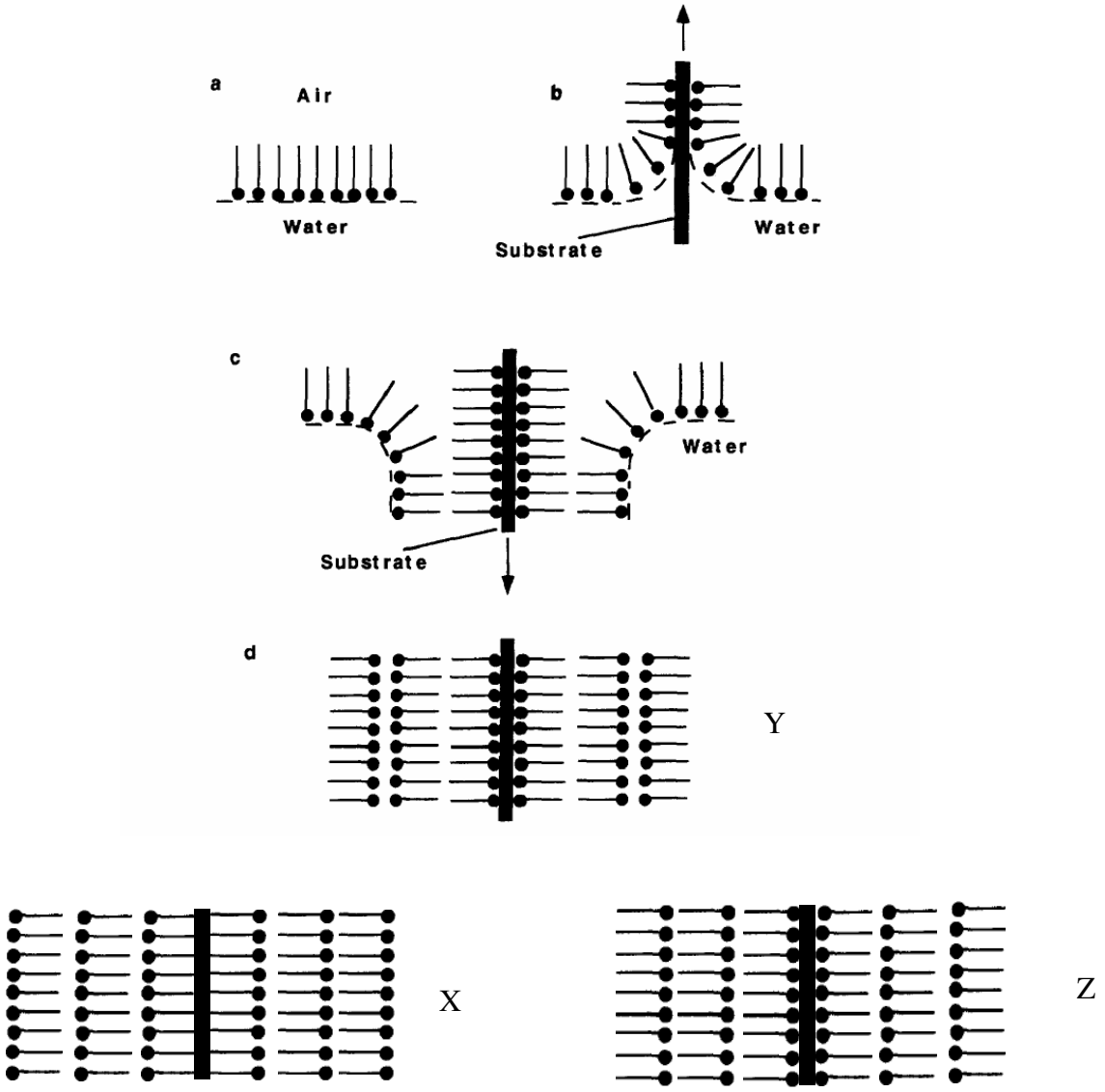

Figure 3.1. Conventional schematic of the LB technique using a hydrophilic substrate. In the first step (a), a suitable amphiphilic molecule is dissolved in a volatile solvent that is then spread at the air water interface to form a Langmuir monolayer. With a barrier, the area of the trough can be altered to change the local density of the molecules, and usually the local organization and order as well. To form the LB film (b), a substrate is passed through the interface a given number of times, with each pass adding another monolayer to the LB film with alternating molecular orientations (c) and (d). And X and Z- types are the other two types of deposition of LB multilayers (noncentrosymmetric).[16]

The LB deposition is traditionally carried out in the "solid" phase. The surface pressure is then high enough to ensure sufficient cohesion in the monolayer, i.e., the attraction between the molecules in the monolayer is high enough so that the monolayer does not fall apart during transfer to the solid substrate.[15]

The LB-technique is one of the most promising techniques for preparing such thin films as it enables (i) the precise control of the monolayer thickness, (ii) homogeneous deposition of the monolayer over large areas, and (iii) the possibility to make multilayer structures with varying layer composition. An additional advantage of the LB technique is that monolayers can be deposited on almost any kind of solid substrate.

Transfer ratio

The quantity and the quality of the deposited monolayer on a solid support are measured by a so called transfer ratio.[16] This is defined as the ratio of the area of film deposited to the change in area at the air/water interface corresponding to this deposition. For ideal transfer, the ratio is equal to 1. Depending on the behavior of the molecule the solid substrate can be dipped through the film until the desired thickness of the film is achieved. If the deposition ratio is near unity for both upward and downward strokes, the materials is said to be deposited in the Y mode. If this ratio is near unity on the upstroke and near zero on the down stroke, the deposition is said to be in the Z mode and the converse situation is said to lead to deposition in the X mode.

Applications

Due to their inherently 2-D structure, the LD films are model membranes and offer the potential to be built up, layer by layer, into waveguides and novel optoelectronic, nonlinear optical and sensory devices.

Surface plasmons are collective oscillations of the free electrons at the boundary of a metal and a dielectric. The surface plasmons are basically guided waves,[17] and their resonance conditions are very sensitive to changes in the thickness and refractive index of the medium adjacent to the metal. Indeed, this effect has been used for the study of oxidation of metals and to evaluate optical constants for deposited overlayers. One of the most promising optical devices is that of the surface plasmon resonance (SPR).[11,17,18] A schematic diagram of the SPR gas detection system is illustrated in Figure 3.2. Lloyd *et al.* used SPR to investigate the interaction between NO_x and LB films of tetra-4-tert-butylphthalocyanine containing silicon.[19]

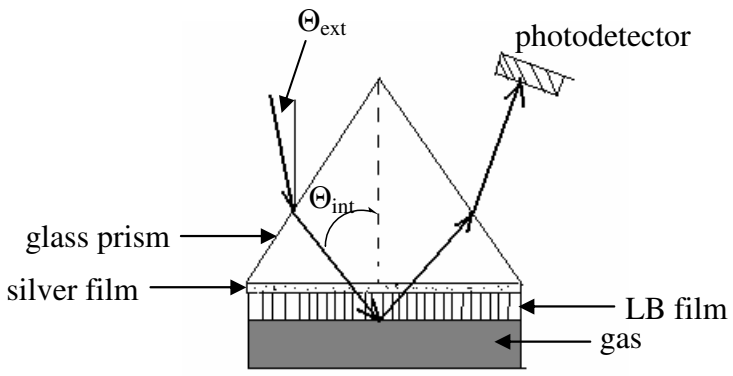

Figure 3.2. A schematic diagram on SPR gas detection system.[11]

3.1.2. Self-assembled monolayers

Features and applications

Self-assembly monolayers (SAMs) are ordered molecular assemblies formed spontaneously by the immersion of an appropriate substrate into a solution of an active surfactant in an organic solvent.[20] SAMs have emerged as a prominent, flexible, and convenient way to present functionality at a surface in a chemically well-defined way. The formation, characterization, and properties of SAMs have been described and reviewed extensively.[11,27-29] Several features of SAMs are attractive. First, they provide a simple way to produce relatively ordered structures at the molecular scale. Second, they provide a way of presenting a wide variety of chemically well-defined terminal functional groups to a surface. The roles of these functional groups have been suggested above. Third, variation in the length of the chain between the head and tail groups offers some control over the interaction between the underlying substrate and the chemical environment above the SAM. For all of these reasons they have a strong appeal to surface chemists.

In addition to the elements of SAMs highlighted above, they offer unique opportunities to increase fundamental understanding of self-organization, structure-property relationships, and interfacial phenomena. The ability to tailor both head and tail groups of the constituent molecules makes SAMs excellent systems for a more fundamental understanding of phenomena affected by competing intermolecular, molecular-substrates and molecule-solvent interactions like ordering and growth, wetting, adhesion, lubrication, and corrosion. That SAMs are well-defined and accessible makes them good model systems for studies of physical chemistry and statistical physics in two dimensions, and the crossover to three dimensions.[30]

In contrast to ultrathin films made by, for example, molecular beam epitaxy, and chemical vapor deposition, SAMs are highly ordered and oriented and can incorporate a wide range groups both in the alkyl chain and at the chain terminal. Therefore, a variety of surfaces with specific interactions can produced with fine chemical control. [31] Due to their dense and stable structure, SAMs have potential applications in corrosion prevention, wear protection, and more. In addition, the biomimetic and biocompatible nature of SAMs makes their applications in chemical and biochemical sensing promising.[32] Their high molecular order parameter in SAMs makes them ideal as components in electro-optic devices. Recent works on nanopatterning of SAMs suggest that these systems may have applications in patterning of gallium arsenide semiconductors and in the preparation of sensor arrays.

History

The formation of monolayers by self-assembly of surfactant molecules at surfaces is one example of the general phenomena of self-assembly. In nature, self-assembly results in supermolecular hierarchical organizations of interlocking components that provides very complex systems.[21] Early work initiated in Kuhn's laboratory, applying many years of experience in using chlorosilane derivative to glass, was followed by the more recent discovery, when Nuzzo and Allara showed that SAMs of alkanethiolates on gold can be prepared by adsorption of di-*n*-alkyl disulfides from dilute solutions.[22] Getting away from the moisture-sensitive alkyl trichloroslianes, as well as working with crystalline gold surfaces, were two important reasons for the success of these SAMs. Many self-assembly systems have been investigated, but monolayers of alkanethiolates on gold are probably the most studied SAMs to date.

Structure

From the energetic point of view, a self-assembling surfactant molecule can be divided into three parts (Figure 3.3). The first part is the head group that provides the most exothermic process, i.e., chemisoption on the substrate surface. The very strong molecular-substrate interactions result in an apparent pinning of the head group to a specific site on the surface through a chemical bond. This can be a covalent Si-O bond in the case of alkyltrichlorosilanes on hydroxylated surfaces; a polar covalent, Au-S bond in the case of alkanethiols on gold; or an ionic $-CO_2^-Ag^+$ bond in the case of carboxylic acids on AgO/Ag.

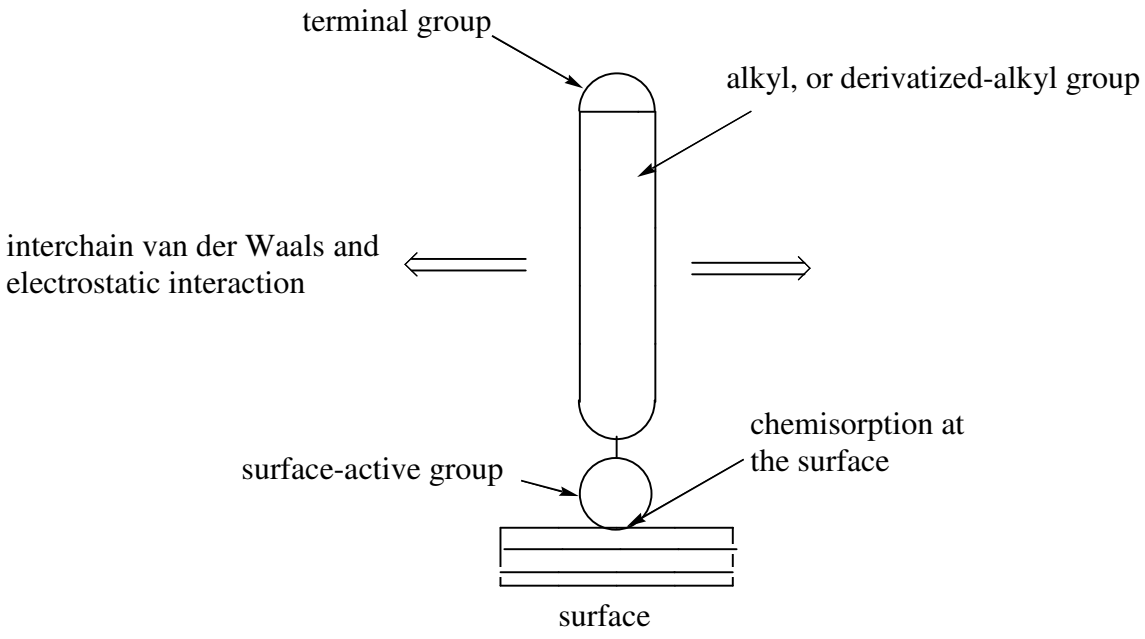

Figure 3.3. A schematic view of the structure and the forces in a self-assembled monolayer.[11]

The energies associated with the chemisoption are at the order of tens of kcal/mol (e.g., ~40-45 kcal/mol for thiolate on gold).[23,24] As a result of the exothermic head group-substrate interactions, molecules try to occupy every available binding site on the surface, and in this process they push together molecules that have already adsorbed.

The second molecular part is the alkyl chain, and the energies associated with its van der Waals interactions are on the order of few (<10) kcal/mol (exothermic). Van der Waals interactions are the main forces in the case of a simple alkyl chain (C_nH_{2n+1}). On the other hand, when a polar bulky group is substituted into the alkyl chain, there also are long-range electrostatic interactions that, in some case, are energetically more important than the van der Waals attractions.

The third molecular part is the terminal functionality, which, in the case of a simple alkyl chain, is a methyl group. These surface groups are thermally disordered at room temperature. [11]

3.1.3. Monolayers of alkanethiols on gold

There are several types of SAMs methods that yield organic monolayers. These include organosilicon on hydroxylated surfaces (SiO_2 on Si, Al_2O_3 on Al, glass, etc.);[33-39] alkanethiols on gold,[22,40-47] silver,[48] and copper;[49,50] dialkyl sulfides and dialkyl disulfides on gold;[43,51] alcohols and amines on platinum;[51] and carboxylic acids on aluminum oxide[52-54] and silver.[55] Among them, because of the strong specific interaction between gold with sulfur and the relatively stablity under ambient condition, SAMs of molecules or macromolecules with free thiols group on the gold surface have been studied

intensively since Nuzzo and Allara published the first paper in this area showing that dialkyldisulfides (RS-SR) form oriented monolayer on gold surface in 1983.[56-58]

Features

The utility of thiols adsorbed on gold as a monolayer system is based on three considerations. First, gold is a relatively inert metal: it does not form a stable oxide surface.[59] Therefore, its surface can be cleaned simply by removing the physically and chemically adsorbed contaminants and it can be handled in ambient conditions. Second, gold has a strong affinity to sulfur and selenium compound [60] because those compounds can form multiple bonds with surface metal clusters.[61] The bonding of the thiolate group to the gold surface is very strong (homolytic bond strength is approximately 40 kcal/mol).[28] That allows us to form monolayers in the presence of many other functional groups. Third, long-chain alkanethiols form a densely packed, crystalline or liquid-crystalline monolayer on gold.[42,62]

Mechanism and kinetics of the formation

A fresh, clean, hydrophilic gold substrate is usually immersed into a dilute solution (10^{-3} M) of the organosulfur compound in an organic solvent. Immersion times vary from several minutes to several hours for alkanethiols, while an immersion time of several days are needed for sulfides and disulfides. The result is closed-packed, oriented monolayer.

In case of alkanethiols, the mechanism of binding is considered to be an oxidative addition of the hydrogen, thus resulting in the formation of a thiolate species.[11,30,32] The eliminated hydrogen is thought to combine to form molecular hydrogen, although there has been no report of hydrogen being measured following the self-assembly process.

$$R\text{-}S\text{-}H + Au_n^0 \rightarrow R\text{-}S\text{-}Au^+ \bullet Au_n^0 + \tfrac{1}{2} H_2 \qquad (1)$$

The kinetics of the formation of alkanethiol monolayers on gold was studied by Bain *et al*. with contact angle and ellipsometry experiments.[41] For a typical solution of 1 mM in ethanol, the contact angle and film thickness were observed to reach ~90% of their final values within the first minute of growth. A slower second step was observed in which the final film properties were reached after only a few hours. This suggested multiple processes at work, with time scales differing by ~2 orders of magnitude. The initial step, which was described well by diffusion-controlled Langmuir adsorption, was found to strongly depend on thiol concentration. At 1 mM solution the first step took ~1 min, while it required longer than 100 min at 1 μM concentration.[41,63] The second step can be described as a surface crystallization process, where alkyl chains get out of the disordered state and into unit cells, thus forming a two-dimensional crystal. Therefore, the kinetic of the first step is governed by the surface-head group reaction, and activation energy may depend on the electron density of the adsorbing sulfur. On the other hand, the kinetics of the second step is related to chain disorder (e.g., gauche defects), the different components of chain-chain interaction (van der Waal, dipole-dipole, etc.), and the surface mobility of the chains. They also noted that the monolayers properties of longer-chain *n*-alkyl thiol (n>8) were consistent but that shorter-chain thiol monolayers were qualitatively different in a way that suggested greater disorder.[41]

Application in biotechnology

The recent development in alkanethiol self-assembly technology has been applied to protein surface modification. The simplicity and adaptability of SAMs and the control

over biomolecule surface orientation suggest that SAMs will play an important role in the construction of artificial biomolecular recognition surfaces and particularly in the future development of biosensors.

Many fundamental and central biological recognition and transduction processes occur at biological surfaces.[64] To investigate these in vitro, and possibly the in vivo, molecular behavior of biomolecules (e.g. proteins, enzymes, nucleic acids and carbohydrates) at biological surfaces must be understood. The well defined and flexible system SAMs technology provides a powerful tool to generate monomolecular films of biological molecules on a variety of substrates. The formation of such monolayer systems is extremely versatile and can provide a method for the in vitro development of bio-surfaces which are able to mimic naturally occurring molecular recognition processes.[65] SAMs also permit reliable control over the packing density and the environment of an immobilized recognition center, or multiple centers, as a substrate surface.

Molecular interactions occurring at biomolecular monolayer surfaces can by studied using a wide range of analytical techniques such as: surface plasmon resonce (SPR),[66,67] scanning probe microscopies, (e.g., STM and AFM),[68] reflection absorption infrared spectroscopy (RAIRS),[65] surface-enhanced Raman spectroscopy,[69] and electrochemical techniques.[70]

3.1.4. Motivation: formation of SAMs with functionalized polyguanidines

More recently, to facilitate bio-related applications such as DNA sequencing and gene mapping technologies,[71,72] studies have increasingly focused on biopolymers, including thiol-functional DNA[73-78] and polypeptides,[79-81] immobilized on gold surfaces.

In particular, SAMs formed from rigid helical polypeptides is a new structural motif being explored (Figure 3.4). Our interests are to prepare thiol-terminated polyguanidines and investigate their behavior when covalently bound to surfaces.

As we discussed before, polyguanidines show some interesting characteristics including being built up from guanidine repeat units, which are ubiquitous entities in biological systems. They adopt approximate 6/1 helical conformations in both solution and the solid state, and their dimensions are comparable to helical polypeptides. Since polyguanidines can be synthesized by living polymerizations,[82-85] which allows for control over the polymer chain length, we should be able to easily adjust the monolayer thickness on the surface. Furthermore, because the structure and conformation of the polyguanidines can be controlled by different methods,[86-89] this type of polymer is a good model for development and study of the surface properties of biomaterials with helical structures and could prove to be a promising candidate for biomimetic applications.

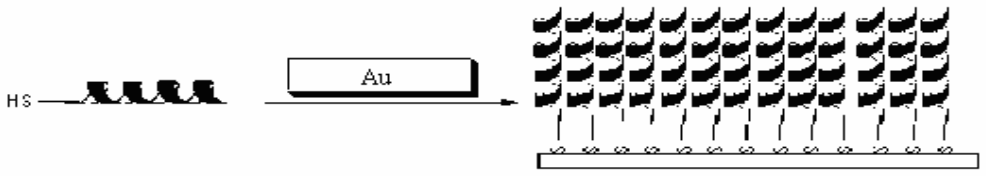

Figure 3.4. SAMs formed by rod-like helical polymers.

Different from other reported methods, herein we report on a new route to place a thiol group onto the polymer chain end in the initiation step. We employed ellipsometry, contact-angle goniometry, and polarization-modulation infrared reflection adsorption spectroscopy (PM-IRRAS) to characterize the films.

3.2. The adsorption of thiol-terminated polyguanidines on gold

3.2.1. Preparation of thiol-terminated polyguanidines

Polyguanidines are synthesized using a titanium-catalyzed polymerization of carbodiimides (Scheme 3.1). This polymerization has been demonstrated to be a living

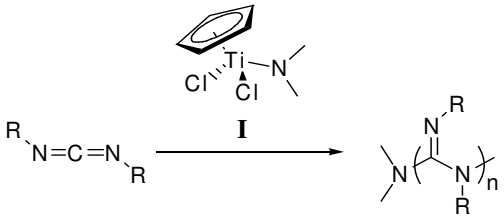

Scheme 3.1. Polymerization of carbodiimide with a Ti catalyst.

polymerization, and the dimethylamino initiating group on the titanium catalyst, **I**, becomes the end group of the polymer chain.[85] This initiation mechanism allows us to selectively place functional groups at the end of the polyguanidines chains. In order to apply this approach, a new catalyst, **II**, possessing a protected thiol, was prepared. The protection of the thiol group was done using 2,4-dinitrofluorobenzene (Sangers reagent). This compound has been shown in the literature to have a high reactivity with a variety of functional groups such as thiol, phenol, or imidazole contained in proteins and peptides.[90] It was found to be particularly suitable as a protecting group, since it may be removed using mild conditions. [91] In addition, it does not interact with the polymerization process, and it provides an excellent NMR and UV/Vis handle useful for characterization purposes. The protection reaction itself involves an aromatic nucleophilic substitution of the activated fluoride of

2,4-dinitrofluorobenzene by the thiol of mercaptoethanol catalyzed by triethylamine as a base (Scheme 3.2).[92] The polymerization of carbodiimides with catalyst **II** yields polyguanidines with a protected thiol group at the chain end. The deprotection step unmasking the thiol endgroup was monitored by both ^{1}H NMR and UV/Vis spectroscopy.

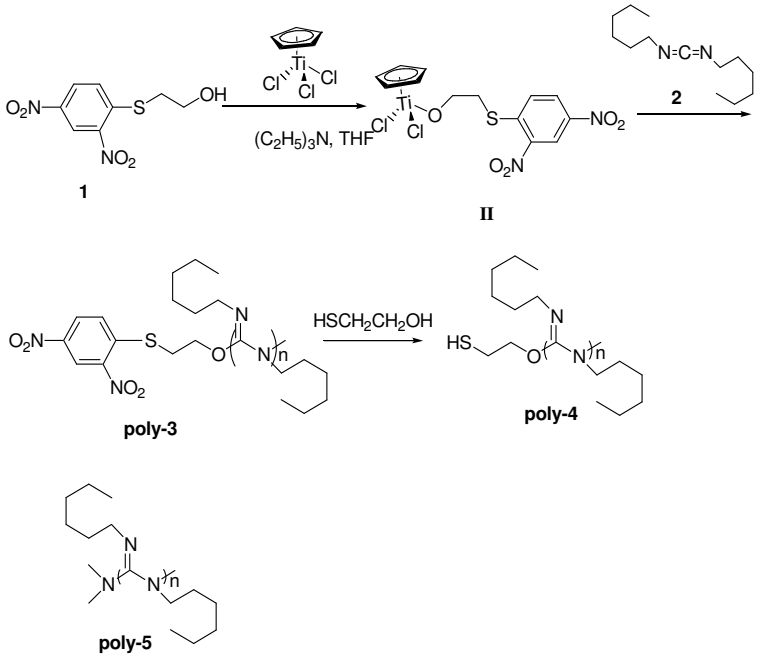

Scheme 3.2. Synthetic route of initiator **II** and poly-**4**.

3.2.2. Analysis of the SAMs by polarization-modulation infrared reflection adsorption spectroscopy (PM-IRRAS)

Polarization modulation-infrared reflection-adsorption spectroscopy (PM-IRRAS) is used for characterization of thin films or monolayer on metal substrates. This technique has the advantages of high surface sensitivity, and of surface selection rules. In addition, the

advantage over the conventional IRRAS mode is that modulated reflectivity is independent of the isotropic adsorption from gas or bulk water. Consequently the interfering effect of water vapor and carbon dioxide can be eliminated to a high degree. Due to its salient features, this technique has broad applications in surface chemistry, especially in the characterization of DNA on the gold surfaces, including the investigation of its hybridization behavior on gold.[93-96]

Infrared reflectance spectra of the SAMs on gold derived from the polyguanidines are shown in Figure 3.5. The thiol-terminated polyguanidines lead to the stronger absorbance.

As in Figure 3.5, the band at 2960 cm^{-1} is assigned to the CH_3 asymmetric in-plane CH stretching mode, and the bands at 2930 and 2859 cm^{-1} are assigned to the C-H asymmetric and symmetric stretching of methylene groups in the side chains, respectively.

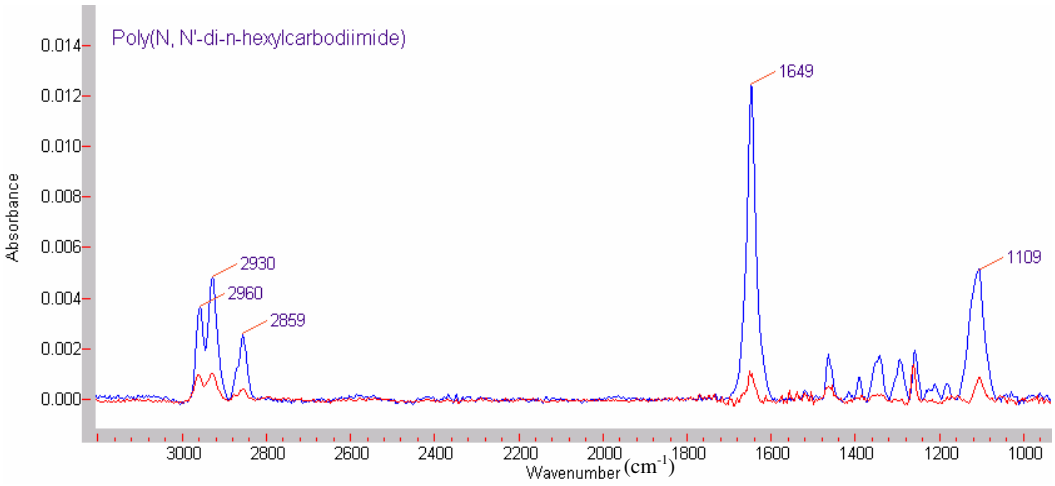

Figure 3.5. The PM-IRRAS spectra measured for the monolayers formed from poly-**4** (blue line). Non-specfic adsorption of poly-**5** is shown by the red line.

Another strong absorbance at 1649 cm^{-1} is assigned to the C=N imine stretching mode of the guanidine repeat units. These characteristic absorbances indicate monolayer formation on the gold surface.

In order to prove that the thiol groups plays an important role for the formation of SAMs, a control experiment was carried out with a polyguanidines possessing no thiol end group. As can be seen in the Figure 3.5, in contrast to the absorbance for the poly-**4** samples, the control sample, poly-**5**, gave a weaker absorbance with a larger signal to noise ratio. The weak signal probably results from small amounts of polymer physisorbed on the substrate.

The distinction in intensity between the poly-**4** and poly-**5** indicates that the adsorption of the polymer on the surface is strongly promoted by the thiol end group.

3.2.3. Properties of monolayer films formed from polyguanidines as a function of the chain length.

We examined the effects on the properties of monolayers of varying the chain length, *n*, in the homologous series of repeat units, using PM-IRRAS, ellipsometric and contact angle measurements.

SAMs from polymers of different chain lengths were prepared. The PM-IRRAS results are shown in Figure 3.6. Unlike the spectra of SAMs formed with the *n*-alkanethiols, which show pronounced peaks shifting with variance of the alkyl chains length,[42] the positions of C=N bands for the polyguanidines do not change. This implies that the orientation of the polymer chain does not vary with different chain length. This observation is consistent with the fact that the polyguanidines have relatively rigid backbones.

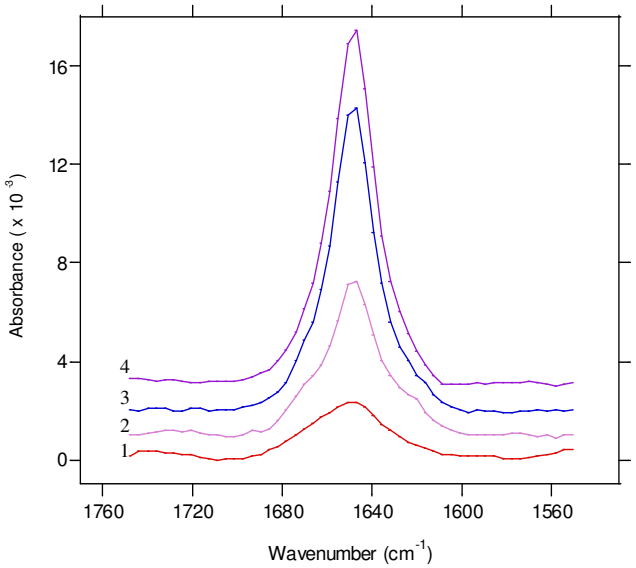

Figure 3.6. Evolution of PM-IRRAS spectra of imine stretching mode with increasing poly-**4** chain length. (The ratios between the monomer and initiator for samples from 1-4 are 5, 10, 50 and 100, respectively.)

Samples prepared from poly-**4** with shorter chains have weaker C=N adsorption and the adsorption intensity increases for increasing chain lengths. This indicates that the amount of imine groups on gold surface increases with increasing numbers of repeat units and not because of increasing numbers of chains.

The Figure 3.7 shows a plot of the ellipsometric thickness against the number of repeat units, *n*, in the polymer chain. The measurements indicate that the monolayers become thicker as the polymer chains increase in length. The data are described by a straight line with a slope of 0.46 Å/guanidine unit and a *y* intercept of 12.6 Å. Two aspects of the experimental data require comment: the flat slope and the relatively larger intercept. According to the literatures, the bond length of C-N is about 1.47 Å, which is much larger

than the experimental result. This tells us that the guanidine chain is not stretched from its helical state. The experimental data is even smaller than the theoretical slope of 1.33 Å, which represents the thickness expected for a monolayer tilted 25° (the mean tilt inferred from reflectance infrared spectra for the long chain alkyl monolayer)[42] from the normal to the surface. However, the specific structure of the polyguanidines must be considered. The polymer backbone adopts and maintains a helix structure. The polymer chains are not extended but coiled as they extend from the surface, which results to the diminution of the overall chain length of the polymer.

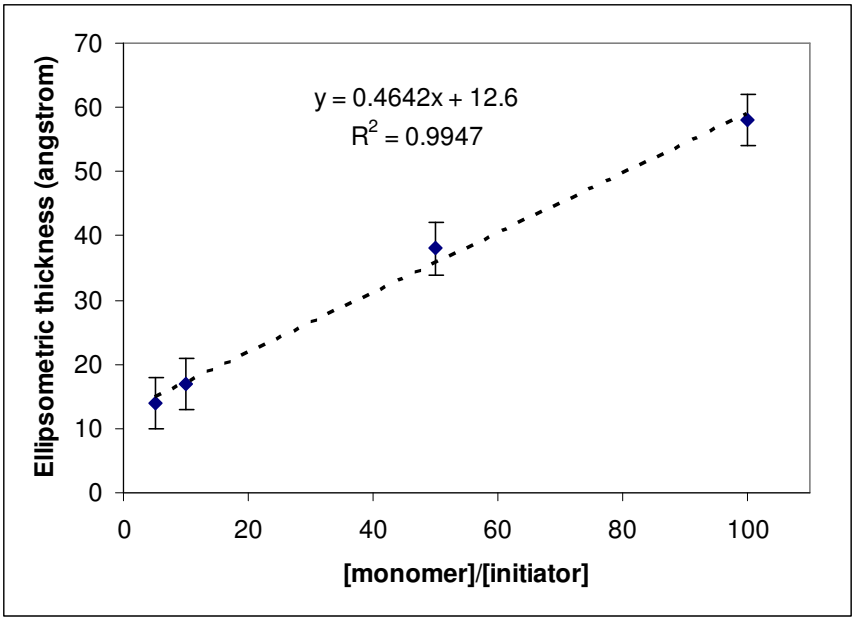

Figure 3.7. Ellipsometric thickness as the function of the repeat unit in the polyguanidines chains.

The intercept value should correspond to the length of the $-OCH_2CH_2SH$ group. Of course, if a tilt of 25° is taken into account, the estimated value is only 5.63 Å. Three

factors stand out as possible contributors to the considerable discrepancy between theoretical data and that estimated by ellipsometry: the refractive index of the gold substrate, the refractive index of the adsorbed film, and the surface coverage (and therefore, the packing of the monolayer). It seems that one may not be able to obtain a true optical response of a bare, unreacted gold substrate unless ultrahigh vacuum is used. This is because even with most careful operation, there will always be a film of contaminants on gold surface, such as, chemisorbed CO, O_2, H_2O, and hydrocarbons, and phsisorbed H_2O, hydrocarbons, and other organic compounds that exist in the laboratory.[11,41] Apparently, this contaminant-film affects only the kinetics of adsorption, and is displaced by the thiols in the process of monolayer formation. But if some of the metal oxide has been reduced by the thiol, the refractive index of the substrate following adsorption may be different as well. Part of the discrepancy may arise from our use of a constant refractive index, independent of the chain-end or backbone and also independent of the chain length.

Another possible explanation is our assumption of a plane, parallel model for the monolayer on gold, even though the surface is not rigorous flat. We expect that roughness would result in a systematic error in the calculated film thickness across the series of samples.

Figure 3.8 shows the advancing contact angles on the polyguanidine layers adsorbed on gold. The advancing contact angles of water for those polymers with different chain length have the range from 104º to 110º, which is similar to the SAMs formed by the alkanethiol. The wettability of the surface has been obviously modified. The advancing contact angles were observed to increase slightly with increasing chain length across the

series of methyl-terminated SAMs. This phenomenon probably arises from one or both of the following effects: (1) the probe liquid might be sensing attractive van der Waals interactions from the underlying gold substrate, which would be stronger for the SAMs having shorter chain lengths, and/or (2) the probe liquid might be interacting with exposed methylene groups, which are likely to be more prevalent in SAMs having short chain lengths because of their relatively looser structure.[42,97,99,100]

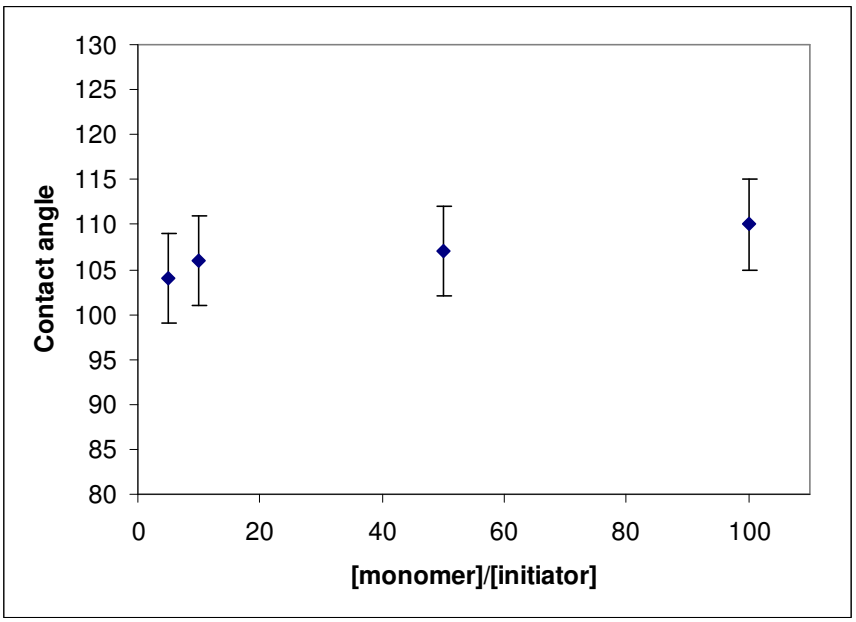

Figure 3.8. Contact angles as the function of the number of repeat units in the polguanidines chains.

3.2.4. Kinetics of formation of monolayers.

The rate of formation of a self-assembled monolayer is influenced by many factors, some of which can be controlled relatively easily, such as temperature, solvent, concentration, chain length of the adsorbate, the cleanliness of the substrate, and others,

such as the rate of reaction with the surface and the reversibility of adsorption of the components of the monolayer, that are inherent to the system.[41] We have used PM-IRRAS and ellipsometry to investigate immersion time dependence of the SAMs formation.

The C=N stretching intensity is used to monitor the rate of SAMs formation. The results are shown in Figure 3.9. The intensity of the imine absorbance reaches its maximum rapidly within 30 min, and does not change significantly as the immersion time increases. This indicates that the formation of polyguanidine monolayer on gold is a rapid process. The result is in agreement with kinetics of alkyl thiol obtained by Bain *et al.*[41] This behavior can be rationalized by rapid adsorption if an imperfect monolayer followed by a slower process of additional adsorption and consolidation, possibly involving displacement

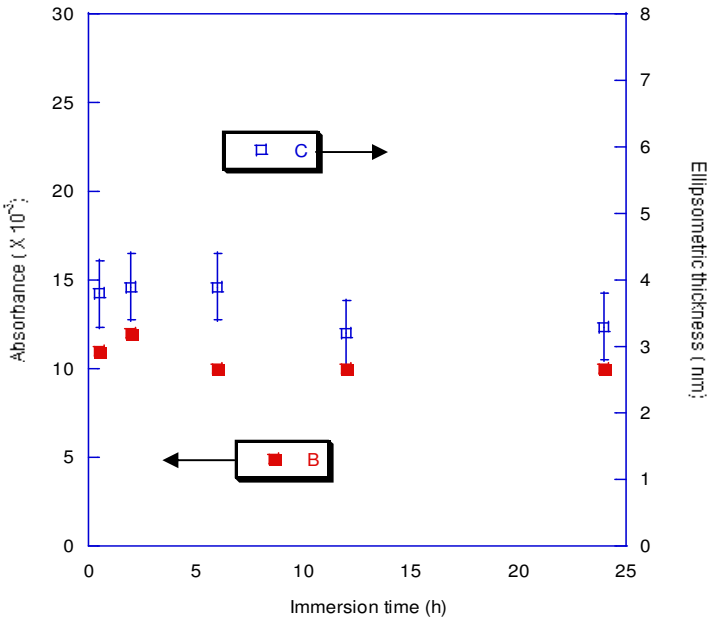

Figure 3.9. The immersion time dependence of SAMs formation.

of contaminants, expulsion of included solvent from the monolayer, and lateral diffusion on the surface to reduce defects and enhancing packing.

Further strong evidence for monolayer formation is that the layer thickness remains at constant of 3.7 nm as a function of time.

3.2.5. Solvent effect on monolayer formation

Most of the work reported in the literatures on the formation of SAMs suggests the use of ethanol as the preferred solvent. However, other solvents can also be used, and sometimes are preferred. Practically, the solubility properties of the polyguanidines dictate the choice of the solvent. In this experiment, to explore a wider range of solvents and to gain insight into the effect of solvent on the properties of monolayer films, we prepared SAMs by exposing gold substrates to 1 mM solutions of polyguanidines in various organic solvent for at room temperature for 30 min. Figure 3.10 and 3.11 present the results of ellipsometry, contact angle and PM-IRRAS measurements.

Apparently, there is no considerable solvent influence except for the SAMs formed in benzene. The SAMs formed from benzene, have properties that are significantly different from the other SAMs. In the PM-IRRAS spectra, the intensities of the absorbance are higher, and the ellipsometric thickness and contact angles are slight larger as well.

During the self-assembly process, thiol molecules must displace solvent molecules from the metal surface and those solvating the assembling chains prior to forming densely packed domains.[101] The solvent polarity might be expected to influence the properties of the formed SAMs. A highly polar solvent can interact with thiol headgroups and might alter

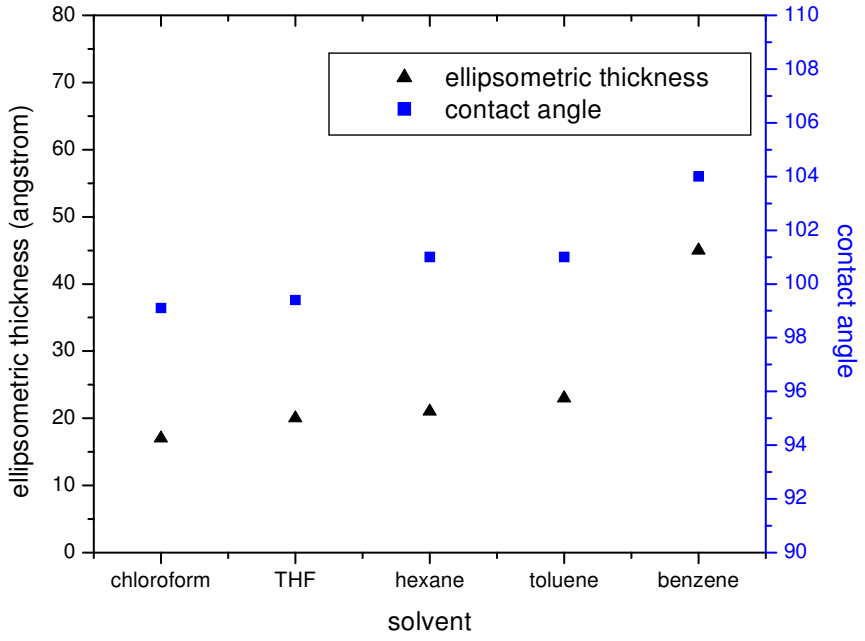

Figure 3.10. The effect of solvent on the formation of thiol-terminated polyguanidines.

the binding between the thiol and the gold surface.[30,102] The relatively weak interaction of the nonpolar solvent, benzene, with the gold surface and polymer chains likely facilitates the formation of densely packed domains of the thiolates with few defects (adsorbate vacancies, domain boundaries, etc.). Such orderly packed monolayer might result in the different properties from the SAMs formed in other solvents. However, it is not possible to correlate the properties of the SAMs simply with the polarity or dielectric constant of the solvent. For example, the hexane also shows different effect than with benzene. The size of solvent molecules has been mentioned as a factor as well.[102] The detail of the effect of solvent on the properties is not clearly understood as of yet.

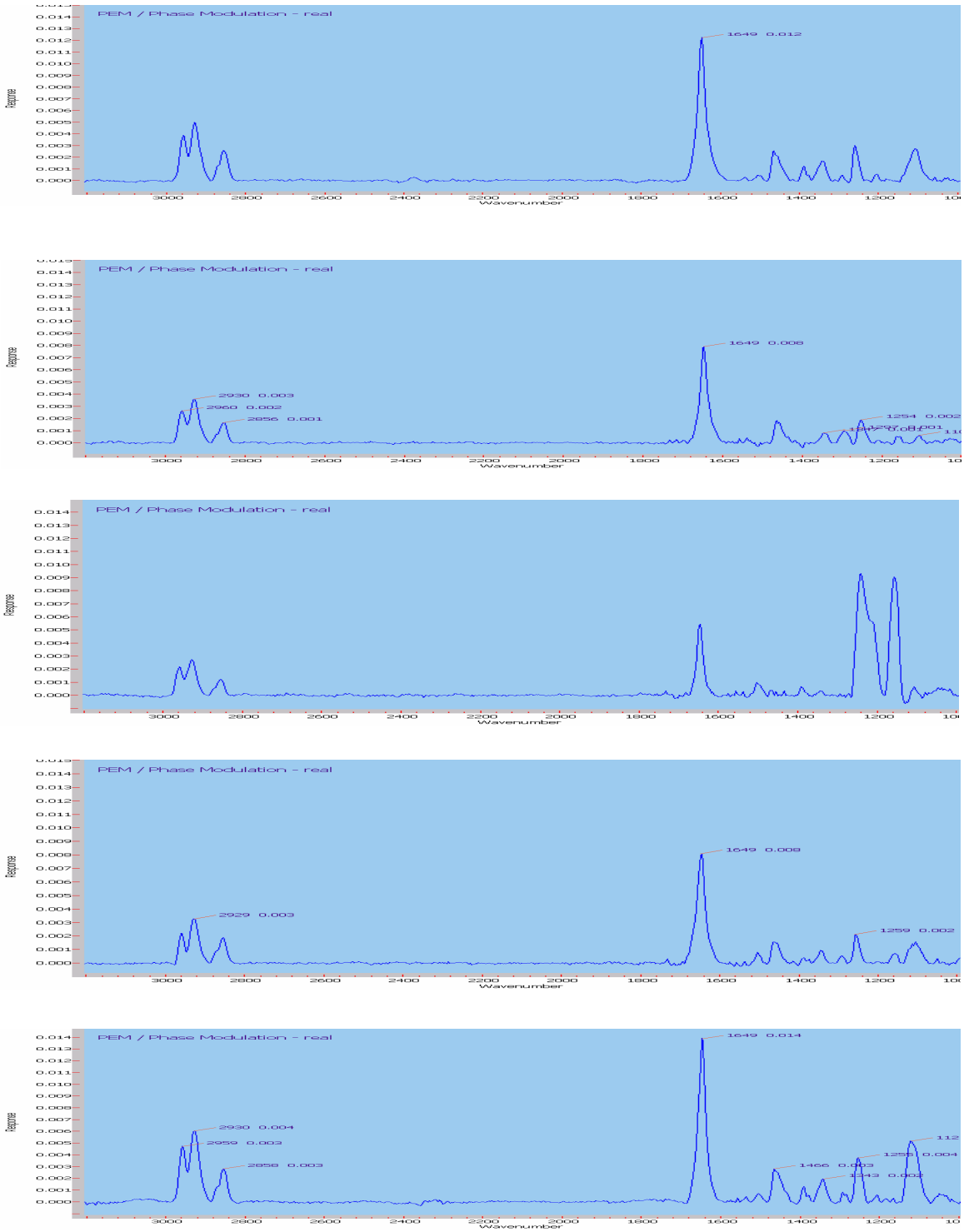

Figure 3.11. PM-IRRAS measurements of the SAMs formed in different solvents (from top to bottom: chloroform, toluene, THF, hexane and benzene.

3.2.6. AFM images of the SAMs of polyguanidines on gold

Since the invention of scanning tunneling microscopy (STM) in 1982 and atomic force microscopy (AFM) in 1986, surface structures have been studied with unprecedented and striking detail.

Characterization of the topography of adsorbed thin films was accomplished by tapping mode AFM. Herein, we took the images of the SAMs formed by poly(*N,N'*-di-*n*-hexylcarbodiimide) with repeat units of 50 and 100, respectively. And all of the adsorbed films prepared from the benzene, since monolayers formed in benzene show significant difference with other solvents. Topological and surface images measured by tapping mode AFM for the adsorption of the two samples are shown in Figure 3.12 and 3.13. The results indicate that the surfaces appeared homogeneous with the root mean square roughness of approximately 1.9 nm and 2.5 nm. From the height images, it is reasonable to observe that the longer polymer chain would result in the thicker monolayer films.

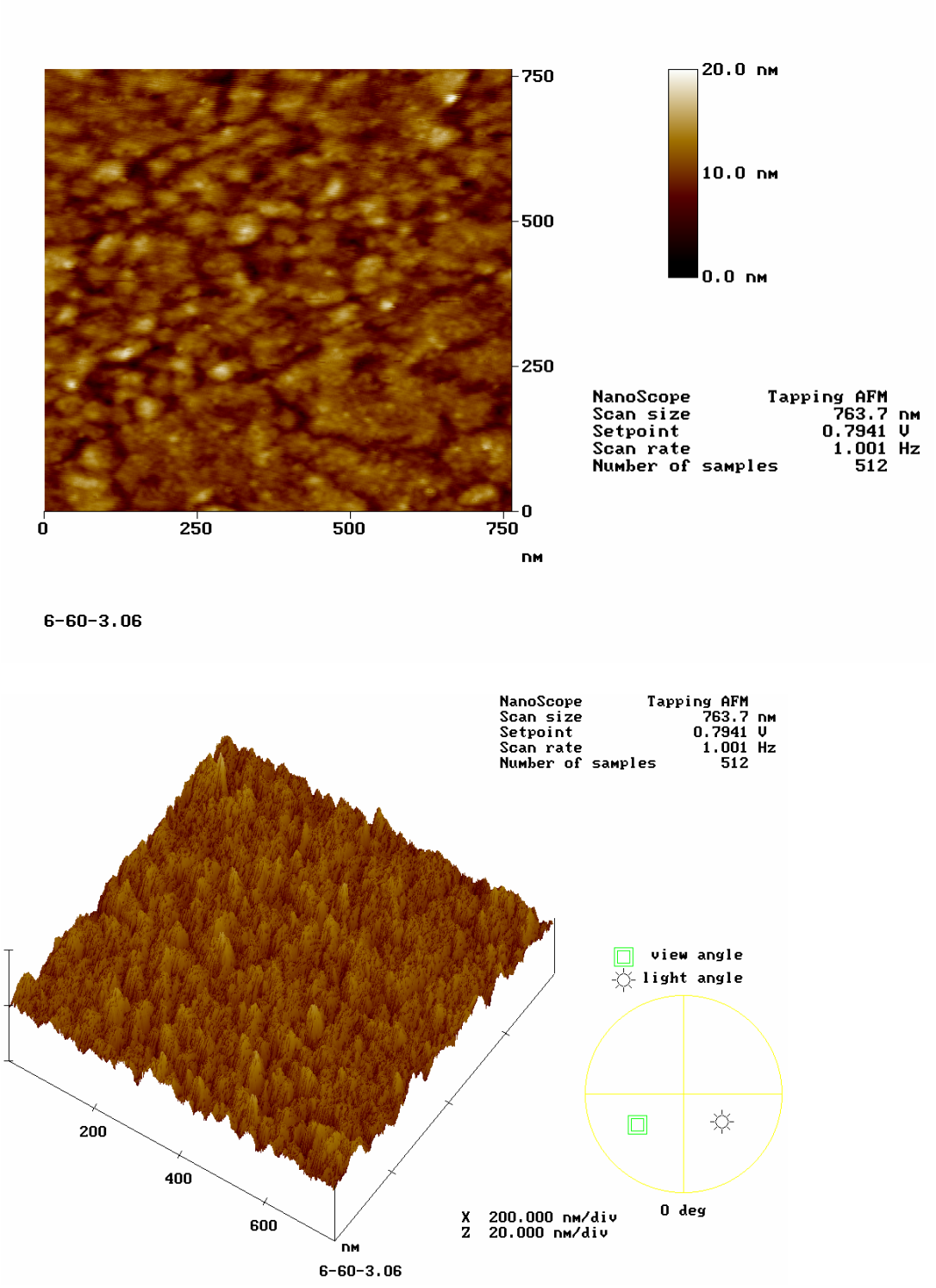

Figure 3.12. AFM tapping mode analysis of a SAMs of 50:1 poly(N,N'-di-*n*-hexylguanidine) absorbed from benzene to gold substrate. The pictures are topological (top), surface (bottom).

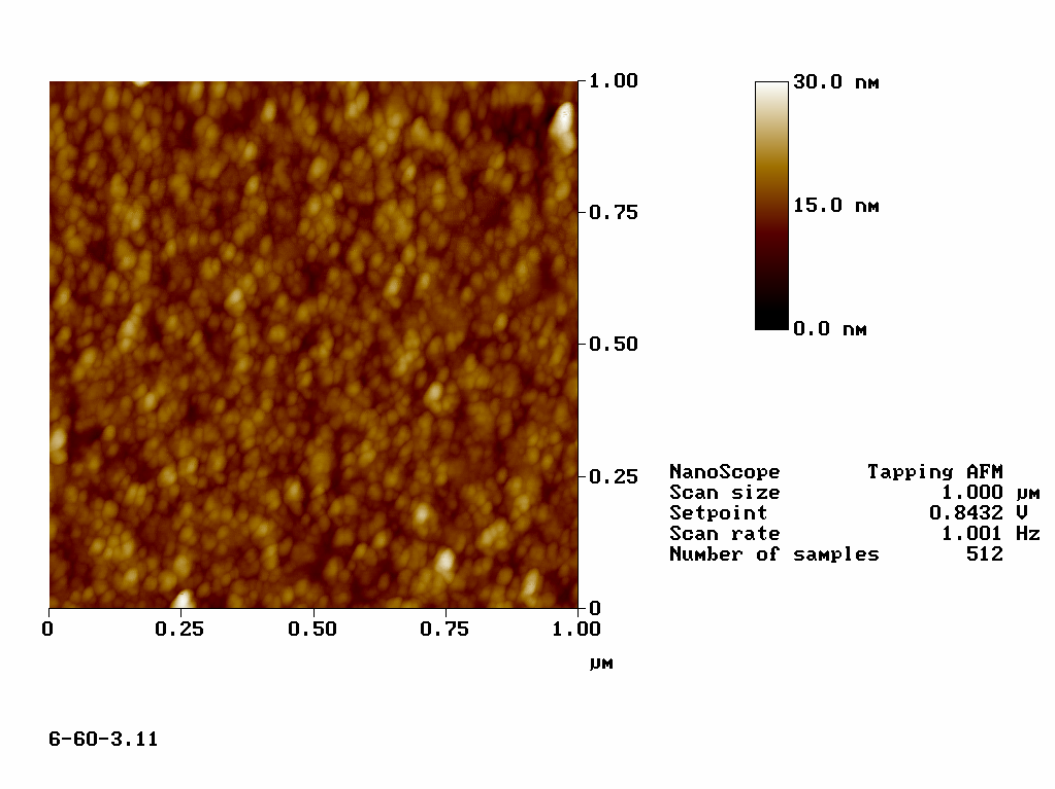

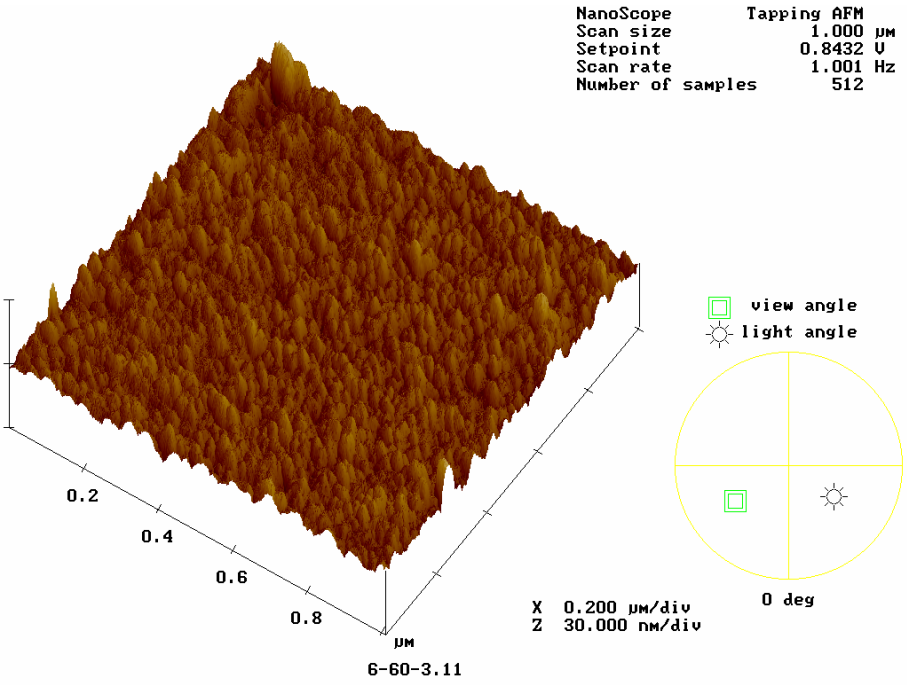

Figure 3.13. AFM tapping mode analysis of a SAMs of 100:1 poly(N, N'-di-*n*-hexylguanidine) absorbed from benzene to gold substrate. The pictures are topological (top), surface (bottom).

3.3. Gold-polyguanidine nanocomposites.

Gold nanoparticles have been widely used in nano-science research to bind or adsorb a variety of functional molecules. These surface-capped gold nanoparticles have many useful applications, including biological markers,[104] DNA sensors,[105] molecular recognition systems,[106] and nanoscale electronics.[107] Herein, we employed surface initiated polymerization to prepare uniform and densely grafted polymer brushes on gold nanoparticles.

We have investigated a novel system consisting of a hydroxyl initiator group attached to a gold particle, that is capable of coordinating titanium(IV), and the subsequent use of this coordinated titanium to catalyze the polymerization of carbodiimide monomers.

Analogous surface modification can be performed with α-hydroxythioalkanes, or with mixtures of alkanethiols, which act as the spacers, and hydroxythioalkanes, as done here. Gold nanoparticles were stabilized with a carefully controlled mixture of benzenethiol and 4-mercaptophenol, leading to a nanoparticle with a well defined proportion of terminal hydroxyl groups. These alcohol groups are extremely reactive towards titanium tetrachloride, reacting rapidly to produce a surface bound titanium trichloroalkoxide.

Our strategy started with growing the metallic clusters with simultaneous attachment of the self-assembled thiol monolayers on the growing nuclei.[108] In order to allow the surface reaction to take place during metal nucleation and growth, the particles were grown in a two-phase system. Two-phase redox reaction can be carried out by an appropriate choice of redox reagents present in the adjointing phases. In the our case, $AuCl_4^-$ was transferred from aqueous solution to toluene using tetraoctylammonium

bromide as the phase transfer reagent and reduced with aqueous sodium borohydride in the presence of 4-mercaptophenol and benzenethiol, which is the spacer between each hydroxyl group. The overall reaction is summarized by Scheme 3.3, where the source of electrons is BH_4^-.

$$AuCl_4^- (aq) + N[CH_3(CH_2)_7]_4^+ (C_6H_5Me) \longrightarrow N[CH_3(CH_2)_7]_4^+ AuCl_4^- (C_6H_5Me)$$

$$m\ AuCl_4^- (C_6H_5Me) + n\ HOC_6H_4SH (C_6H_5Me) + 4n\ C_6H_5SH (C_6H_5Me) + 3\ m\ e^- \longrightarrow 4m\ Cl^-(aq) + (Au)_m(-S\ C_6H_4OH)_n\ (-S\ C_6H_5)_{4n}(C_6H_5Me)$$

$$(Au)_m(-SC_5H_4OH)_n\ (-SC_6H_5)_{4n} + TiCl_4 \longrightarrow (Au)_m(-S\ C_6H_4O\text{-}TiCl_3)_n\ (-S\ C_6H_5)_{4n} + HCl$$

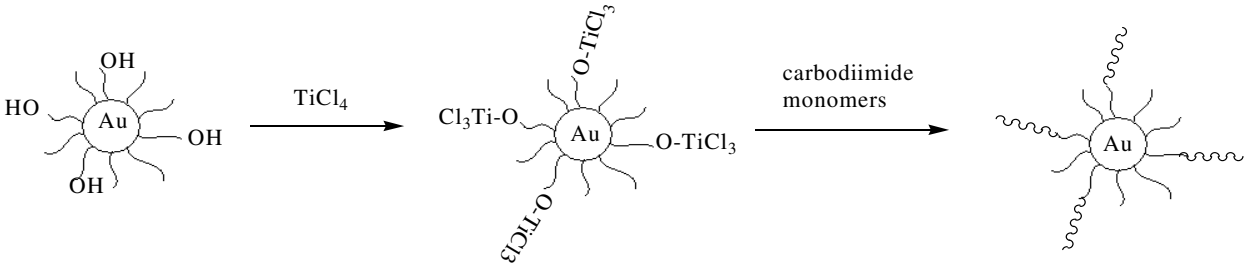

Scheme 3.3. Preparation of gold-polyguanidines nanocomposites.

The product after polymerization possessed a light purple color, which is different from the typical white polyguanidines. The gold-polyguanidines nanocomposites were characterized by UV-Vis, light scattering and transmission electron microscopy.

Gold nanoparticles exhibit strong plasmon resonance absorption that is dependent on the particle size and shape. For roughly spherical gold nanoparticles, the plasmon band maximum generally falls between 520 and 530 nm.[109,110] Figure3.14 shows the UV-Vis absorption spectra of the gold seeds and the nanocomposites of the gold-polyguanidines. Centers of absorption bands moving from 520 nm to 570 nm indicates that aggregation takes place, which might result from the instability of the gold particles in the reaction of the hydroxyl group with titanium complex. From the results of light scattering in the Figure 3.15, we found the average size of the particles in the solutions increased significantly.

Transmission electron microscopy (TEM) images of typical gold seeds and gold-polyguanidines nanocomposites in Figure 3.16 show that polymers grew up from the gold surface like hair. And from the images, we could find aggregation of the gold seeds which is also found in the UV-Vis results. Such aggregation results because the nanocomposites are not quite uniform. Further studies are needed for us to understand how to reduce the aggregation and how to control the size of the nanocomposites.

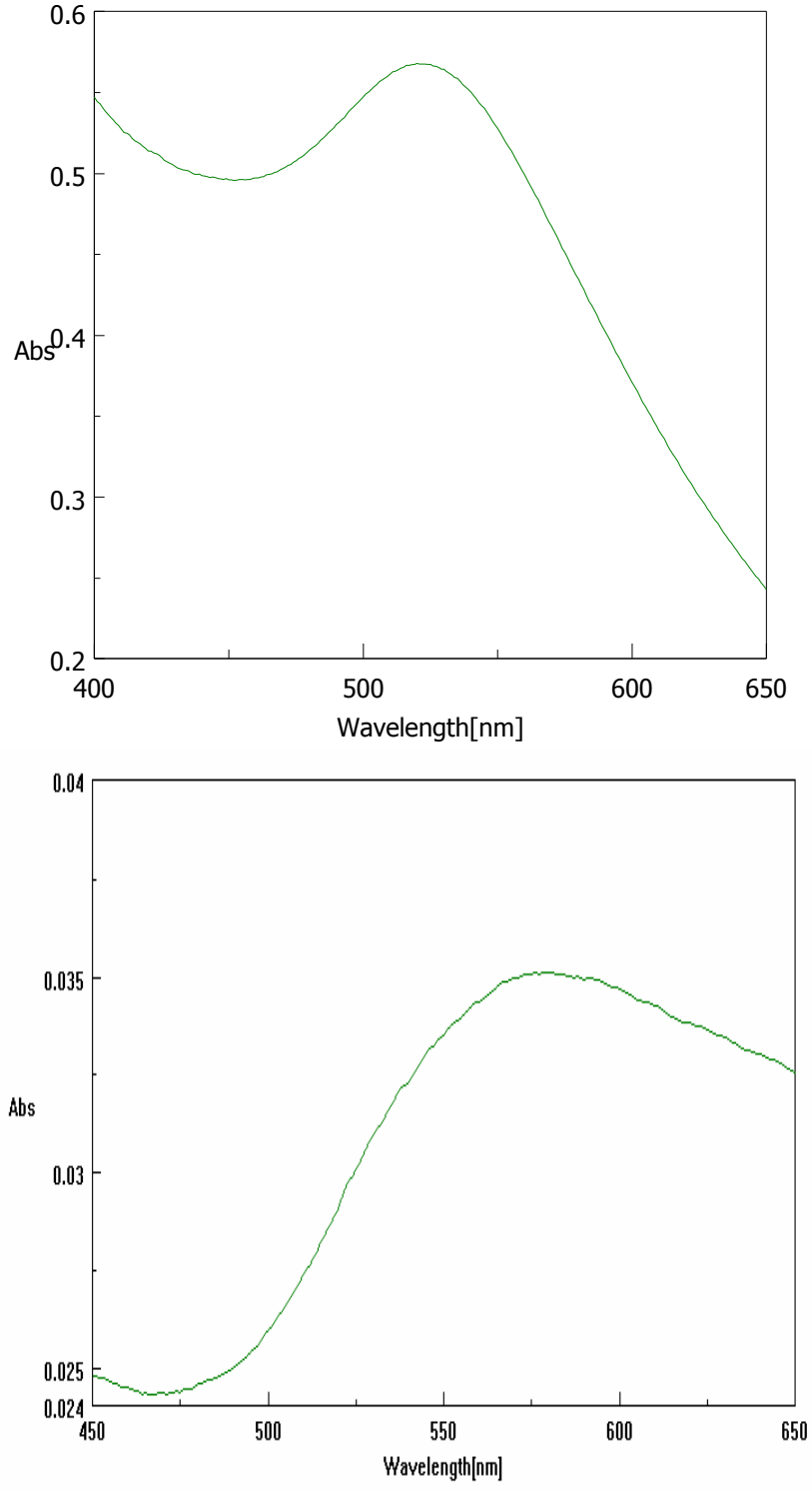

Figure 3.14. UV-Vis absorption spectra of gold seeds (top) and gold-polyguanidine nanocomposites (bottom).

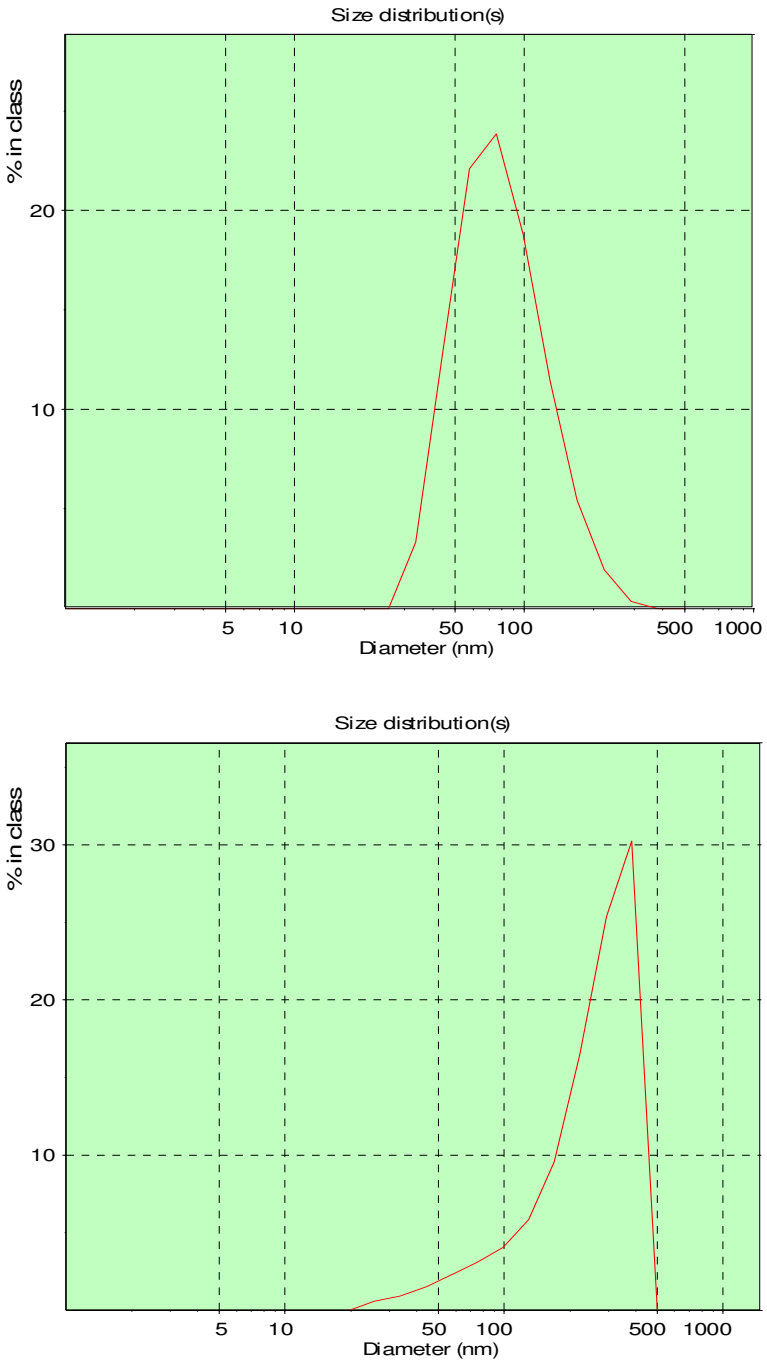

Figure 3.15. Size distributions of the particles by light scattering: gold seeds (top) and gold-polyguanidines nanocomposites (bottom).

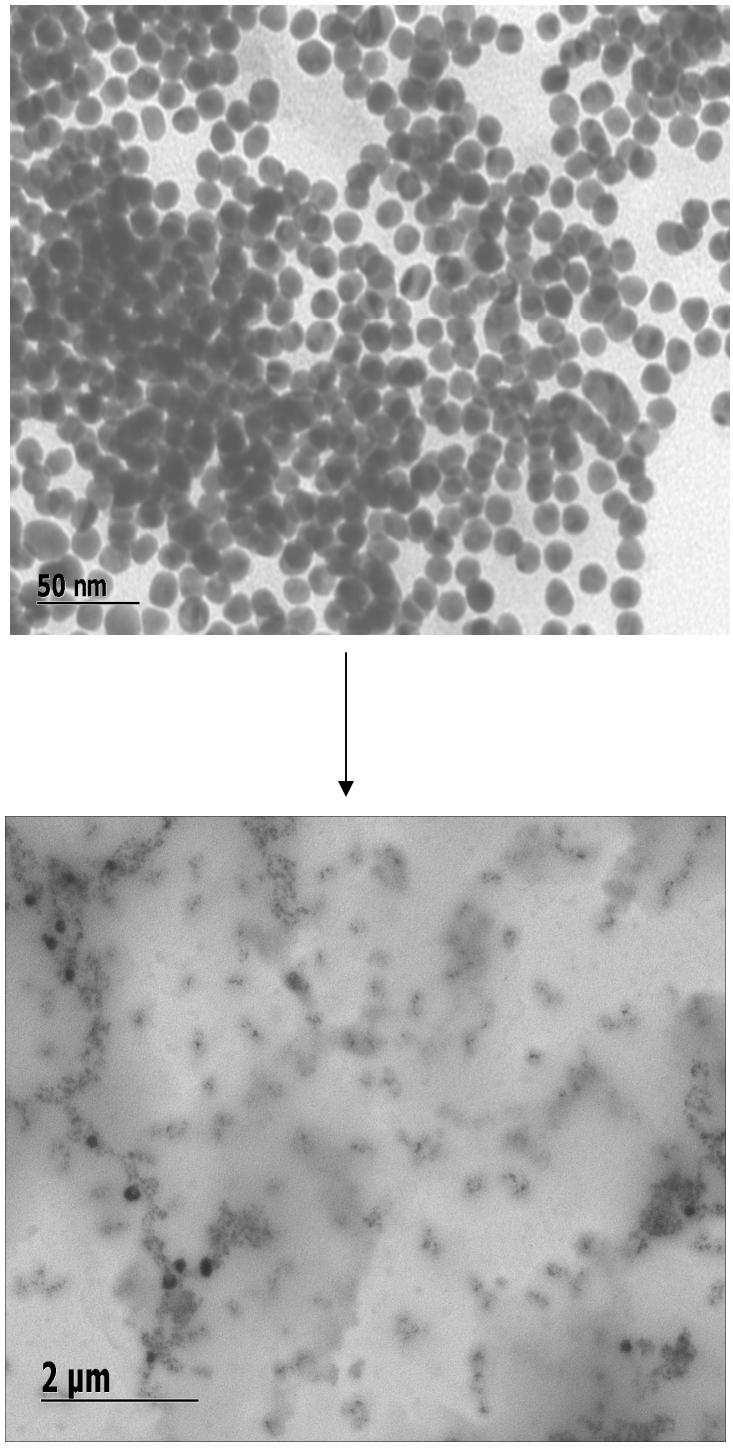

Figure 3.16. TEM images of gold seeds (top) and gold-polyguanidines nanocomposites (bottom).

3.4. Experimental section

3.4.1. General procedures and characterizations

Instruments

Air and moisture sensitive procedures were carried out using standard Schlenk techniques or in the Unilab glove box under an atmosphere of nitrogen. All glassware was either flame dried or oven dried overnight. All infrared spectra (cm^{-1}) were recorded on NaCl plates and were acquired on a JASCO FT/IR-410 spectrometer. Wavenumbers in cm^{-1} are reported for characteristic peaks. The ^{1}H and ^{13}C NMR spectra were measured in $CDCl_3$ on a Mercury 300 or 400 spectrometers. Chemical shifts are reported in δ (ppm) relative to tetramethylsilane as internal standard.

Reagents

Unless otherwise noted all reagents used were obtained from a commercial supplier and were used without further purification.

The solvents used for air and water sensitive procedures were purified via chromatography except for the THF, which was distilled from a Na/benzophenone ketyl under nitrogen. The solvents used for the measurement of optical rotation and CD are A.C.S. spectrophotometic grade. Unless otherwise noted, all other solvents were reagent grade and used without further purification.

3.4.2. Experimental procedures and characterizations

α-(2,4-Dinitrophenylthio)ethanol, 1

Compound **1** was synthesized prepared with a slight modification of literature procedures.[90] Mercaptoethanol (26 mmol) in 20 mL of $CHCl_3$ was slowly added to a

solution of 5 g (26 mmol) of 2,4-dinitroflurorbenzene mixed with 7 mL of triethylamine at room temperature. Extractions were carried out with HCl (1 M) and then twice with water. The product was separated, dried over magnesium sulfate ($MgSO_4$) and filtered. Yellow crystals were then recrystallized from $CHCl_3$ with yield of 5.55g (87.5%). ^{1}H NMR (300 MHz, $CDCl_3$) δ: 9.08 (d, 1H), 8.39 (dd, 1H), 7.70 (d, 1H), 4.04 (t, 2H), 3.31 (t, 2H).

Synthesis of the bischloro-η^5-cyclopentadienyl-(2,4-dinitrophenylthio) ethoxytitanium(IV) (**II**).

To a solution of $CpTiCl_3$ (0.86 g, 3.9 mmol) in THF (5 mL), **1** (0.95 g, 3.9 mmol) and $(C_2H_5)_3N$ (0.54 mL, 3.9 mL) in THF (10 mL) was added dropwise over 30 min. After the mixture was stirred at r.t. for 2 h, the insoluble solid was removed by filtration. Evaporation of the solvent yielded the crude product. The pure **II** was obtained by recystallization from benzene. Yield (1.08 g, 65.0%). ^{1}H NMR (300 MHz, $CDCl_3$) δ: 9.09 (d, J = 2.4, 1H, -Ar), 8.41 (dd, J = 9, J = 2.4, 1H, -Ar), 7.71 (d, J = 9, 1H, -Ar), 6.78 (s, 5H, Cp), 4.97 (t, J = 6, 2H, CH_2), 3.39 (t, J = 6, 2H, CH_2). ^{13}C NMR (75 MHz, $CDCl_3$) δ: 145.4, 127.8, 127.6, 122.0, 120.9, 120.5, 119.8, 117.6, 80.6, 34.8.

Preparation of poly(*N,N'*-di-*n*-hexylcarbodiimide) (**poly-3**).

Polymerization were carried out at r. t. in a dry box. The initiator **II** was dissolved in THF and added to the neat monomer. Unless otherwise noted, the ratio between monomer and initiator was 50:1 for the polymers used in these studies. The mixture was stirred overnight and a red solid was formed. The poly-**3** was purified three times by reprecipitation from a chloroform solution into methanol. ^{1}H NMR (400 MHz, $CDCl_3$) δ: 9.09, 8.44, 7.64, 4.20-4.00 (br), 3.49, 3.20-2.80 (br), 2.88, 1.47-1.00 (br), 1.00-0.60 (br).

General thiol deprotection reaction.

To the solution of poly-**3** and $HSCH_2CH_2OH$ (100 equiv.) in chloroform, $(CH_2CH_3)_3N$ was added to bring the solution to an apparent pH = 8. After stirring overnight, **poly-4** with deprotected thiol end group was precipitated in methanol.[25] ^1H NMR (400 MHz, $CDCl_3$) δ: 4.20-4.00 (br), 3.49, 3.20-2.80 (br), 2.53, 1.47-1.00 (br), 1.00-0.60 (br).

Preparation of poly(*N,N'*-di-*n*-hexylcarbodiimide) (**poly-5**).

As a control experiment, monomer **2** was polymerized by the bischloro-η^5-cyclopentadienyl-dimethylaminotitanium(IV) (**I**) to give poly(*N,N'*-di-*n*-hexylcarbodiimide) (poly-**5**) without the thiol functionality. The procedure of polymerization was similar to the polymerization employed above. ^1H NMR (400 MHz, $CDCl_3$) δ: 4.20-4.00 (br), 3.20-2.80 (br), 1.47-1.00 (br), 1.00- 0.60 (br).

SAMs formation.

Clean polycrystalline gold films deposited on glass slides containing a chromium oxide passivation layer (Evaporated Films Inc.) were used. The wafers were cleaned using a "piranha solution" (70% conc. H_2SO_4/30% H_2O_2) (CAUTION: Piranha solution should be handle with care due to unexpected detonation hazard). The substrates were immersed in 1 mM of poly-**4** in toluene for times ranging from 30 min to 24 h. Upon removal from the solution, the substrates were rinsed and placed in fresh solvent to remove any physisorbed materials before characterization procedure. As a control, similar samples were prepared using the same procedure with poly-**5**.

Characterization of SAMs.

Polarization Modulation Infrared Reflection Absorption Spectroscopy.

The PM-IRRAS spectra were recorded on a Digilab FTS 7000 (Randolph, MA) spectrometer equipped with a step scan interferometer, a liquid nitrogen cooled narrow band MCT detector, a globar source, and a UDR-8 filter. The IR radiation was typically phase modulated at frequencies of 400 or 800 Hz at an amplitude of 1.0 or 2.0 λ HeNe while stepping at 0.5-2.5 Hz. A gold grid polarizer was used to obtain either s- or p-polarized radiation, which was then modulated by a Hinds ZnSe PEM operating at 37 kHz and an amplitude of 0.5 λ (strain axis 45° to the polarizer) before reflecting off the sample at an incident angle of 80° from the surface normal. The spectra were recorded at room temperature at a resolution of 8 cm^{-1} and were the result of four scans with a spectral range of 900-3500 cm^{-1}. The digital signal processing (DSP) algorithm incorporated into the Bio-Rad spectrometer software was used to obtain the spectra. This instrument allowed the gold slide containing the monolayer to also be the reference to obtain the absorption spectra. This technique eliminated the need for a separate reference bare gold slide.

Ellipsometric thickness measurement

The thickness of SAM and the polymer layer was measured using a single-wavelength fixed geometry ellipsometer (AutoEL II, Rudolph Technologies). The thickness was evaluated from the experimentally measured ellipsometric angles Ψ and Δ using the supplied software (DafIMB and WVASE32). The ellipsometric angles Ψ and Δ were collected for a series of wavelengths ranging from 240 to 1000 nm. The incident angle is 70° and the effective refractive index of the polyguanidines was assumed as n = 1.62.[103] The thickness is only moderately sensitive to the exact value of n chosen,[41] so the measurement results are reliable as a comparison for same materials.

Contact angles measurements

Advancing contact angles of DI water were measured with a CAM 200 optical contact angle meter (KSV instrument Ltd.). Water drops were dispersed onto the polymer film surface as the probe liquid. The detailed procedure we employed is: A drop of DI water with the fixed size is formed on the end of a hydrophobic needle and lowered to the surface. As the needle is raised, the drop detaches itself from the tip and advances across the surface. The corresponding software was used for calculation. At least 3 drops were used for each surface sample.

AFM

The topology and roughness measurement of polymer surface were obtained using a Digital instrument Nanoscope III (Digital Instruments, Inc.) in tapping mode. All measurements were conducted after drying the samples.

Synthesis of Gold Nanoparticles.

The gold seeds were synthesized utilizing a modification of the two phase synthesis published by Brust and coworkers.[108] An aqueous solution of gold salt, hydrogen tetrachloroaurate (30 mL, 0.030M) was stirred with a toluene solution containing tetraoctylammonium bromide, a phase transfer catalyst (80 mL, 0.050 M). The solutions were stirred together for one hour. The transfer to the toluene phase was complete, as evidenced by the deep red color of the toluene phase, and the lack color of the aqueous phase. The 4-mercaptophenol and benzenethiol (0.04 g and 0.14 g respectively, a 1:4 mole ratio) were dissolved in about 2 mL toluene and added to the reaction. A freshly prepared aqueous solutions of sodium borohydride (25 mL, 0.4 M) was added dropwise to reduce the

gold (III) to gold (0). The two phase reaction is stirred for 0.5 h, then the organic phase was decanted. Most of the solvent were removed by vacuum and the product were precipitated into methanol. The precipitate was filtered, then was redissolved in toluene and reprecipitated in the methanol to get a dark, waxy, dense solid. The neutral gold combines to form nanometer scale particles, with surface consisting of thiol-functionalized gold.

Polymerization on Gold Nanoparticles

In the glove box, 8 mg of the products of the preceeding synthesis was dissolved in methylene chloride (2 mL) and dropwise add the 2 mL methylene chloride solution containing 4 μL titanium tetrachloride. The mixture was stirred for 2 h. The solution was freeze dried, and kept under vacuum for 24 h to remove all volatiles. The titanium alkoxide bearing nanoparticles was dissolved in 2 mL chloroform, and 0.2 g of *N*,*N'*-di-*n*-hexylcarbodiimide monomer was added under a nitrogen atmosphere. Light purple gold-polyguanidine nanocomposite was obtained after regular work-up.

Characterization of gold-polyguanidine nanocomposites

UV-vis/CD spectra were recorded on a JASCO J-600 spectropolarimeter.

3.5. References and notes

1. Roberts, G., Ed. *Langmuir-Blodgett Films*, Plenum Press, New York **1990**.
2. Swalen, J. D.; Allara, D. L.; Andrade, J. D.; Chandross, E. A.; Garoff, S.; Israelachvili, J.; McCarthy, T. J.; Murray, R.; Pease, R. F.; Rabolt, J. F.; Wynne, K. J.; Yu, H. *Langmuir*, **1987**, *3*, 932.
3. Breton, M. *J. Macromol. Sci. –Rev. Macromol. Chem*, **1981**, *21*, 61.
4. Petty, M. C. *Thin Solid Films*, **1992**, *210/211*, 417
5. Pockels, A. *Nature*, **1892**, *46*, 418.
6. Pockels, A. *Nature*, **1892**, *43*, 437.
7. Langmuir, I. *J. Am. Chem. Soc*. **1917**, *39*, 1848.
8. Blodgett, K. A. *J. Am. Chem. Soc*. **1935**, *57*, 1007.
9. Blodgett, K. A. *Phys. Rev.* **1937**, *51*, 964.
10. Vincett, P. S.; Roberts, G. G. *Thin Solid Films* **1980**, *68*, 135.
11. Ulman, A. *An Introducation to Ultrathin Organic Films, from Langmuir-Blodgett to Self-Assembly*, Academic Press, San Diego, **1991**.
12. Binks, B. P. *Adv. Colloid Interface Sci*., **1991**, *34*, 343.
13. Peterson, I. R. *J. Phys. D: Appl. Phys*. **1990**, *23*, 379.
14. Corkery, R. W. *Langmuir*, **1997**, *9*, 3591.
15. Knobler, C. M.; Schwartz, D. K. *Current Option in the Colloid and Interface Science*, **1999**, *4*, 46.
16. Trengold, R. H. *Order in Thin Organic Films*. Cambridge University Press, **1994**.
17. Raether, H. *Phys. Thin Films* **1977**, *9*, 145.
18. Barnes, W. L.; Sambles, J. R. *Thin Solid Films*, **1986**, *143*, 237.
19. Lloyd, J. P.; Pearson, C.; Perry, M. C. *Thin Solid Films*, **1988**, *160*, 431.
20. Admason, A. W. *Physical Chemistry of Surface*, Wiley: New York, 1976.
21. Kuhn, H. Ulman, A. *Thin Films*, Academic Press: New York, 1995, Vol. 20.
22. Nuzzo, R. G.; Allara, D. L. J. *Am. Chem. Soc*. **1983**, *105*, 4481.
23. Dubois, L. H.; Zegarski, B. R.; Nuzzo, R. G. *Proc. Natl. Acad. Sci. U. S. A*. **1987**, *84*, 4739.
24. Dubois, L. H.; Zegarski, B. R. ; Nuzzo, R. G. *J. Am Chem. Soc*. **1990**, *112*, 570.
25. Benza, V.; Bassetti, B.; Jona, P. Phys. Rec. R. 1987, 36, 7100.
26. Kirkpatrick, S.; Gelatt, C. D., Jr.; Vecchi, M. P. *Science*, **1983**, *220*, 671.
27. Schreiber, F. *Prog. Surf. Sci.* **2000**, *65*, 151.

28. Dubois, L. H.; Nuzzo, R. G. *Annu. Rev. Phys. Chem*. **1992**, *43*, 437.

29. Poirier, G. E. *Chem. Rev.* **1997**, *97*, 1117.

30. Ulman, A. *Chem. Rev*. **1996**, *96*, 1533.

31. Ulman, A.; Evans, S. D.; Shnidman, Y. Sharma, R.; Eiler, J. E.; Chang, J. C. *J. Am. Chem. Soc*. **1991**, *113*, 1499.

32. Ferretti, S.; Paynter, S.; Russell, D. A.; Sapsford, K. E. Richardson, D. J. *Trends in Analytical Chemistry*, **2000**, *19*, 530.

33. Sagiv, J. *J. Am. Chem. Soc.* **1980**, *102*, 92.

34. Finklea, H. O.; Robinson, L. R.; Blackburn, A.; Richter, B.; Allara, D.; Bright, T. *Langmuir*, **1986**, *2*, 239.

35. Maoz, R.; Sagiv, J. *Thin Solid Films* **1985**, *132*, 135.

36. Maoz, R.; Sagiv, J. *Langmuir* **1987**, *3*, 1045.

37. Netzer, J.; Sagiv, J. *J. Am. Chem. Soc*. **1983**, *105*, 674.

38. Tillman, N.; Ulman, A.; Schildkraut, J. S.; Penner, T. L. *J. Am. Chem. Soc.* **1988**, *111*, 6136.

39. Tillman, N.; Ulman, A.; Penner, T. L. *Langmuir*, **1989**, *5*, 101.

40. Troughton, E. B; Bain, C.D.; Whitesides, G. M.; Nuzzo, R. S.; Allara, D. L.; Porter, M. D. *Langmuir* **1988**, *4*, 365.

41. Bain, C. D.; Troughton, E. B.; Tao, Y. T.; Evall, J.; Whitesides, G. M.; Nuzzo, R. G. *J. Am. Chem. Soc*. **1989**, *111*, 321.

42. Porter, M. D.; Bright, T. B.; Allrar, D. L.; Chidsey, C. E. D. *J. Am. Chem. Soc*. **1987**, *109*, 3559.

43. Nuzzo, R. G.; Fusco, F. A.; Allara, D. L. *J. Am. Chem. Soc*. **1987**, *109*, 2358.

44. Nuzzo, R. G.; Dubois, L. H.; Allara, D. L.; *J. Am. Chem. Soc*. **1990**, *112*, 558.

45. Rubinstein, I.; Steinberg, S.; Tor, Y.; Shanzer, A.; Sagiv, J. *Nature*, **1988**, *332*, 426.

46. Whitesides, G. M.; Laibinis, P. E.; *Langmuir* **1990**, *6*, 87.

47. Bain. C. D.; Whitesides, G. M. *J. Am. Chem. Soc*. **1989**, *111*, 7164.

48. Maroncelli, M.; Strauss, H. L.; Snyder, R. G. *J. Chem. Phys*, **1985**, *82*, 2811.

49. Benza, V.; Bassetti, B.; Jona, P. *Phys. Rev. B*. **1987**, *36*, 7100.

50. Mouritsen, O. G.; Ipsen, J. H.; Zuckermann, M. J. *J. Colloid Interf. Sci*. **1989**, *129*, 32.

51. Troughton, E. B.; Bain, C. D.; Whitesides, G. M.; Nuzzo, R. G.; Allara, D. L.; Porter, M. D. *Langmuir* **1988**, *4*, 365.

52. Allara, D. L.; Nuzzo, R. G. *Langmuir* **1985**, *1*, 45.

53. Allara, D. L.; Nuzzo, R. G. *Langmuir* **1985**, *1*, 52.

54. Ogawa, H.; Chihera, T.; Taya, K. *J. Am. Chem. Soc*. **1987**, *105*, 1365.

55. Schlotter, N. E.; Porter, M. D.; Bright, T. B.; Allara, D. L. *Chem. Phys. Lett*. **1986**, *132*, 93.

56. Camillone, N.; Eisenberger, P.; Leung, T. Y.; Pschwartz, P.; Scoles, G. *J. Chem. Phys.* **1994**, *101*, 11031.

57. Ulman, A.; Kang, J. F.; Shnidman, Y.; Liao, S.; Jordan, R.; Choi, G. Y.; Zaccaro, J.; Myerson, A. S.; Rafailovich, M.; Sokolov, J.; Fleischer, C. *Review in Molecular Biotechnology* **2000**, *74*, 175.

58. Kim, B.; Tripp, S.; Wei, A. *J. Am. Chem. Soc*. **2001**, *123*, 7955.

59. Somorjai, G. A.; *Chemistry in Two Dimensions-Surfaces*; Cornell University Press: Ithaca, NY, 1982.

60. Nuzzo, R. G.; Fusco, F. A.; Allara, D. L. *J. Am. Chem. Soc*. **1987**, *109*, 2358.

61. Seller, H.; Ulman, A.; Shnidman, Y.; Eilers, J. E. *J. Am. Chem. Soc*. **1993**, *115*, 9389.

62. Strong, L.; Whitesides, G. M. *Langmuir* **1988**, *4*, 546.

63. Schwartz, D. K. *Annu. Rev. Phys. Chem*. **2001**, *52*, 107.

64. Strder, C. D.; Fong, T. M.; Tota, M. R.; Underwood, D.; Dixon, R. A. *Annu. Rev. Biochem.* **1994**, *63*, 101.

65. Revell, D. J.; Knight, J. R.; Blyth, D. J.; Haines, A. H.; Russel, D. A. *Langmuir* **1998**, *14*, 4517.

66. Sigal, G. B.; Bamdad, C.; Barberis, A.; Strominger, J.; Whitesides, G. M. *Anal. Chem*. **1996**, *68*, 490.

67. Lahiri, J.; Isaacs, L.; Tien, J.; Whitesides, G. M. *Anal. Chem*, **1999**, *71*, 777.

68. Leggett, G. J.; Roberts, C. J.; Williams, P. M.; Davies, M. C.; Jackson, D. E.; Tendler, S. J. B. *Langmuir* **1993**, *9*, 2356.

69. Meuse, C. W.; Niaura, G.; Lewis, M. L.; Plant, A. L. *Langmuir*, **1998**, *14*, 1604.

70. Bardea, A.; Katz, E.; Buckmann, A. F.; Willner, I. *J. Am. Chem. Soc*. **1997**, *119*, 9114.

71. Maskos, U.; Southern, E. M. *Nucleic Acids Res*. **1993**, *20*, 4663.

72. Lee, G. U.; Chrisey, L. A.; Colton, R. J. *Science* **1994**, *266*, 771.

73. Brewer, S. H.; Anthireya, S. J.; Lappi, S. E.; Drapcho, D. L.; Franzen. S. *Langmuir* **2002**, *18*, 4460.

74. Petrovykh, D. Y.; Kimura-Suda, H.; Whitman, L. J.; Tarlov, M. J. *J. Am. Chem. Soc*. **2003**, *125*, 5219.

75. Huang, E.; Satjapipat, M.; Han, S.; Zhou, F. M. *Langmuir* **2001**, *17*, 1215.

76. Herne, T. M.; Tarlov, M. J. *J. Am. Chem. Soc*. **1997**, *119*, 8916.

77. Georgiadis, R.; Peterlinz, K. P.; Peterson, A.W. *J. Am. Chem. Soc*. **2000**, *122*, 3166.

78. Sauthier, M. L.; Carroll, R. L.; Gorman, C. B.; Franzen, S. *Langmuir* **2002**, *18*, 1825.

79. Williams, A. J.; Gupta, V. K. *J. Phys. Chem. B* **2001**, *105*, 5223.

80. Williams, A. J.; Gupta, V. K. *Thin Solid Films* **2003**, *423*, 228.

81. Buffeteau, T.; Calvez, E. L.; Castano, S.; Desbat, B.; Blaudez, D.; Dufourcq, J. *J. Phys. Chem. B* **2000**, *104*, 4537.

82. Goodwin, A.; Novak, B. M. *Macromolecules* **1994**, *27*, 5520.

83. Goodwin, A. *Ph.D. Thesis*, University of California at Berkeley, **1996**.

84. Larson, R. J. *Ph.D. Thesis*, University of Massachusetts Amherst, **2000**.

85. Shibayama, K.; Seidel, S. W.; Novak, B.M.; *Macromolecules* **1997**, *30*, 3159.

86. Schlitzer, D.S.; Novak, B. M. *J. Am. Chem. Soc*. **1998**, *120*, 2196.

87. Tang, H. Z.; Lu, Y. J.; Tian, G. L.; Capracotta, M. D.; Novak, B. M. *J. Am. Chem. Soc*. **2004**, *126*, 3722.

88. Tian, G. L.; Lu, Y. J.; Novak, B. M.; *J. Am. Chem. Soc*. **2004**, *126*, 4082.

89. Deming, T. J.; Novak, B. M.; *J. Am. Chem. Soc*. **1992**, *114*, 7926.

90. Carrot, G.; Hilborn, J. G.; Trollsas, M.; Hedrick, J. L. *Macromolecules* **1999**, *32*, 5264.

91. Shaltiel, S. *Biochem. Biophys. Res. Commun*, **1967**, *29*, 178.

92. Goudie, R. S.; Preston, P. N. *J. Chem. Soc*. C **1970**, 1718.

93. Mose, S.; Brewer, S. H.; Lowe, L. B.; Lappi, S. E.; Gilvey, Lauren B. G.; Sauthier, M.; Tenent, R. C.; Feldheim, D. L.; Franzen, S. *Langmuir* **2004**, *20*, 11134.

94. Wenzl, I.; Yam, C. M.; Barriet, D.; Lee, T. R. *Langmuir* **2003**, *19*, 10217.

95. Williams, A. J.; Gupta, V. K. *Thin Solid Films* **2003**, *423*, 228.

96. Shon, Y.S.; Lee, S.; Perry, S. S.; Lee, T. R. *J. Am. Chem. Soc*. **2000**, *122*, 1278.

97. Wenzl, I.; Yam, C. M.; Barriet, D.; Lee, T. R. *Langmuir* **2003**, *19*, 10217.

98. Yam, C. M.; Cho, J.; Cai, C. *Langmuir* **2003**, *19*, 6862.

99. Shon, Y. –S.; Lee, S.; Colorado, R. Jr.; Perry, S. S.; Lee, T. R. *J. Am. Chem. Soc*. **2000**, *122*, 7556.

100. Miller, W. J.; Abbott, N. L. *Langmuir* **1997**, *13*, 7106.

101. Xu, S.; Cruchon-Dupeyrat, S.; Garno, J. C.; Liu, G. Y.; Jenning, G. K.; Young, T. H.; Laibinis, P. E. *J. Chem. Phys*. **1998**, *108*, 5002.

102. Yan, D.; Jenning, G. K.; Weinstein, R. D. Ind. Eng. *Chem. Res*. **2002**, *41*, 4528.

103. Larson, R. J. *Ph.D. Thesis*, University of Massachusetts Amherst, **2000**.

104. Slot, J. W.; Geuze, H. J. *J. Cell. Biol.* **1981**, *90*, 533.

105. Storhoff, J. J.; Elghanian, R.; Mucic, R. C.; Mirkin, C. A. Letsinger, R. L. *J. Am. Chem. Soc.* **1998**, *120*, 1959.

106. Liu, J.; Xu, R.; Kaifer, A. E. *Langmuir* **1998**, *14*, 7337.

107. Esumi, K.; Hosoya, T.; Suzuki, A.; Torigoe, K. *Langmuir* **2000**, *16*, 2978.

108. Brust, M.; Walker, M.; Bethell, D.; Schiffrin, D. J.; Whyman, R. *J. Chem. Soc., Chem, Commun*., **1994**, 801.

109. Kuo, C-H.; Chiang, T-F.; Chen, L-J.; Huang, M. H. *Langmuir*, **2004**, *20*, 7820.

110. Jana, N. R.; Gearheart, L.; Murphy, C. J. *Langmuir*, **2001**, *17*, 6782.